# UNIVERSITÀ DEGLI STUDI DI FERRARA

**DOTTORATO DI RICERCA IN**

**"SCIENZE DELLA TERRA"**

**CICLO XXVI°**

COORDINATORE Prof. **Massimo COLTORTI**

# Primary magmas, fractionation modelling and mantle source of Etnean lavas

Settore Scientifico Disciplinare **GEO/07**


**Dottorando**

Dott. Alesci Giuseppe

**Tutore**

Prof. Coltorti Massimo

**INDEX**

# 1. INTRODUCTION AND AIMS OF THE RESEARCH

"Mt. Etna is one of the most active and emblematic Volcano in the World, it represents a reference point for a lot of Earth Sciences disciplines from Volcanology to Geophysics, representing an open-air laboratory. With this motivation the UNESCO committee decided during his 2013 annual session in Phnom Penh to include this volcano into the UNESCO World Heritage List. Mt. Etna, 3343 meters high, is the highest European Volcano and one of the most active in the world. With his about $10^3$ $m^3$ of volcanic material emitted every year is one the most studied volcanoes worlwide and a touristic destination of primary importance. For this reason is fundamental to take into account the hazard that could occurs to tourists, inhabitants, infrastructures and air-traffic in the area surrounding the volcano. In the last decades several eruptive events caused the closure of the "Fontane Rosse" Airport of Catania for few days and the destruction of edifices and roads along the southern (Rifugio Sapienza and Nicolosi) and northern flank (Piano Provenzana) of the Volcano. In order to reduce the risk connected to these events, it is necessary trying to understand the eruptive dynamics starting from the deep "roots" of the volcano. The investigation of the deep and shallow feeding system of Mt. Etna, and subsequently of his mantle source could give us some information about the eruptive style thus helping to predict future volcanic events and to reduce the hazard of them. This PhD project research wants to give some support to the Etnean volcanic hazard. It's organized as following:

1) Stratigraphically controlled sampling of the whole Etnean magmatic suites.

2) Whole rock analyses of major and trace elements by X-rays fluorescence (XRF) (Laboratories of the Department of Physics and Earth Sciences – University of Ferrara).

3) Whole rock analyses of trace elements by Inductively Coupled Plasma Mass Spectrometer (ICP-MS) (Laboratories of the Department of Physics and Earth Sciences – University of Ferrara).

4) "In situ" major elements analyses of olivine, clinopyroxene, plagioclase, Ti-magnetite and amphibole phenocrysts by Electron Microprobe (EMP) (Laboratories of Padova, IGG-CNR).

5) Fractionation modeling for each magmatic suites.

6) First volume estimation of the volcanic edifice.

7) Melt modeling to investigate the Etnean mantle source.

8) Comparison between Mt. Etna and Mt. Iblei magmatism.

## 2. GEOGRAPHIC BACKGROUND

Mt. Etna is the highest active Volcano in Europe (is named Mongibello from the Arabic word *gebel*). It's located in the northeastern sector of Sicily region and has an oval base area of 1418 $km^2$ (47 km N-S and 38 Km E-W) (Tanguy et al., 1997). The Volcanic edifice lies on a big anticlinal structure dipping eastward, that is made up of tertiary and quaternary sedimentary rocks which constitute the base of the volcano. The maximum thickness of the volcanic pile resting on the sedimentary cover is estimated about 2000 meters (Tanguy et al., 1997). Mt. Etna is confined to the north by Alcantara River and Peloritani Mountains, to the east, for about 30 km, by the Ionian Sea, to the west by Simeto River and to the South by the Gela-Catania Plain that separate it from Mt. Iblei (Fig. 2.1). The volume of the whole volcanic edifice is estimate in about 370 $Km^3$ of material (Neri and Rossi, 2002).


**Fig. 2.1 -** Satellite image of Sicily and Mt. Etna.

# 3. GEOLOGICAL BACKGROUND

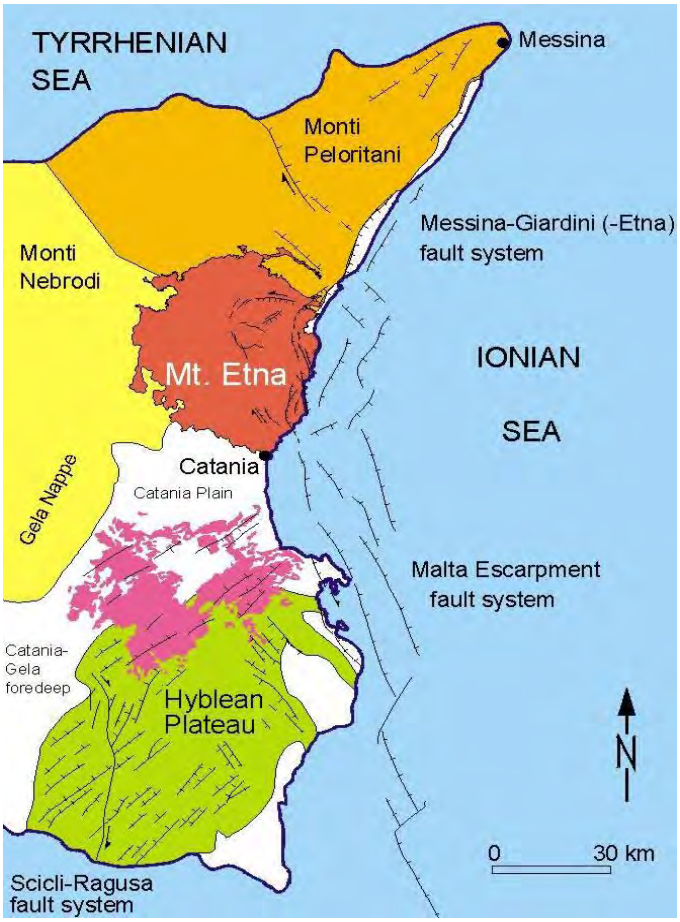


**Fig. 3.1.1** – Geological map of Sicily.

Mt. Etna is located in a complex geodynamic contest, at the intersection of the Maghrebian Chain, the Peloritani Mountains and the Iblean foreland (Catalano e D'Argenio, 1982; Ben Avraham and Grasso, 1990) (Fig. 3.1.1). Two main domains identify the structural setting of Sicily: i) the foredeep-foreland system of the southeastern part of the Island (Gela-Catania foredeep and Iblean foreland) and ii) the southward sedimentary successions related to the Eocene-Quaternary deformation of the paleogeographic domains into the northern sector of the Sicilian region.

The ***Iblean Foreland*** represents the southeastern corner of Sicily (Fig. 3.1.1) and reach 986 meters in altitude close to Mt. Lauro (Schmincke et al., 1997). It's made up of an upper Triassic-Pleistocene massive, prevalently carbonatic succession with intercalations of basaltic

lavas of submarine and subaereal origin and from tholeiitic to nephelinitic affinity (Beccaluva et al. 1998). It is connected, by a NE-SW oriented fault system, to the Gela-Catania foredeep that is an upper Triassic tectonic depression interpreted as external foredeep (Cristofolini et al. 1979; Schmincke et al., 1997) filled by quaternary and recent sediments that cover the Pliocene and Lower Pleistocene Etnean volcanic products. All the main Iblean Plio-Pleistocene tectonic displacements occurred along a N-NE trust system faults located in the western sector of the Plateau (Grasso and Reuther, 1988; Schmincke et al., 1997). To the east The Iblean foreland is delimitated by the Ibleo-Maltese Escarpment. This is a trastensive fault system oriented NNW-SSE (N170°) and extending for 300 kilometers from the oriental Sicilian coast to the south with maximum vertical displacements of 2000 meters. The Gela Nappe is the most external front of the Maghrebian overthrust belt (Butler et al., 1992), generated by continental collisions between the African Plate and the Calabro-Peloritano Arc.

The ***Maghrebian Chain*** (Eocene - Quaternay) connects the Appennines with the Northern African Chains (Fig. 3.1.1) and is formed by successions identified in three distinct structural – stratigraphical Units that were formed during the Miocene - Pliocene continental collisional tectonic (Catalano and D'Argenio, 1982).

The external Units:

I. ***Monte Judica Unit***. Constitutes the Numidian Flysch

II. ***Imerese Unit***. Identified by a thicker Numidian Flysch which is formed by an alternation of brown clays and yellow quarzarenites (Upper Oligocene – Lower Miocene). They outcrop next to the Etnean western flank (Bronte).

The intermediate Units:

I. ***Panormide Unit***. It took place after the Panormide carbonatic platform deformation (Catalano and D'Argenio, 1982) and is represented by reef and back-reef facies. At the top, this succession is covered by the Gratteri Formation, marls and calcarenites with intercalations of quarzarenites that together with the Numidian Flysch represent the crustal xenolites found inside the 2001 and 2002-2003 eruptions lava flows (Michaud, 1995; Ferlito et al., 2009).

II. ***Sicilide Complex.*** Constituited by the Sicilide Unit and Mt. Soro Unit. They are related to intense overtrusting events.

III. ***Calabridi Unit.*** It is made up of Paleozoic metamorphic successions, that lie tectonically on the Mt. Soro Flysch (Catalano e D'Argenio, 1982). They could by divided into four more subunits: 1) Longi-Taormina Unit formed by a metamorphic basement and a Meso – Cenozoic sedimentary cover (it is delimitated by the Taormina lineation that separates it from the northern sector of the Appennine – Maghrebian Chain); 2) Fondachelli – Portella – Mandrazzi Unit; 3) Mandanici Unit constituited by epimetamorphites and 4) Aspromonte Unit (at the base of the succession) with high degree metamorphic rocks and intrusions of granites (Catalano e D'Argenio, 1982). They are covered by Capo D'Orlando Flysch made up of conglomeratic lenses and alternations of sandstones and marly – silty clays.

IV. ***Post – orogenic Units.*** This sedimentary succession that took place after the main Miocene tectonogenic stage. In the southern sector of Mt. Etna they form most of the Gela Nappe and were involved into the recent tectonic deformations. They cover volcanites and old sedimentary deposites along Mt. Etna flanks (Catalano e D'Argenio, 1982).

## 3.1 STRUCTURAL SETTING

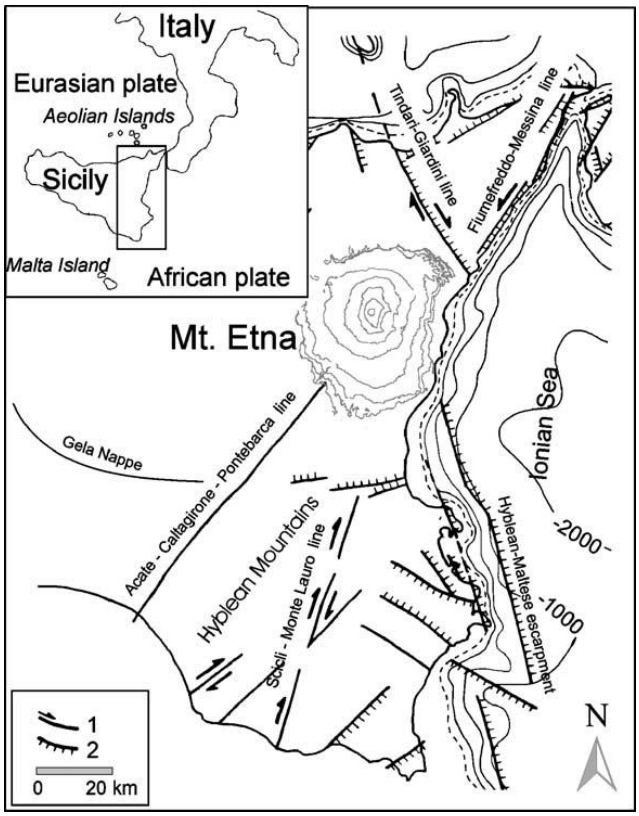


**Fig. 3.1.2 –** Geological map of eastern Sicily 1) Tectonic lineations; 2) Main faults (from Patanè et al., 2006)

The tectonic setting of Mt. Etna is due to the interaction between regional tectonic dynamics and local processes concentrated into the Etnean area. It grew up at the intersection of three main regional fault system (Fig. 3.1.2):

I. ***Tindari – Giardini*** lineation, directed NW-SE and connected with the Ibleo – Maltese Escarpment towards SE.

II. ***Messina – Fiumefreddo*** fault System, oriented NE-SE.

III. ***Kumeta – Alcantara*** fault System, directed ENE-WSW, that intersect the others lineation just north of the volcanic edifice.

Recently The Ibleo – Maltese Escarpment assumed a more important role than Messina – Fiumefreddo and Kumeta – Alcantara Systems. It is considered as the superficial expression of a main regional asymmetric rifting (Continisio et al., 1997; Torelli et al., 1998). The continental crust is 23 kilometers in thickness under the central portion of Sicily and becomes thinner reaching only 13 to 11 kilometers eastward under the Ionian Sea. This could represents a transition to an oceanic crust (Torelli et al., 1998). In this hypothesis the Ibleo – Maltese Escarpment would represents a passive continental margin separating the Sicilian continental domain from the adjacent Jurassic – Cretaceous oceanic basin (Reuther et al., 1993; Torelli et al., 1998). Another hypothesis argues against the oceanic nature of the Ionian crust and identifies this fault system as a deep intra-continental fracture, reactivated during the Miocene which separates the Sicily region from the nearby Ionian Sea (Scandone et al., 1981). The main Etnean tectonic structures are located in the eastern sector of the volcanic edifice and are represented by the "Timpe" system, extension to the north of the Ibleo – Maltese Escarpment. It is a normal-trust fault system, oriented NNW – SSE, that reaches 200 meters of displacement decreasing towards the Ionian sea (Azzaro, 1998; Nicolich et al., 2000). This system is very active and contributes to the topographic raising of the southwestern Etnean flank. Northward it is cut by the Pernicana Fault that is oriented E-W and separate a wide sector of the volcanic edifice, and by the Naca Fault System directed NE-SW. The Ragalna Fault System, oriented N-S and with a main normal-right displacement, borders the Etnean complex along his western flank. Finally in the southern volcanic flank two main isolated structures are found, the Trecastagni Fault and the Tremestieri Fault (Azzaro, 1998, Nicolich et al., 2000). Most of the earthquakes occur within the first 5 kilometers in the eastern sector of the volcano and although the low magnitude (M<4,8) they can generate destructive effects and extended shallow fractures. The geodynamic behavior of the volcanic edifice seems to be controlled by flank instability processes, like the oriental sector eastward dislocation. This is named "Valle del Bove", a horseshoe shaped depression 7 kilometers long and 5 kilometers wide, bounded by steep wall up to 700-800 meters (Nicotra et al., 2011). It is interpreted as the result of a complex interaction between regional tectonic stresses and the gravity on the volcanic edifice. Pernicana Fault and Trecastagni and Tremestieri Faults identify respectively the northern and southern margin of this unstable sector (Azzaro, 1998). Valle del Bove has been extensively studied by numerous authors (Romano, 1982; Calvari et al., 1994; Coltelli et al., 1994, D'Orazio et al., 1997) because it exposes most of the Ancient Alkaline Centers products. The "Pernicana Fault System" (PF) is a E-W oriented fracture system 18 kilometers in length (Neri et al. 2004) of great importance for the Etnean eruptive dynamics. Here occur

most of the displacements after each eruptive event. As a result of the 2002-2003 Etna eruption, it propagated eastward with a predominant lateral-left displacement (Neri et al., 2005). Currently the PF can be subdivided into two main portions with different degree of displacement. The occidental one, 9 kilometers long, is associated with an intense shallow seismicity. The oriental one is the aseismic portion of recent formation (Fig. 3.1.3). The distinct seismic behavior could be related to different physics properties of the substratum (Neri et al., 2004). The NE-Rift (NE-SW) and the S-Rift (N-S) represent, in recent times, two other important fracture systems, directly connected to the main Etnean tectonic lineaments. They generated very dangerous lateral eruption with extended lava flows that could be able to invade the densely populated low Etnean flanks.

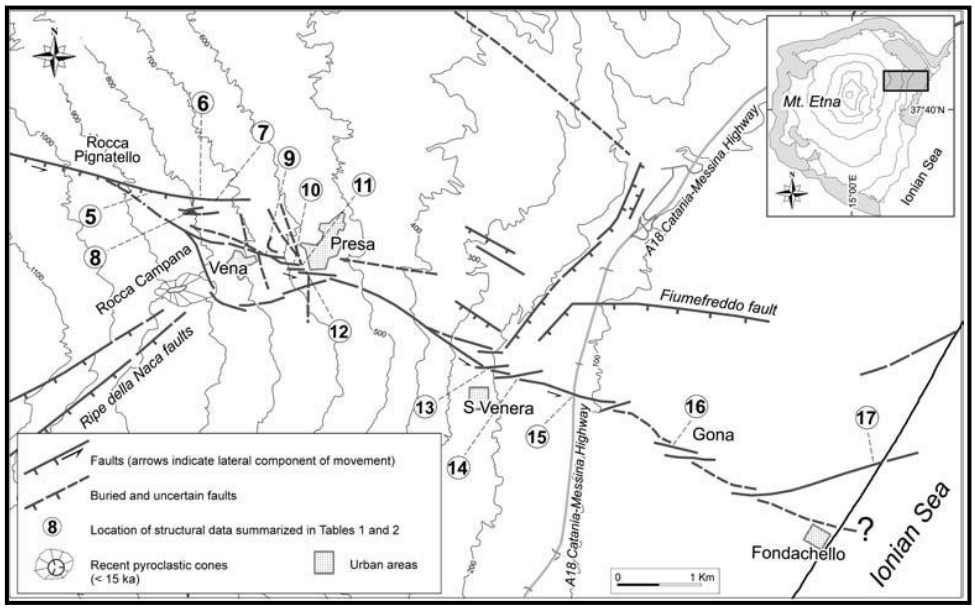


**Fig. 3.1.3** - Structural map of eastern sector of Pernicana Fault, after the 2002-2003 eruption (from Neri et al. 2004)

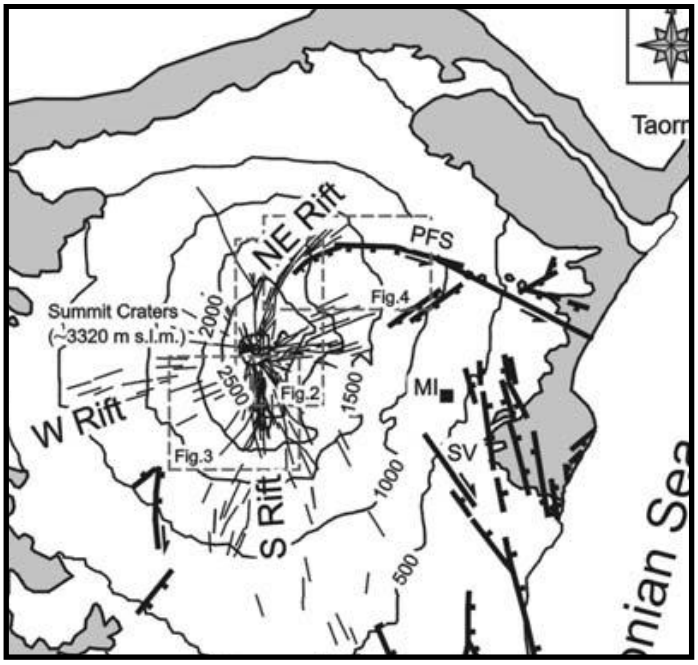


**Fig. 3.1.4** – Map of the Etnean Rift-systems (from Andronico et al. 2005)

# 4. VOLCANOLOGICAL EVOLUTION

The Mt. Etna volcanological evolution has been debated for three decades taking into account the Etnean volcano-stratigraphic units (Romano 1982) and several isotopic analyses. Condomines et al. (1982) utilized the $^{230}Th/^{238}U$ method followed by Gillot et al. (1994) that based on K/Ar measurements was able to identify clear temporal limits inside the Romano et al. (1982) chronological reconstruction. Recently Branca et al. (2008), on the basis of new stratigraphical data, recognized four main evolutional stages: Basal Tholeiitic (BT), Timpe (TI), Valle del Bove Centers (VDB) and Stratovolcano (SV). This marks a shift from the usual Romano's chronology that distinguished the entire volcanological evolution in 5 different stratigraphic units: The Tholeiitic phase, Ancient alkaline eruptive centers, Trifoglietto Unit, Ancient Mongibello and Recent Mongibello Units. Branca et al. (2008) constrained his reconstruction using the K/Ar age determinations published by Gillot et al. (1994) and Tric et al. (1994).

One of the aim of this PhD research project was to establish a well defined and internationally acknowledged volcanological evolution of Mount Etna taking into account volcano-stratigraphic features, age determinations but specially geochemical and petrological affinities. For this reason was implemented a new volcanological evolution that could integrate all data from previous works (Condomines et al., 1982; Romano, 1982; Gillot et al., 1994; Tric et al., 1994; Branca et al., 2008; Nicotra et al., 2011 and reference therein):

***Tholeiitic and transitional phase (500 – 220 ka ago)***

The volcanic activity started about 500 Ka ago (Gillot et al., 1994), several kilometers southeastward the actual Mt. Etna position, with fissural and submarine volcanism with tholeiitic affinity. The products emitted in this first stage represent only 10% of the whole volcanic edifice. Olivine-tholeiites lava flows (520 – 400 Ka ago) emitted by not connected fissures outcrop Near Aci Trezza, Ficarazza and Aci Castello towns (Tanguy et al., 1997).

Younger basaltic lava flows and pigeonite tholeiites can be observed in correspondence of Adrano - Biancavilla and Santa Maria di Licodia - Paternò (300 Ka ago) respectively (Tanguy et al., 1997).

This first period is characterized by sub-volcanic bodies, pillow lavas and volcanoclastic breccia of tholeiitic affinity intercalated in the Gela – Catania foredeep's marly-clay succession (Pleistocene) (Branca et al., 2008; Corsaro and Cristofolini, 2000). Several important outcrops are shown at the Castle Rock of Acicastello. Here pillow lavas are laterally associated to volcanoclastic breccia emitted by the same N-S oriented eruptive fissure. Marly-clay material is founded among the "pillows" indicating a shallow water depositional environment with intense clay accumulation (Simeto river's paleo-alluvional plain). Adjacent to the pillow lavas hypoabissal masses and well developed colonnade lava flows are shown (Corsaro and Cristofolini, 2000). Pillow lavas and pillow breccias formed by angular pillow fragments inside a hyaloclastitic matrix outcrop westward. The oldest subaerial lavas are exposed in the volcano western flank, along the Simeto River's left bank (Romano, 1982; Corsaro and Cristofolini, 2000; Branca et al., 2008). They form a basaltic succession (tholeiitic), from 5 to 25 meters thick, with pillow lavas facies and marly claystones at the bottom of the succession (Adrano and Santa Maria di Licodia) (Tanguy et al., 1997; Branca et al., 2008). Tanguy et al. (1997) in his detailed work recognized three main type of eruptive products with peculiar petrographic and geochemical features:

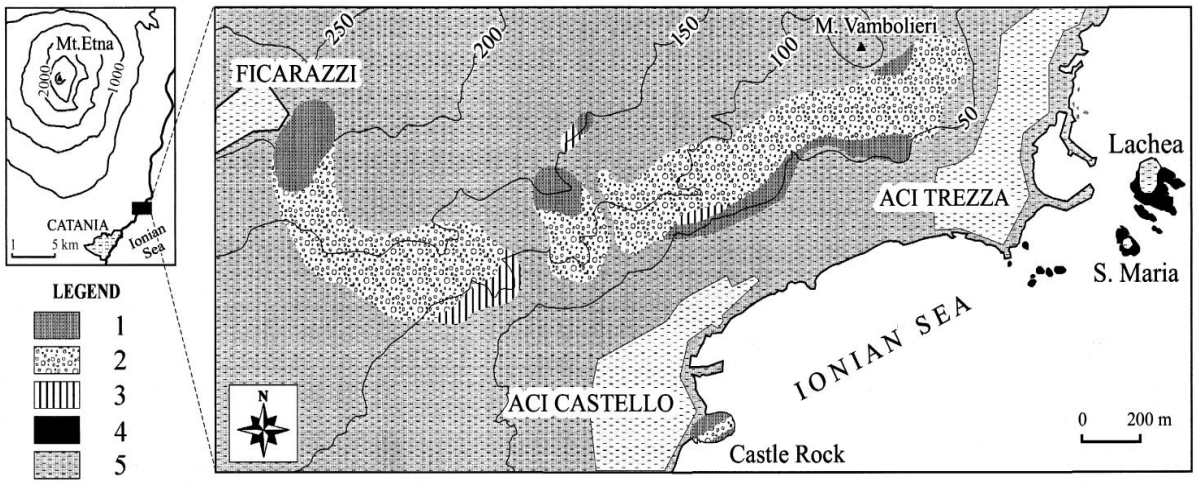


**Fig. 4.1.** - Sketch map of the tholeiitic lithotypes in the Acicastello–Acitrezza–Ficarazzi area. 1) Pillow-lavas and pillow breccia. 2) Volcaniclastic deposits. 3) Subvolcanic rocks with closely spaced columnar joints. 4) Subvolcanic rocks with widely spaced columnar joints. 5) Younger alkaline volcanics and sedimentary rocks chiefly marly claystones; sands and gravels (Corsaro and Cristofolini, 2000).

*i.* ***Olivine-tholeiites.*** They show subaphyric texture with olivine phenocrysts in a course groundmass mostly made up of plagioclase and clinopyroxene with dark-brown glass of rhyodacitic composition. These lavas are primary magmas (or at least primitive magmas), the

earliest and less evolved emitted at Mount Etna. They show high Mg, Cr, Ni and low alkalies and U and Th.

*ii.* ***Pigeonite-tholeiites.*** Less primitive magmas with a decidedly aphyric texture, rare olivine phenocrysts and lower content in Mg, Cr and Ni than olivine-tholeiites type.

*iii.* ***Transitional tholeiites.*** They have lower normative olivine and hypersthene contents than the two previously described groups. The texture varies from subaphyric - doleritic (as in a typical tholeiite) to porphyritic (as in basaltic alkaline lavas).

***Ancient alkaline volcanism – AAV (220 - 60 Ka ago)***

About 220 Ka ago the volcanic activity shifted northward along the Ionian coast with fissural eruptions of Na-alkaline products (Tanguy et al., 1997; Branca et al., 2008). This first alkaline stage generated a shield volcano, 15 km in diameter (oriented N-S) and 7 kilometers southeastward the actual volcano edifice (Branca et al., 2008). His products, with variable thickness from 10 to 100 meters, outcrop along the Acireale-Moscarello Timpa and form the bottom of the Acireale Timpa. Here the passage from a transitional to a Na-alkaline magmatism can be observed (from the base to the top of the succession). Contemporaneously some monogenic Na-alkaline volcanic centers were active close to the actual southern flank of Mt. Etna.

About 121 Ka ago the volcanic activity migrated (westward) to the "Valle del Bove" area and was characterized by the emplacement of the polygenic volcanic centers of "Tarderia" (106 Ka ago) and "Rocche" (102 Ka ago) recording the beginning of a central conduit type volcanic activity (Branca et al., 2008). Their products outcrop in the central zone of the volcano, along the northern rim of "Valle del Bove" (Val Calanna and Tarderia) (Nicotra et al., 2011). Afterwards some others ancient alkaline centers took place named Calanna, Triglioletto I and II, Zoccolaro, Vavalaci-Belvedere, Giannicola, Salfizio and Cuvigghiuni. Trifoglietto is the largest volcanic center developed from 80 to 60 Ka ago. It was located WNW of the primordial Etnean edifice (Tanguy et al., 1997).

***Ellittico (60 – 15 ka ago)***

About 60 ka ago, the main Etnean feeding system moved northwestward inducing the development of the Ellittico Center, the large Stratovolcano which constitutes the skeleton of the actual edifice (more than $^1/_3$ of the whole volcanic edifice). It covered to the west the ancient shield volcano products and to the southeast the Trifoglietto Unit lava flow successions (Romano, 1982; Tanguy et al., 1997). It was formed by an alternation of lavas and pyroclastic material that cover a wide compositional range and constituted a large volcanic edifice with steep flanks. About 15 Ka ago four sub-plinian eruptions partially destroyed the Ellittico Center (Branca et al., 2008) producing several $Km^3$ of trachytes as fall and pyroclastic flow deposits. These events generated a 4 x 3 kilometers wide caldera filled by the subsequent Recent Mongibello products and lavas (Romano, 1982; Tanguy et al., 1997; Branca et al., 2008 and reference therein). Actually the Ellittico products outcrop along the western and southern rim of Valle del Bove. Their thickness range from 100 to 400 meter (Belvedere) and represent 90% of the whole Stratovolcano volume (Romano, 1982).

***Recent Mongibello (15 ka ago – present day)***

The last 15 Ka volcanic persistent activity formed the Recent Mongibello Volcano over-imposed on the Ellittico caldera (Romano, 1982; Tanguy et al., 1997; Branca et al., 2008). Its activity is characterized by different eruptive mechanisms related to the presence of an extensional tectonic regime. In general effusive activity prevailed on explosive phenomena but it showed always a wide range of eruptive styles. About 2 Ka the Recent Mongibello summit area collapse generated the "Caldera del Lago" filled by the actual summit craters products. All lavas and product emitted belong to Na-alkaline series and in lesser extent to K-alkaline series although since 1971 the K-affinity prevails on the Na-one.

***Recent activity***

Recent studies on the last decades eruptions (Allard et al., 2006) investigate the relationship between magma raising, flank instability and changes in eruptive style (summit and eccentric). Three periods were identified, the first from 1993 to 1995 with simply degassing from the summit area; the second from 1995 to 2001 with lava flows, strombolian activity and lava

fountains concentrated in the summit craters area (Fig. 4.2). In this second period were recorded the most intense eruptive events in the last 330 years of Etnean activity. Finally the third from 2001 to the present day with strong explosive activity and lateral eruptions (2001 and 2002-03 eruptions) (Andronico et al., 2009; Giacomoni et al., 2012) and an intense effusive activity from summit craters (2004, 2006, 2008, 2010 and the 2011-12 eruptions) (Neri et al., 2004; Ferlito et al., 2010).

The 2001 (Viccaro et al., 2006; Ferlito et al., 2008) and 2002-03 eruptions (Andronico et al., 2005 and 2009; Ferlito et al., 2009; Spampinato et al., 2008; Giacomoni et al., 2012) were hybrid and highly explosive events characterized by both central and eccentric activity. The 2002-03 eruption interested for the first time, after 70 years, both the NE and S-Rifts. The NE Rift is formed by a fissures system starting from the North East Crater (NEC, formed after the 1911 eruption) and going northeastward, constituting a topographic ridge, 5 kilometers long and 1 kilometer wide, made up of pyroclasts and lava flows (Ferlito et al., 2009). This structure is part of a more important and extended fracture system (NE-SW) from the summit of South East Crater (SEC; fig. 4.2) to the northern margin of Valle del Bove (Monaco et al., 2005; Patanè et al., 2006). The S Rift cuts the southern flank of the volcano and forms a fracture and fissures system directed N-S and SSW-NNE extending from "Montagnola" to "Nicolosi" town for about 10 kilometers. These structures constitute a volcanic ridge marked by a series of aligned eccentric cones (Patanè et al., 2006).

The 2004 effusive activity was followed by the 2006 eruption, culminated with the 16$^{Th}$ November paroxysm, that radically changed the summit area morphology (Ferlito et al., 2010). After the partial SEC collapse, the alternative emission of lava flows and strombolian activity until the 15$^{th}$ December originated the New South East Crater (NSEC). The 2008 eruption lasted 11 months and was very similar to the 2004 one with lava flows emission into Valle del Bove and weak strombolian activity confined to the summit craters. The 2010 activity was characterized by several strombolian events that generated dense ash plumes up to 1 km high. Between January 2011 and April 2012, 25 eruptive events were recorded, all of them lasted from several hours to 2-3 days and were characterized by rare lava flows and very intense strombolian explosions and lava fountains, in some cases up to 800 meters high (Braiato 2011-12).

The explosive behavior for 2001 and 2002-03 eruptions was strictly related (Ferlito et al., 2009; Giacomoni et al., 2012) to the presence of shallow magma batches and to the arrival of primitive and volatile rich magma bodies (Metrich et al., 2004) under the two Etnean Rift Systems, reactivated after long time. Otherwise the most recent activity involved only the

summit craters area in a open-conduit system where magmas can easily degas. A detailed study of 2001 and 2002-03 eruptions is reported in Ferlito et al., (2009) and Giacomoni et al. (2012). 2011 and 2012 strombolian and lava fountains events are well descripted in Braiato 2011-2012 that analyzed samples from most of the cited paroxysms.. During every strombolian event, the magma is replaced by a new and more primitive one. In this complex contest is very important to integrate these data investigating the shallow and deep plumbing system, the Etnean mantle source and his original volatile content to understand the future eruptive mechanisms.


**Fig. 4.2** - Satellite image of Etnean summit craters.

# 5. SAMPLING AND ANALYTICAL METHODS

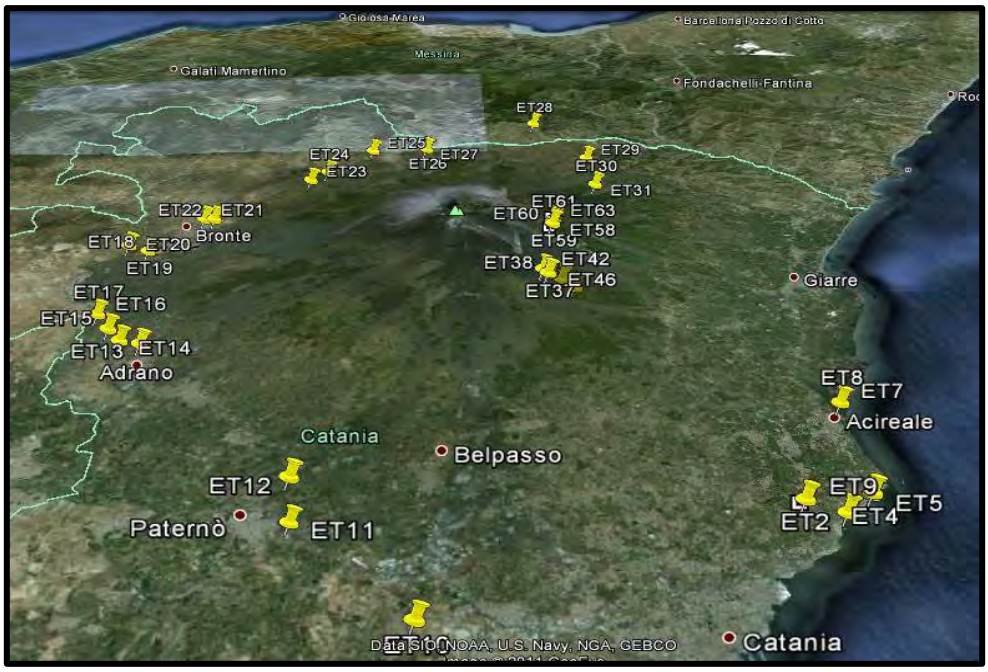


**Fig. 5.1 -** Map showing the sampling of Mt. Etna succession.

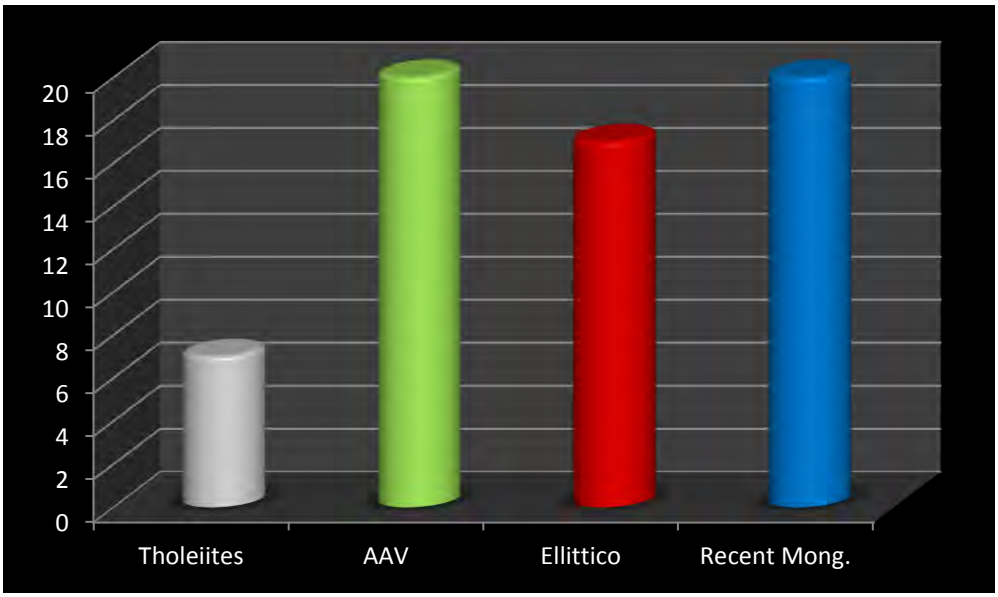


**Fig. 5.2 –** Statistical distribution of sampled rocks.

A detailed stratigraphically-controlled sampling was performed on the whole volcanic edifice for a total amount of 64 samples (lavas flows, pillow lavas and dykes). Position, elevation and typology of all the samples are reported in Table 1. GPS coordinates and altitude values were

taken by a Magellan Meridium Platinum. A representative number of rocks were sampled for each evolutionary stage of Mt. Etna volcanic activity (Fig. 5.1) in order to have a complete framework. This sampling helped also to complete the analyses for both Tholeiitic and AAV periods which are rather scarce in literature (7 Tholeiites, 20 AAV, 18 Ellittico and 19 Recent Mongibello) (Fig. 5.2 and Table 1). In some cases a detailed sampling of the entire volcanic successions was performed as for the ancient eruptive centers of Trifoglietto (AAV - Valle del Bove) and Ellittico (Fig. 5.3) with the aim to observe any geochemical variation during their evolution.

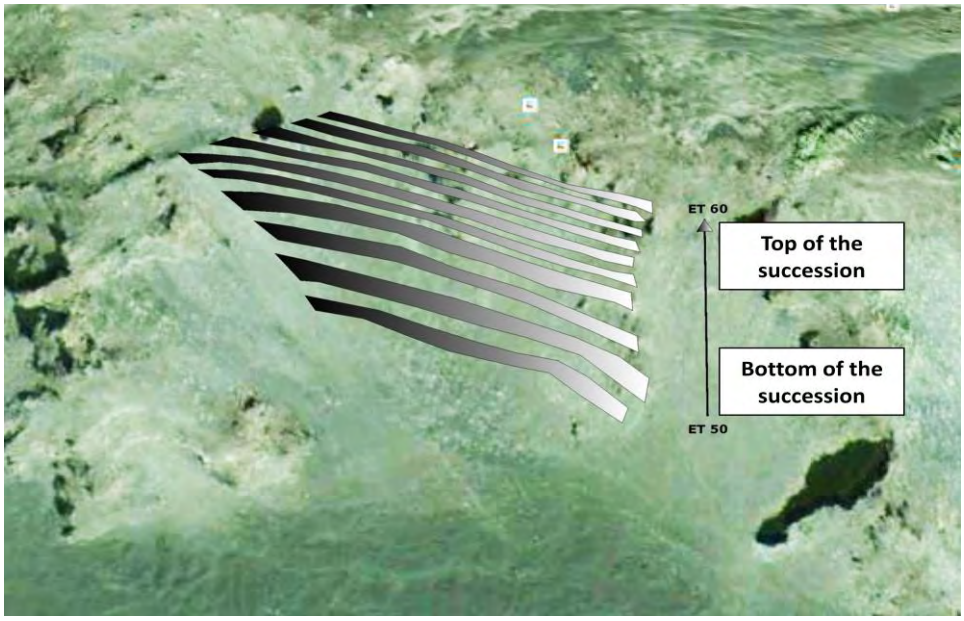


**Fig. 5.3** – Satellite image of sampled Ellittico succession.

All samples were analyzed for whole-rock major and trace elements using X-ray fluorescence (Thermo ARL Advant XP). Intensities were corrected for matrix effects following the method of Lachance and Trail, (1996). Loss on Ignition (L.O.I.) was determinate by gravimetric method. All samples were left 12 hours at 100° Celsius to eliminate the hygroscopic water. After a first precision balance weight they were calcined in a muffle for 12 hours at 1100° Celsius and reweighed. L.O.I. values (wt%) were finally calculated using:

L.O.I. = (Weight Precalcination – Weight Postcalcination) / (Weight Precalcination – Weight Crucible)

All the values were corrected assuming $Fe_2O_3$ as 15% FeO

$FeO = Fe_2O_3\,TOT / (1{,}2613)$

$Fe_2O_3 = FeO * 0{,}15$

26 Representative samples were selected for Th, U, and REE analyses by means of Inductively Coupled Plasma Mass Spectrometry (ICP-MS, Plasma Quad 2Plus VG Elemental). Both major and trace element analyses were carried out at the Department of Physics and Earth Sciences of the University of Ferrara. Accuracy and precision were calculated by analyzing a set of international rock standards with certified values. Geostandards include: JP-1, JGb-1, BHVO-1, UB-N, BE-N, BR, GSR-3, ANG, MAG-1, JLs1 and JDo1. Accuracy for analyzed elements is in the range of 0.9 – 7.9 %. Conservatively, its assumed an accuracy of 10 % for all elements. Detection limits for U and Th are 0,01 ppm.

Porphyritic index (P.I.) was determined by means of Scion Corporation image elaboration program (www.scioncorp.com).

Major and minor elements for olivines, clinopyroxenes, plagioclases, amphiboles, spinels and apatites were carried out by an electron microprobe (EMP-Cameca SX-50) at laboratories of Padova, IGG-CNR, using both energy and wavelength dispersive spectrometry (EDS and WDS).

Routine WDS data were carried out on carbon-coated polished thin sections with an accelerating voltage of 20 KV, 40 nA beam current, and a counting time on peak of 120-130 seconds for ten elements analysis. Natural and synthetic standards were used for calibration. Phenocrysts of the main mineralogical phases were analyzed from 12 representative samples of the four evolutionary stages. Profiles were made following a step of 10-20 μm resulting in more than 650 analyses (see “In-situ geochemistry” chapter).

**Table 1 – Latitude, longitude and elevation**

| Sample | Unit | Latitude | Longitude | Elevation (m) | Type | Location |
|---|---|---|---|---|---|---|
| ET1 | Tholeiites | 37°33'14.58"N | 15° 8'55.91"E | 15 | Pillow lava | Acicastello |
| ET2 | Recent Mongibello | 37°33'14.88"N | 15° 8'55.50"E | 16 | Subaereal lava flow | Acicastello |
| ET3 | Recent Mongibello | 37°33'14.21"N | 15° 8'55.30"E | 17 | Subaereal lava flow | Acicastello |
| ET4 | Tholeiites | 37°33'50.23"N | 15° 9'47.03"E | 5 | Pillow lava | Acitrezza |
| ET5 | Tholeiites | 37°33'47.43"N | 15° 9'45.14"E | 7 | Pillow lava | Acitrezza |
| ET6 | Tholeiites | 37°33'47.08"N | 15° 9'43.25"E | 8 | Subaereal lava flow | Acitrezza |
| ET7 | AAC | 37°37'9.90"N | 15°10'9.46"E | 161 | Lava flow | Acireale |
| ET8 | AAC | 37°37'11.05"N | 15°10'9.54"E | 161 | Lava flow | Acireale |
| ET9 | Tholeiites | 37°33'38.33"N | 15° 7'59.09"E | 175 | Lava flow | Ficarazzi |
| ET10 | Tholeiites | 37°30'42.64"N | 14°58'16.68"E | 250 | Lava flow | Motta San Anastasia |
| ET11 | Tholeiites | 37°33'33.57"N | 14°55'12.24"E | 299 | Lava flow | Paternò - railway |
| ET12 | Ellittico | 37°34'58.11"N | 14°55'1.82"E | 322 | Lava flow | highway Santa Maria di Licodia |
| ET13 | Tholeiites | 37°40'27.78"N | 14°49'55.41"E | 597 | Lava flow | Adrano |
| ET14 | Ellittico | 37°40'40.39"N | 14°49'15.91"E | 424 | Lava flow | Adrano |
| ET15 | Recent Mongibello | 37°41'14.72"N | 14°48'46.47"E | 362 | Lava flow | From Adrano to Simeto Valley |
| ET16 | Recent Mongibello | 37°41'59.14"N | 14°48'14.14"E | 374 | Lava flow | From Adrano to Simeto Valley |
| ET17 | AAC | 37°42'2.88"N | 14°48'0.14"E | 360 | Lava flow | Saraceno Bridge |
| ET18 | Recent Mongibello | 37°45'30.94"N | 14°48'57.60"E | 605 | Lava flow | Mt. Barca |
| ET19 | AAC | 37°45'55.11"N | 14°48'8.00"E | 502 | Lava flow | Mt. Barca |
| ET20 | Recent Mongibello | 37°45'56.77"N | 14°48'11.51"E | 508 | Lava flow | Lava flow Monte Barca |

| Sample | Unit | Latitude | Longitude | Elevation (m) | Type | Location |
|---|---|---|---|---|---|---|
| ET21 | Recent Mongibello | 37°47'20.19"N | 14°50'32.99"E | 855 | Lava flow | Bronte |
| ET22 | Recent Mongibello | 37°47'16.26"N | 14°50'55.04"E | 889 | Lava flow | Bronte |
| ET23 | Recent Mongibello | 37°49'59.47"N | 14°54'4.60"E | 1010 | Lava flow | Maletto-Randazzo |
| ET24 | Recent Mongibello | 37°50'37.88"N | 14°54'39.99"E | 947 | Lava flow | Maletto-Randazzo |
| ET25 | Recent Mongibello | 37°52'25.80"N | 14°56'19.58"E | 795 | Lava flow | Randazzo |
| ET26 | Recent Mongibello | 37°52'31.82"N | 14°58'29.41"E | 734 | Lava flow | Randazzo |
| ET27 | Recent Mongibello | 37°52'10.18"N | 15° 2'15.36"E | 667 | Lava flow | Pisciaro Pass |
| ET28 | Recent Mongibello | 37°54'40.38"N | 15° 3'4.37"E | 611 | Lava flow | Mt. Mojo |
| ET29 | Recent Mongibello | 37°51'33.46"N | 15° 4'55.96"E | 688 | Lava flow | Salicchiata |
| ET30 | Recent Mongibello | 37°48'43.28"N | 15° 4'51.45"E | 1308 | Lava flow | Piano Provenzana |
| ET31 | Ellittico | 37°48'43.25"N | 15° 4'51.43"E | 1473 | Lava flow | Ragabo Refuge |
| ET32 | AAC | 37°41'57.93"N | 15° 3'12.98"E | 1379 | Lava flow | Acqua Rocca |
| ET33 | AAC | 37°42'17.64"N | 15° 2'50.38"E | 1499 | Dyke | Acqua Rocca |
| ET34 | AAC | 37°42'19.20"N | 15° 2'48.72"E | 1530 | Lava flow | Acqua Rocca |
| ET35 | AAC | 37°42'18.52"N | 15° 2'47.94"E | 1527 | Lava flow | Acqua Rocca |
| ET36 | AAC | 37°42'31.57"N | 15° 2'29.38"E | 1768 | Dyke | Schiena dell'Asino |
| ET37 | AAC | 37°42'32.50"N | 15° 2'26.70"E | 1800 | Dyke | Schiena dell'Asino |
| ET38 | AAC | 37°42'30.96"N | 15° 2'25.77"E | 1815 | Lava flow | Schiena dell'Asino |
| ET39 | AAC | 37°42'38.43"N | 15° 2'19.42"E | 1720 | Lava flow | Valle del Bove - southern margin |
| ET40 | AAC | 37°42'38.93"N | 15° 2'18.72"E | 1716 | Lava flow | Valle del Bove - southern margin |

| Sample | Unit | Latitude | Longitude | Elevation (m) | Type | Location |
|---|---|---|---|---|---|---|
| ET41 | AAC | 37°42'40.90"N | 15° 2'19.60"E | 1683 | Lava flow | Valle del Bove - southern margin |
| ET42 | AAC | 37°42'40.83"N | 15° 2'17.25"E | 1686 | Lava flow | Valle del Bove - southern margin |
| ET43 | AAC | 37°42'41.27"N | 15° 2'16.93"E | 1683 | Lava flow | Valle del Bove - southern margin |
| ET44 | Recent Mongibello | 37°42'40.98"N | 15° 2'18.20"E | 1683 | Lava flow | Valle del Bove |
| ET45 | Recent Mongibello | 37°42'41.12"N | 15° 2'17.99"E | 1683 | Lava flow | Valle del Bove |
| ET46 | AAC | 37°42'32.50"N | 15° 2'28.77"E | 1777 | Lava flow | Schiena dell'Asino |
| ET47 | AAC | 37°42'32.50"N | 15° 2'28.77"E | 1777 | Lava flow | Schiena dell'Asino |
| ET48 | AAC | 37°42'32.50"N | 15° 2'28.77"E | 1777 | Lava flow | Schiena dell'Asino |
| ET49 | AAC | 37°42'32.50"N | 15° 2'28.77"E | 1777 | Lava flow | Schiena dell'Asino |
| ET50 | Ellittico | 37°45'8.56"N | 15° 2'50.24"E | 1964 | Lava flow | Valle del Bove - ColleSerra |
| ET51 | Ellittico | 37°45'9.03"N | 15° 2'50.53"E | 1971 | Lava flow | Valle del Bove - ColleSerra |
| ET52 | Ellittico | 37°45'10.01"N | 15° 2'50.45"E | 1983 | Lava flow | Valle del Bove - ColleSerra |
| ET53 | Ellittico | 37°45'10.80"N | 15° 2'51.12"E | 2001 | Lava flow | Valle del Bove - ColleSerra |
| ET54 | Ellittico | 37°45'11.88"N | 15° 2'50.90"E | 2019 | Lava flow | Valle del Bove - ColleSerra |
| ET55 | Ellittico | 37°45'12.83"N | 15° 2'51.33"E | 2023 | Lava flow | Valle del Bove - ColleSerra |
| ET56 | Ellittico | 37°45'13.66"N | 15° 2'51.67"E | 2030 | Lava flow | Valle del Bove - ColleSerra |
| ET57 | Ellittico | 37°45'14.52"N | 15° 2'51.36"E | 2034 | Lava flow | Valle del Bove - ColleSerra |
| ET58 | Ellittico | 37°45'15.17"N | 15° 2'52.21"E | 2039 | Lava flow | Valle del Bove - ColleSerra |
| ET59 | Ellittico | 37°45'15.72"N | 15° 2'51.72"E | 2044 | Lava flow | Valle del Bove - ColleSerra |
| ET60 | Ellittico | 37°45'16.31"N | 15° 2'52.37"E | 2052 | Lava flow | Valle del Bove - ColleSerra |
| ET61 | Ellittico | 37°45'22.13"N | 15° 2'53.21"E | 2031 | Lava flow | Citelli Refuge pathway |
| ET62 | Ellittico | 37°45'24.21"N | 15° 2'55.34"E | 2010 | Lava flow (Cicirara) | Citelli Refuge pathway |
| ET63 | Ellittico | 37°45'28.07"N | 15° 2'55.30"E | 1992 | Lava flow | Citelli Refuge pathway |
| ET64 | Recent Mongibello | 37°45'50.12"N | 15° 3'1.47"E | 1871 | Lava flow | Citelli Refuge pathway |

# 6. GAS AND VOLUME ESTIMATION

## 6.1 GAS

One of the main feature of Mt. Etna is represented by the persistent degassing from summit craters (this is one of the most commonly observed kind of volcanic activity). Upon their migration from the source region toward the Earth's surface, magmas release volatile species into the gas phases after a decrease in their solubility inside the melt (Carroll and Holloway, 1994). These may induce magma fragmentation during strombolian activity and lava fountaining generating a significant hazard (Cashman et al., 2000). Since the late 1970s explosive eruptive events have been more frequent, especially for the 1995-2001 period that counts about 150 episodes of lava or fire fountaining (many of which generating high ash and gas columns). Mt. Etna is very well monitored by The "Istituto Nazionale di Geofisica e Vulcanologia" (INGV) through continue observation of seismic signals, volcanic tremor, video monitoring (visible and termal maps) and simulations of the volcanic ashes dispersion (taking into account the dominant winds) (Fig. 6.1.1).

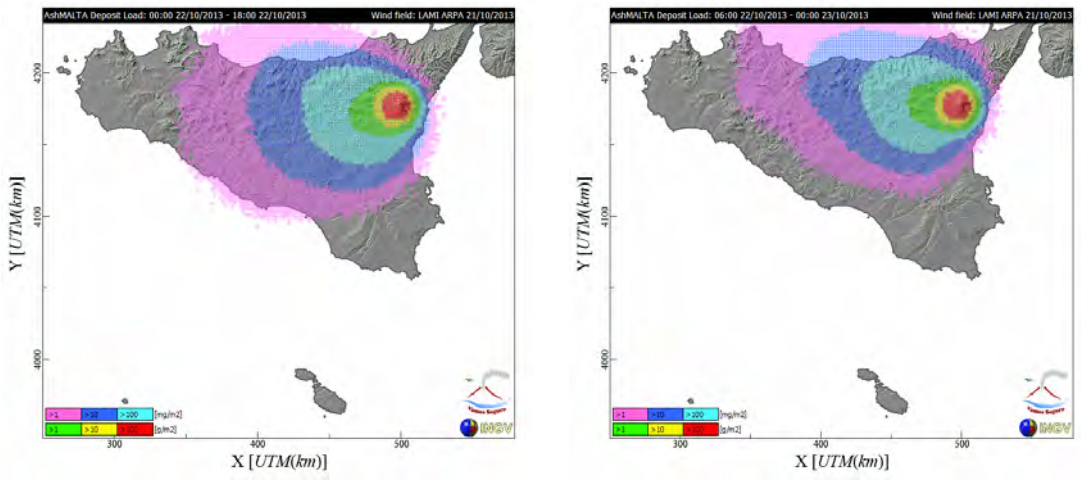

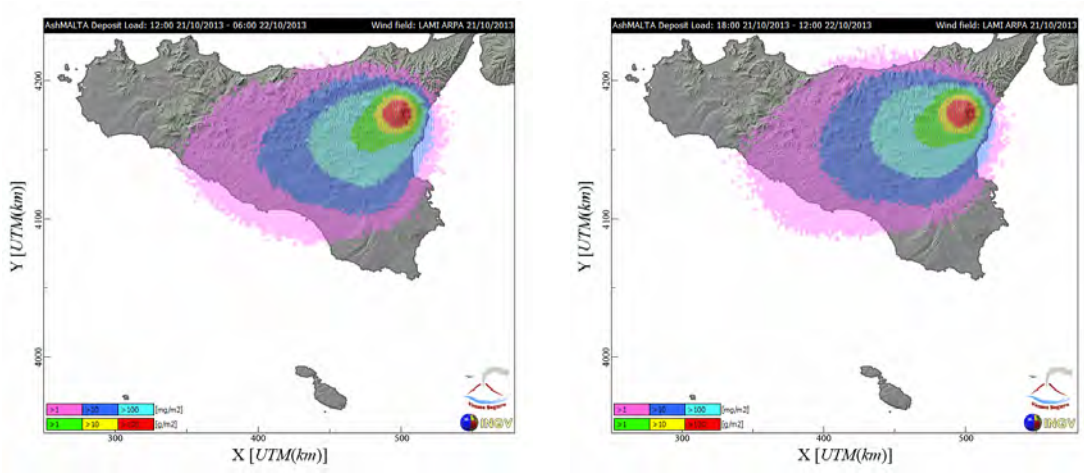


**Fig. 6.1.1.** – Simulations maps of Mt. Etna ash dispersion (www.INGV.it)

Notwithstanding its behavior is poorly understood in many aspects and the composition of volcanic gas can give us some information upon the magma ascent and the eruptive dynamics. Aiuppa et al. (2011) analyzed the H content in Mt. Etna's gas phases with the aim to discover the redox properties of the shallow magmatic system. Magma redox state controls the iron partition thus contributing in controlling magma crystallization sequence and differentiation, and volatile partitioning between gas and melt. The fugacity in gases is buffered by oxidation-reduction reactions among ferromagnesian minerals in the surrounding silicate (rock/melt) matrix. Aiuppa et al. (2011) performed hydrogen determinations in the volcanic gas plume of Mt. Etna with an upgraded MultiGAS apparatus (Fig. 6.1.2). When the magmatic gas phase is directly injected in the atmosphere at high temperature, as at open vents (Bocca Nuova and Northeast craters), and then rapidly cooled, the $H_2$-$H_2O$ and $SO_2$-$H_2S$ gas ratios are quenched to reflect redox properties of the source magmas (hydrogen-rich gas). Comparison between the model derived compositions and natural data suggests that most of the observed plume compositions closely match those representative of quenched gas-melt equilibria for redox conditions at the NNO buffer and 0.1 MPa Pressure. These data support the shallow (near surface), cold (550 °C) and oxidized (conduit gases have equilibrium redox conditions at NNO + 2.8) environment of final equilibration of H poor gases.

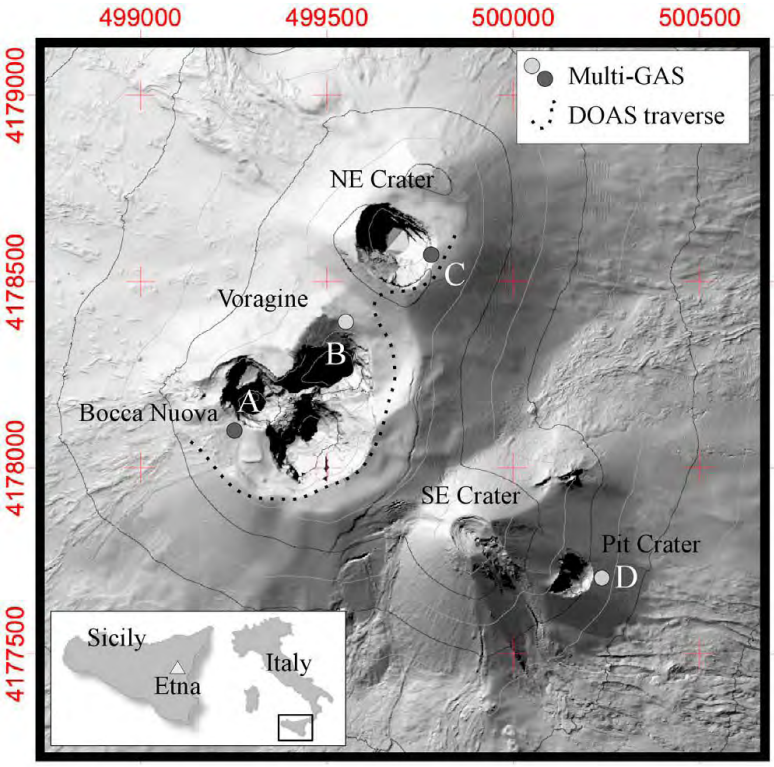


**Fig. 6.1.2 –** Map of Mt. Etna summit craters area, showing the MultiGAS sites measurements (Aiuppa et al. 2011)

Giacomoni et al. (2013) tried to investigate the deep feeding system oxidation state. He calculated $fO_2$ values for Mt. Etna magmas using $Fe^{3+}/Fe^{2+}$ distribution between clinopyroxene-plagioclase phenocrysts and melt (France et al., 2010). At Pressure <0.5 Gpa and Temperature of 1150°, oxygen fugacity varies between $+0.8 < \Delta QFM < +2.3$. According to Kress and Carmichael (1988) this $fO_2$ corresponds to a $Fe^{3+}/Fe^{2+} = 0.15$.

Other important volatile species are represented by $SO_2$ and $CO_2$. The $CO_2/SO_2$ ratio is related to the different solubility of $CO_2$ and sulfur (14 MPa; Stelling et al., 2008) in a silicate melt. In a open conduit degassing system this value gets low because the loss of $CO_2$, until the triggering of new eruptions with the uprising of primitive and volatile-rich magma bodies (Aiuppa et al., 2007). Real time gas measurements of $CO_2$ and $SO_2$ could be used as indicator of incoming eruptions. Mt. Etna is one of the largest $SO_2$ emission source even during non-eruptive periods (Allard et al., 1991; Allard, 1997; Pennisi and Le Cloarec, 1998). Measurements of the $SO_2$ volcanic plume and of $CO_2$ soil emissions indicate an average $SO_2$ outflux between 0.31 and 7.7 Mt $yr^{-1}$ (average of 2.04 Mt $yr^{-1}$ during non eruptive periods; Ferlito et al. 2014) and a $CO_2$ average output of 13±3 Mt $yr^{-1}$ (Allard et al., 1991) (Table 2). Regard to $CO_2$ Mt. Etna produces about the 15 % of the global volcanic emission. Some authors (Clocchiatti et al. 1992) analyzed olivine fluid inclusions and obtained for Etnean

magmas a saturation limit of $CO_2$ at about 700 MPa (at 1200 °C) that corresponds to a minimum exsolution depth of approximately 24 km. D'Alessandro et al. (1997) calculated the involvement of 0,7 $km^3$/a of magma in generating the estimated $CO_2$ emission rate (Table 2). However a lot of authors (Azzaro and Neri, 1992; Barberi et al., 1993; Calvari et al., 1994) measured a lava emission rate in the order of 0,035 $km^3$/a for the 1971-1995 period (GPS techniques were used to measure the lava thickness enabling to calculate the final volume and emission rate), that is 1/20 of the value requested to balance the gas emissions (Table 2). This reveals a very low ratio between erupted and degassed magma and opens a lively debate that affects other well studied volcanoes such as Izu – Oshima, Japan (Kazahava et al., 1994); Stromboli, Italy (Allard et al., 1994); Erebus, Antarctica (Oppenheimer and Yirgu, 2002) and Masaya, Nicaragua (Rymer et al., 1998) that exhibit continued degassing in the absence of significant magma eruptions. Allard et al. (1997) tried to explain this great Mt. Etna's $CO_2$ emission rate with the thermal decarbonatation of limestones present in Etna's sedimentary basement.

D'Alessandro et al., (1997), provided constraints on $CO_2$ magmatic origin in the Etnean area (excluding the decarbonatation origin proposed by Allard et al., 1997) by means of isotopic data on carbon in $CO_2$ from Allard et al., (1991), Anzà et al., (1989), D'Alessandro et al. (1997) and Giammanco and Inguaggiato, (1996). Values of $\delta^{13}C$ ($CO_2$) in gas from both the lower flanks and the summit craters area of Etna, generally fall in the range of –6 to 1‰ vs PDB (Pee Dee Belemnite) that are slightly more positive than the values commonly accepted for magmatic $CO_2$. This could be explained by a slight crustal contamination of the magmatic source as suggested by - $^3He/^4He$ ratio (5.8–7 R/Ra), which is slightly lower than ratios typical of a MORB source (8±1 R/Ra according to Lupton, 1983).

However Etna is also a strong emitter of $SO_2$, whose output alone would account for a huge amount of degassing magma and the S-isotopic composition ($\delta^{34}S$ ($SO_2$) + 0.8‰ vs Canyon Diablo Troilite) indicate a mantle source (Allard, 1986). The high output of both $CO_2$ and $SO_2$ might be typical of alkaline volcanoes such as Etna. D'Alessandro et al. (1997) hypothesize a model conceptually consistent with these isotopic data suggesting that the asthenosphere beneath Etna rises to a depth where reduced lithostatic pressure allows exsolution of $CO_2$ from the magma. This hypothesis is supported by seismic refraction studies that showed a significant upwarp of the lower-crust boundary beneath the eastern flank of Etna (Nicolich et al. 1996). These authors suggest that the deep magma chamber of Etna is a lens atop an upwarped mantle and the presence of convective movements in an uprising asthenosphere

allows the transport of gas rich magma from deeper to shallower parts, making the source of gas practically infinite.

Many authors (Francis et al., 1993; Allard et al., 1994 and references therein), instead, suggest the intrusion of huge amounts of magma and/or the presence of convective movements within the conduits and magma chambers (Oppenheimer and Yirgu, 2002; Oppenheimer et al., 2009; Kazahava et al., 1994; Stoiber et al., 1986; Witham and Llewellin, 2006; Witham et al., 2006; Spilliaert et al., 1996; Witham et al., 2011). The undegassed and volatile-rich magma rises the conduit while the degassing one increases his density and can I) convects back down into the volcanic conduit; II) mixes in large and deep reservoir; III) intrudes the country rock (Huppert and Hallworth, 2007; Francis et al., 1993; Kazahava et al., 1994; Stevenson and Blake, 1998; Witham et al., 2011).

In this contest, mixing represents the main mechanism that may be able to reduce the volatile concentration in magma arriving at an open volcanic vent in a degassing system (that is lower than in melt inclusions analyses). This could explain the rare explosive eruptions because the low gas content cannot induce magma fragmentation (Witham et al., 2011). In addition the escape of gas from shallow depths through a permeable network (Burton et al., 2007) represents another reason for the lack of explosive activity.

Following Ferlito et al., (2014) the solution of magma convection presents some important weakness: i) does not explain why new magmas batches can emplace, lose their volatiles content and don't erupt; ii) the loss of volatiles induces undercooling, promotes crystallization and should "close" the open conduit; iii) all the degassed magma will have to be rearranged beneath the volcanic edifice. The estimated amount of degassed and cold basaltic magma is $3*10^5$ $m^3$ every day and it would be too large if compared with the plutonic complex recognized by Allard et al. (1997) and Patanè et al. (2006).

Ferlito et al., (2014) support the presence of a $CO_2$ flux within the Etnean feeding system, because $CO_2$ exsolves at considerable depths (700 Mpa from Clocchiatti et al. 1992; 600 MPa from Barsanti et al., 2009). The $CO_2$ acting as volatiles carrier (because changes the $CO_2$-$H_2O$ equilibrium of fluxed magma), induces the $H_2O$ exsolution at depth, causing loss of $H_2O$ from the system (Dixon et al., 1995; Papale, 1999; Liu et al., 2005; Collins et al., 2009; Armienti et al. 2013).This can justify the high emissions of $H_2O$ without frequent magma eruptions. Unfortunately the migration mechanism of $H_2O$ is still a not well understood process that necessitate a long series of experimental works (Ferlito et al. 2014).

## 6.2. VOLUME ESTIMATIONS

One of the aim of this study was to obtain an estimation of the magmatic products related to the Etnean activity. First was necessary to calculate the volcanic edifice volume, taking into account the reconstruction of the sedimentary basement underlying Mt. Etna. Neri and Rossi (2002), starting from geoelectric data (Ogniben, 1966) and hydrogeological studies drew a substratum map (Fig. 6.2.1). Most of the wells in literature do not reach the sedimentary succession, so all information on the impermeable substratum come from indirect Vertical Electrical Soundings (VES) (Patella and Quarto, 1987; Loddo et al., 1989). Both wells and VES are less numerous in the summit craters area, making the substratum map not so precise. Evaluating both literature data and hydrogeological studies of private and public companies, Neri and Rossi (2002) reconstructed the sedimentary basement morphology comparing direct and indirect information on the same detected area.

According to this reconstructed map, N-NW respect to the actual summit craters area, it is observable a 1300 meters high-topographic, that could represent an extension of Madonie and Mt. Peloritani formations.

A specific software, that makes tridimensional elaborations of topographic data, was used to calculate the emitted products volume as a simple difference between the actual topographic surface and the reconstructed substratum (Fig. 6.2.2). However, the result of 326 $km^3$ does not consider the Valle del Bove area eroded material. With the aim to obtain this missing volume, they digitalized the apical morphology prior to the Valle del Bove formation from Neri et al., (1995) and subtracted it to the actual topography getting more 13,4 $km^3$. Considering the error given by the use of indirect data and the probable substitution of part of the substratum sediments with magmatic dykes intrusions is reasonable to add 10% to the previous estimated volume. The final result is 374 $km^3$ with an emission rate of 1250 $m^3/y$ (Table 2) that was calculated taking into account that most of the volcanic edifice developed in the last 100 ka. (Neri and Rossi, 2002).

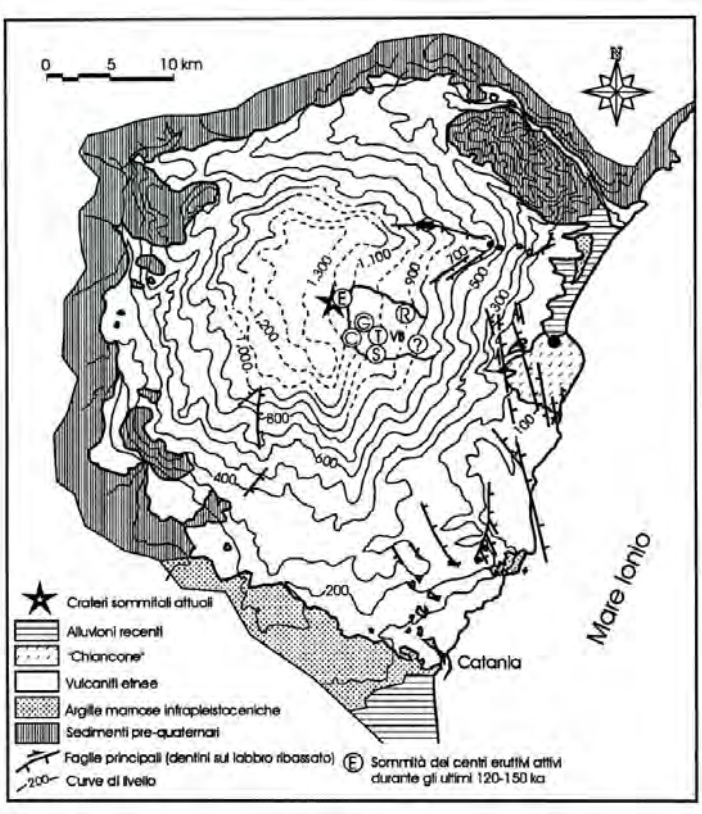


**Fig. 6.2.1** –Substratum morphologic map of Mt. Etna (from Neri and Rossi 2002). In the central area are marked the main Volcanic Centers of the last 150 ka: E= Ellittico, C= Cuvigghiuni; G= Giannicola Grande; S= Salfizio; T= Trifoglietto; R= Rocca Capra; ?= Calanna. The locations derive from Coltelli et al. (1994), Calvari et al. (1994) and Romano (1982).

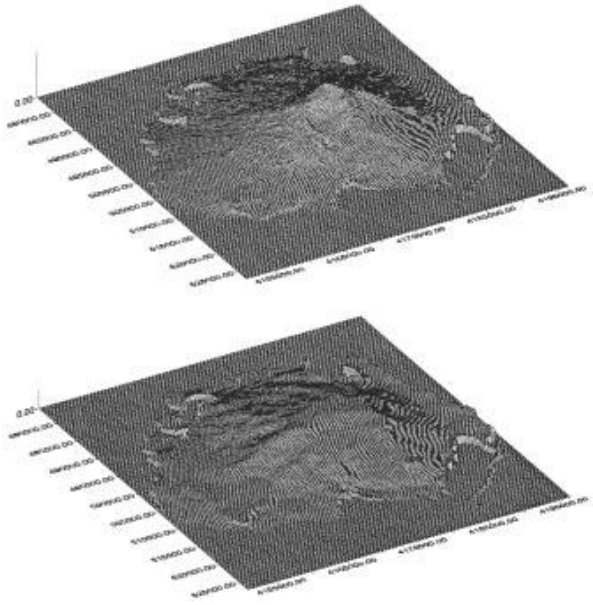

**Fig. 6.2.2 -** Tridimensional reconstruction of Etnean sedimentary basement (at the bottom) and actual topographic surface (at the top). Vertical scale $1=^{2}/_{3}$h. (from Neri and Rossi 2002).

# 7. MELT INCLUSIONS

Silicate melt inclusions represent trapped silicate melt that can give us important information on the evolution of the magma. This is possible only on the condition that they remained isolated from the enclosing magma after their entrapment (Frezzotti, 2001). Studies of melt inclusions in early crystallization phases (for example olivine) allow the characterization of primary magmas while in differentiated products they can provide information on the petrological evolution of the magmas. The concentrations of volatile species ($H_2O$, $CO_2$, Cl, S) are very important to recognize the presence of metasomatic agents in the mantle source (possible recycling of subducted material) and to better understanding the degassing processes. Matching these data with geochemical and petrological information is useful in order to increase our knowledge of magmatic processes (Frezzotti, 2001). Melt inclusions (MI) are constituted by glass ± one or more glass bubbles ± daughter mineral phases and are often very small (< 30 μm) (Fig. 7.1 and 7.2). A very common processe that affects MI is represented by crystallization of daughter-mineral phases within the inclusion (Fig. 7.2). From an original alkali-basalt trapped by the growing crystal, Mg, Ca, Fe and Si will be lost by the crystallization of clinopyroxene at the walls of the inclusion. Complete studies to characterize MI requires: i) Electron microprobe analyses (major and minor elements analyses; Nielsen and Sigurdsson, 1981; Lowenstern and Mahood, 1991); ii) Ion microprobe (trace-element and isotope analyses, HO quantitative analyses; Kovalenko et al., 1988; Ihinger et al., 1994; Deloule et al., 1995); iii) Fourier-transformed infrared spectroscopy ($H_2O$ and $CO_2$ quantitative analyses; Ihinger et al., 1994, Lowenstern, 1994) and more recently iv) Laser-ablation microprobe inductively coupled plasma-mass spectrometry (trace elements; Taylor et al., 1997).

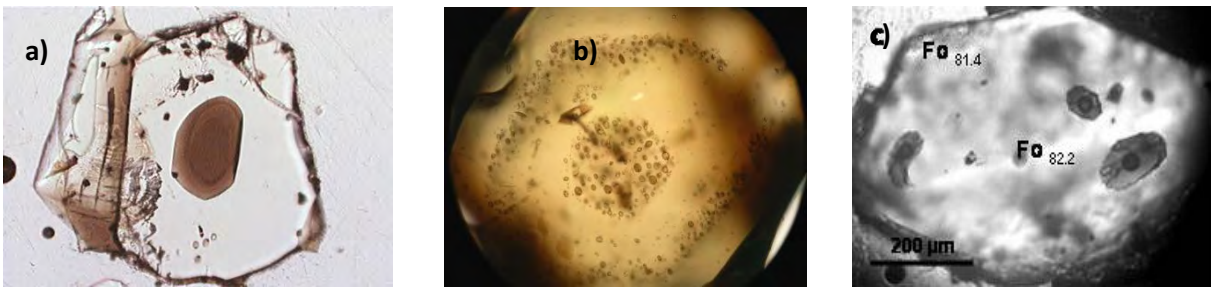


**Fig. 7.1** – Pictures of melt inclusions in olivine phenocrysts from a) Keanakakoi, Kilauea, Hawaii (Metrich and Wallace 2008); b) Stromboli (Faure and Schiano, 2005) and c) 2002-2003 eruption, Mt. Etna (Metrich and Wallace 2008)

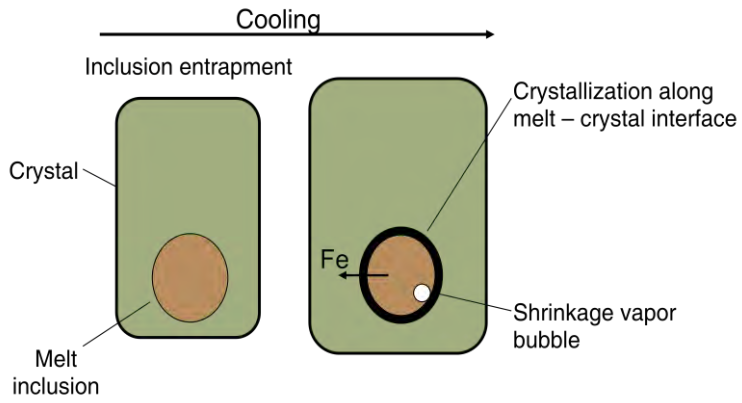


**Fig. 7.2** – Sketch of post-entrapment modifications of Melt inclusions (from Metrich and Wallace 2008).

A common way to check if the silicate-melt inclusions have retained their original composition is to bring the inclusions to homogenization temperatures followed by quenching (Frezzotti, 2001). If inclusions are properly homogenized, their composition should match the major element trends of the host magma.

One of the most important MI's application to the Etnean magmastic system is represented by data on major and trace elements. They allow i) reconstructions of the primary magmas composition and to establish the formation conditions of alkali basaltic melts in the mantle (Clocchiatti and Massare, 1985; Gurenko et al., 1991; Sobolev and Shimizu, 1993; Sobolev and Danyushevsky, 1994); ii) characterization of fractional crystallization processes (Metrich et al., 1991; Lu et al., 1992; Vaggelli et al., 1993) and iii) recognition of mixing phenomena, not observable in whole rock analyses (Anderson, 1976; Anderson and Wright, 1972; Hervig and Dunbar, 1992).

Olivine, represents the best mineralogical phase for the MI study because give us the compositions of primary melts and it is less prone to fracturing. Kamenetsky and Clocchiatti (1994 and 1996) found a range of compositions for Etnean magmas varying from tholeiitic, transitional to alkaline basalts (Fig. 7.3) that could not be related by fractional crystallization but only by partial melting of the mantle source. Melt inclusions from the most primitive olivine (Mt. Maletto alkali basalt) were unusually high in CaO and were very different from the primary melt calculated by Armienti et al. (1988) on the bases of Mt. Maletto whole rock composition (Kamenetsky and Clocchiatti, 1996). Probably this divergence is related to the failure of a complete homogenization of melt inclusions because of the high crystallization

pressure (2-6 Kbar) of the host olivine, indicated by the presence of high-density $CO_2$ fluid inclusions in olivine (Kamenetsky and Clocchiatti, 1996).

Recently, Maugeri (2014; Fig. 7.3) analyzed melt inclusions from Tholeiitic, Ellittico and Post-1971 Recent Mongibello olivine phenocrysts (lavas sampled in this thesis work). In the first period, only one evolved MI was obtained, whereas for Ellittico is shown a primitive composition that fits well with literature data and reconstructed primary magmas described in Fractionation modeling chapter. Melt inclusions from 2002-2003 eruption are differentiated and plot along the alkaline differentiation trend.

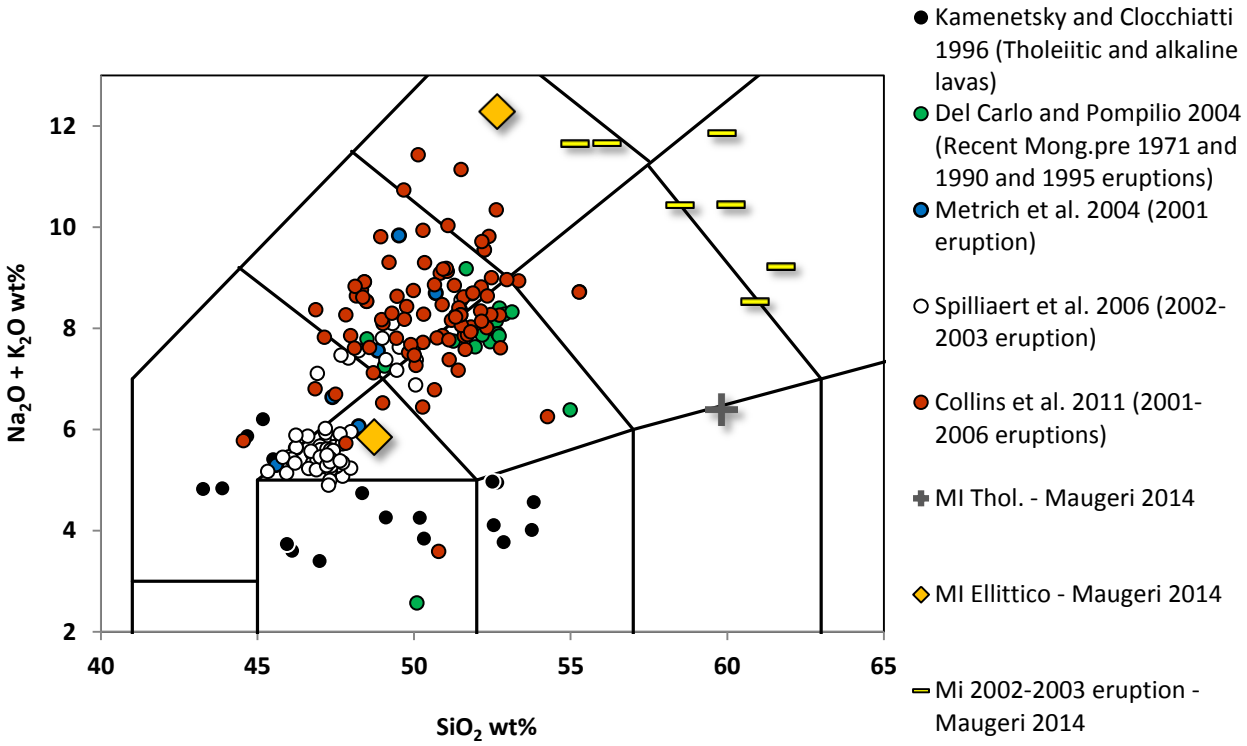


**Fig. 7.3** – TAS diagram of Etnean melt inclusions data from literature (Kamenetsky and Clocchiatti, 1996; Del Carlo and Pompilio, 2004; Metrich et al. 2004; Spilliaert et al. 2006; Collins et al. 2011, Maugeri 2014).

Another important outcome in studying MI is given by the measurements of their $H_2O$ and $CO_2$ content (Fig. 7.4). They allow the estimation of the magmatic volatile content prior and during crystallization processes and the pre-eruptive volatile evolution of the magma (Frezzotti, 2001). Furthermore The $H_2O$ concentration in olivine's MI is representative of the water content in primary magmas directly derived from the partial melting of their mantle source.

At Mt. Etna several authors analyzed the volatiles contents of MI entrapped in olivines (Métrich et al., 2004 and Spilliaert et al., 2006). Metrich et al. (2004) and Spilliaert et al. (2006) on recent erupted lavas (2001 and 2002-2003 eruptive events) obtained a value of 3.5 wt% of $H_2O$ and 4000 ppm of $CO_2$ for MI trapped at 400 and 100 MPa. These high values are normally related to metasomatized mantle source in subduction geodynamic settings (Fig. 7.4). A lot of authors (Tonarini et al., 2001; Schiano et al., 2001; Faccenna et al., 2011) hypothesize the interaction with metasomatizing fluids from the near eolian subduction slab. They relate such a high amount of water with the increase in $K_2O$ and low field rare earth elements observed especially in the post 1971 eruption products, although the subduction imprinting beneath Mt. Etna is still debated because seismic investigations indicate that the active Benioff zone is located beneath the Eolian Islands (Anderson and Jackson, 1987; Selvaggi and Chiarabba, 1995; Finetti, 2005). A possible explanation for the high $H_2O$ content in etnean magmas could be: i) Supercritical fluids carrying alkali Cl-complexes migrating from the deeper to the shallower portion of the pumbling system (Ferlito and Lanzafame, 2010; Ferlito et al., 2014) and ii) Involvement of volatile-bearing phases (amphibole and/or phlogopite) in the partial melting of an heterogeneous and variably enriched mantle source (Beccaluva et al., 1998; Viccaro and Cristofolini, 2008, Alesci et al., 2013). Arguments in support of this last model will be given by data on potential Etnean primary magmas in "Melt modeling" chapter.

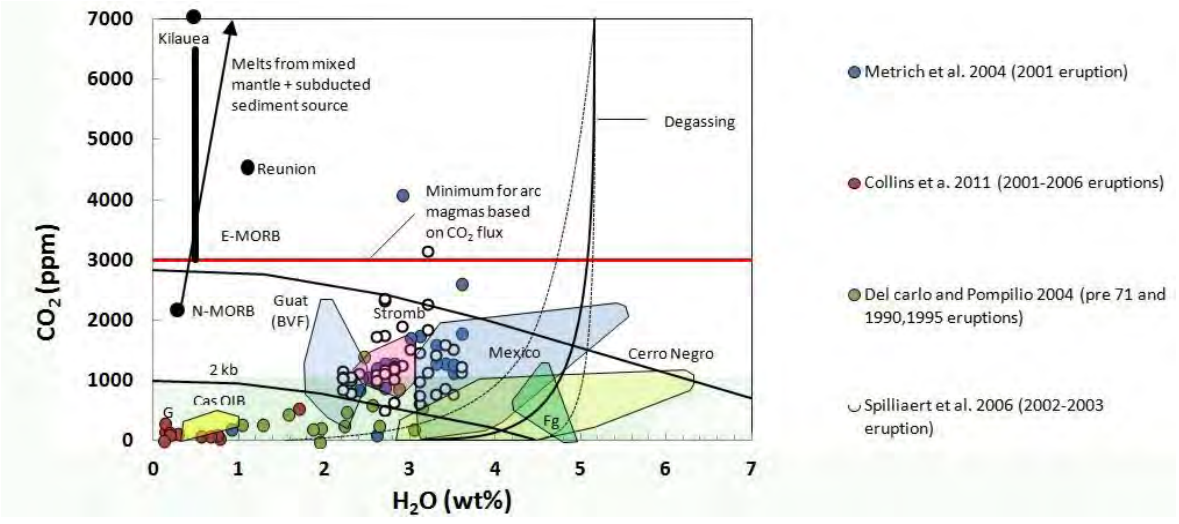


**Fig. 7.4** – $H_2O$ and $CO_2$ contents of Mt. Etna magmas (fields from Wallace, 2005).

| Author | Magma emission rate ($km^3/y^{-1}$) | $SO_2$ flux ($Mt/y^{-1}$) | $CO_2$ flux ($Mt/y^{-1}$) | Saturation limit $CO_2$ (MPa) | Saturation limit $SO_2$ (MPa) | Magmatic $CO_2$ (%) | Magmatic $SO_2$ (%) |
|---|---|---|---|---|---|---|---|
| **Allard et al. (1991)** | | | **13±3** | | | | |
| **Clocchiatti et al.(1992)** | | | | **700 Mpa** | | | |
| **Armienti (1994)** | | | | | | **0,70** | |
| **D'Alessandro (1995)** | | **2,04** | | | | | |
| **D'Alessandro (1997)** | **0,7** | | | | | | |
| **Neri e Rossi (2002)** | **0,00125** | | | | | | |
| **Stelling et al. (2008)** | | | | | **14 Mpa** | | |
| **Metrich et al. (2004)** | | | | | | | **0,3** |
| **Spilliaert et al. (2006)** | | | | | | | **0,3** |
| **Ferlito et al. (2014)** | **0,12** | | | | | | |
| **Azzaro and Neri(1992)** | **0,035** | | | | | | |
| **Barberi et al. (1993)** | | | | | | | |
| **Barsanti et al. (2009)** | | | | **600 Mpa** | | | |

**Table 2 -** Values of the parameters considered In magma emission rate calculations for Mt. Etna. Ferlito et al. (2014) calculated the magma emission rate starting from the $SO_2$ measured flux (Allard 1991) and $SO_2$ content at the saturation limit in the etnean feeding system (Metrich et al. 2004; Spilliaert et al. 2006). D'Alessandro 1997 followed the same approach by means of $CO_2$ measured flux (Allard et al. 1991) and $CO_2$ concentration at the saturation limit (Armienti et al. 1994). The vaules obtained from this two works are quite different, but both of them evidence the low ratio between erupted (Azzaro and Neri, 1992; Barberi et al., 1993; Calvari et al., 1993) and degassed (respectively 4 and 20 times) magma. Neri and Rossi (2002) calculated the emission rate on the base of Mt. Etna volcanic edifice volume (the value is 28 times underestimated).

# 8. PETROGRAPHY

Mt. Etna rocks show peculiar petrographic features for each evolutionary stage. The tholeiitic samples, massive and altered (especially ET1 and ET6), have ophitic to poorly porphyritic textures with P.I. (Porhyritic index vol%) ranging from 5 to 15% and vesiculation up to 10%. Phenocrysts include altered olivine (on average 63%), clinopyroxene (21%), plagioclase (18%) and Cr-spinel (13%) set in a microcrystalline groundmass (composed by plagioclase, clinopyroxene and Cr-spinel) (Table 3). Large-size olivine phenocrysts (millimetric in size; Fig. 8.1a) have Cr-spinel inclusions (Fig. 8.1b), resorbed cores and rims, Peccerillo (2005) and Tanguy et al. (1997) observed rare orthopyroxene inclusions. Clinopyroxene ranges from diopside to salite in composition (Tanguy et al., 1997; Corsaro and Cristofolini, 1997; Armienti et al., 2004; Corsaro and Pompilio, 2004). High dimension plagioclase phenocrysts (Fig. 8.1b) have labradoritic composition, whereas oligoclase to anorthoclase are observable as microlites in the matrix (Tanguy et al. 1997). All tholeiitic sections are markedly altered so it was not possible to study in details the textural features of plagioclase and clinopyroxenes.

Products and lavas from AAV show higher Porphiritic Index (on average P.I.= 35-40%) than tholeiites with abundant and large labradoritic plagioclase phenocrysts (75%) (from euhedral to subeuhedral) followed by clinopyroxene (13%), amphibole (9%), Ti-magnetite (7%), and olivine (6%) in a glassy to microcrystalline groundmass (Table 3). Using the textural plagioclase classification proposed by Viccaro et al. (2010) and Giacomoni et al. (2012) the following textures were recognized: Type 1 (oscillatory zoned), type 4 (sieved), type 5 (resorbed dusty rim) and type 6 (aligned melt inclusions). Sometimes types 1 and 4 or 5 and 6 are found in the same crystal. ASF1, ASF2, ASF3, ASF4 and CAR1, CAR2, CAR4 lavas contain large clinopyroxene phenocrysts (up to 1 cm) that is the most common mineralogical phase (30-35%). They are often zoned (from yellow Ti-augite to green Fe-diopside compositions) (Fig. 8.2a) and sometimes show rounded and resorbed rims. CAR4 has a peculiar phenocryst with Ti-magnetite inclusions at the core ad a clear resorbed rim with aligned melt inclusions (Fig. 8.2b). ASF1 shows zoned clinopyroxenes with “sieved” cores. In all other samples clinopyroxene is smaller and less abundant with Ti-magnetite inclusions and resorbed rims. Olivines in these samples are large in size with resorbed rims and Ti-magnetite inclusions (indicating its early crystallizzation). Plagioclase is smaller and the association between the texture 4 and 5 is quite common (Viccaro et al., 2010; Giacomoni et al., 2012).

All lavas show glomeroporphyritic aggregates fromed by clinopyroxene, olivine and Ti-magnetite phenocrysts (in order of decreasing abundance) (Fig. 8.4, table 3).

Amphibole, founded in ET34, ET35, ET36, ET37, ET40, ET41 and ET42 (up to 25-30%) is abundant (in some cases entirely resorbed), markedly pleochroic (with ά pale yellowish brown and γ dark brown) with high relief and straight extinction (Table 3). These optical characters conform to those of the Ti-rich calcic amphibole classified as kaersutite (Fig. 8.4). The markedly resorbed rim is due to the decreased volatile pressure during the eruptive activity testifying a disequilibrium with the melt. Olivine phenocrysts are rare (up to 15%), small and commonly displaying a brown-reddish iddingsite envelope (hydrothermal alteration). Sometimes clinopyrexene, olivine and Ti-magnetite form glomeroporphyritic aggregates.

Ellittico lavas are the most evolved terms emitted by Mt. Etna and show petrographic features similar to AAV ones. They have a porphyiritc texture (on average P.I.= 35-40%) with abundant plagioclase (on average 71%), olivine (15%), clinopyroxene (11%), and Ti-magnetite (5%) phenocrysts in a glassy to microcrystalline groundmass (Table 3). The Type 5 (resorbed dusty rim) plagioclase texture (Viccaro et al., 2010; Giacomoni et al., 2012) is the most common, followed by type 1 (oscillatory), 4 (sieved), 6 (aligned melt inclusions) and 7 (shallow tailed) (Fig. 8.5, 8.6a and 8.6b). Sometimes the oscillatory zoning is found associated with the 4, 5 or 6 types. Using the "Michel Levy" method and observing the in situ analyses on plagioclase phenocrysts it was possible to determinate the compositions ranging from andesine to bytownite (confirmed by in-situ analyses, Table 5). Olivine (up to centimetric in ET58) and clinopyroxene often are zoned and show Ti-magnetite inclusions (Fig. 8.6a and 8.6b).

Samples from Recent Mongibello have a more primitive character with lower P.I (on average 25-30%) and abundant olivine. Andesitic and labradoritic plagioclase is still the most common phase (on average 60%) that shows prevalently the "sieved" (type 4; Fig. 8.7a and 8.8a), "resorbed dusty rim" (type 5; Fig. 8.7b) and "shallow tailed" (type 7) textures (Viccaro et al., 2010; Giacomoni et al., 2012). All typologies are often mutually associated (1+4; 1+5; 4+6, Fig. 8.8b; 6+7 and 1+6+7) (Table 3). Clinopyroxene phenocrysts (22%), of medium-small size, show germinations (ET22, ET24), zoning (Fig. 8.9b) (hourglass zoning in ET23) and Ti-magnetite and olivine inclusions (Fig. 8.8a, 8.8b and 8.9b). Sometimes form clusters with olivine and Ti-magnetite (ET15, ET44). Olivine (up to 30%), of medium-small size, is frequently fractured and altered along rims and fractures (ET20); sometimes displays resorbed rims (ET22, ET25, ET27) and holds Ti-magnetite phenocrystals (5%) (Fig. 8.9a and 8.9b). Most of the samples have a prevalently glassy matrix (Table 3). Textural relationships

between phenocrysts indicate early crystallization of olivine, clinopyroxene, and Ti-magnetite, followed by massive crystallization of plagioclase.

The petrographic features of Recent Mongibello products are well described by a lot of authors (Cristofolini and Tranchina, 1980; Cristofolini et al., 1987; Viccaro et al., 2010, Giacomoni et al., 2012), especially for the eruptive events of the last three decades. This is related to the increase of the volcanic activity and the emission of K-alkaline terms since the 1971 eruption (Tanguy and Kieffer, 1977; Joron and Treuil, 1984; Tanguy et al., 1997; Clocchiatti et al., 2004). Ferlito et al. (2009) and Giacomoni et al. (2012) studied lavas from the 2002-2003 event (from both NE and S-Rift systems) founding different kind of magmas on the base of geochemical composition and textural features (as well as for the 2001 eruption; Viccaro et al., 2006; Corsaro et al., 2007; Ferlito et al., 2008). These samples are all porphyritic (P.I. from 25 to 40%) while along two NE-Rift fractures, during the 2002-2003 eruption, were emitted oligophyric products with P.I. ranging from 10 to 18%. A detailed textural and petrological study of plagioclase in lavas from the S and NE-Rifts indicates that chemicophysical conditions of the deep feeding system were analogous, while more superficially ascent dynamics were different (Giacomoni et al., 2012). The inhibition of plagioclase growth for the oligophyric NE- Rift products is related to the presence of $H_2O$-satured and undegassed magmas in a closed system. The presence of aligned melt inclusions, (type 6 texture) along the plagioclase phenocryts rims, represents the instant growth of this phase after the sudden loose of water probably in relation to decompression due to fracture opening. On the other hand, the porphyritc samples (prevalently along the S-Rift) in association with the type 5 plagioclase texture (resorbed dusty rims), indicate frequent primitive magma imputs (where clinopyroxene prevails on the other phases; Alesci, 2010) in $H_2O$-undersatured conditions that are the most common for the shallow etnean feeding system (Giacomoni et al., 2012).

If the study of plagioclase textures is useful to constrain the shallow feeding system conditions, clinopyroxene can represent an important tool to obtain information on the deeper part of the Etnean magmatic system. Plagioclase is very susceptible to temperature, pressure and volatile content but its stability field, restricted to low pressure conditions, limits its use to the first 12 km of deepness. Clinopyroxene that crystallizes earlier can provide important information on deeper processes and magmatic parameters. A preliminary study by Fini (2013) investigated the textural features of clinopyroxenes from the four Etnean evolutionary periods.

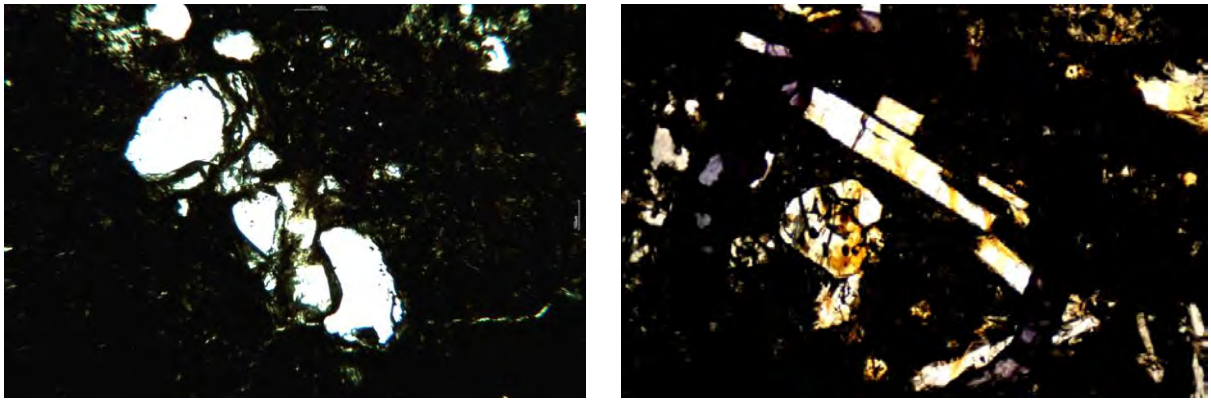

**Fig. 8.1** – a) Olivine phenocryst from ET4 (Tholeiite); b) Olivine and plagioclase phenocryts from ET9 (Tholeiite).

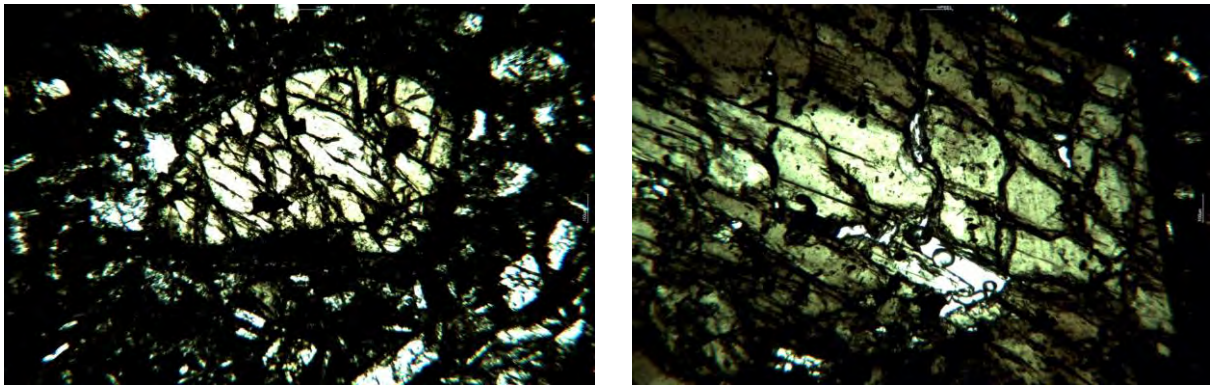

**Fig. 8.2** – a) Cpx with resorbed rim in CAR4 (AAV) and b) Zoned Cpx in CAR4 (AAV).

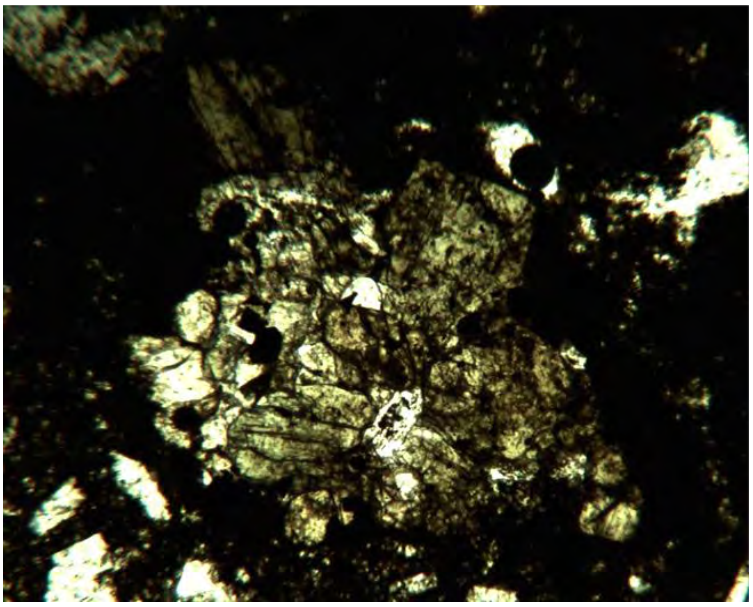

**Fig. 8.3** – Glomeroporphyritic aggregate of Cpx, Ol and Ti-Mt (ET39, AAV).

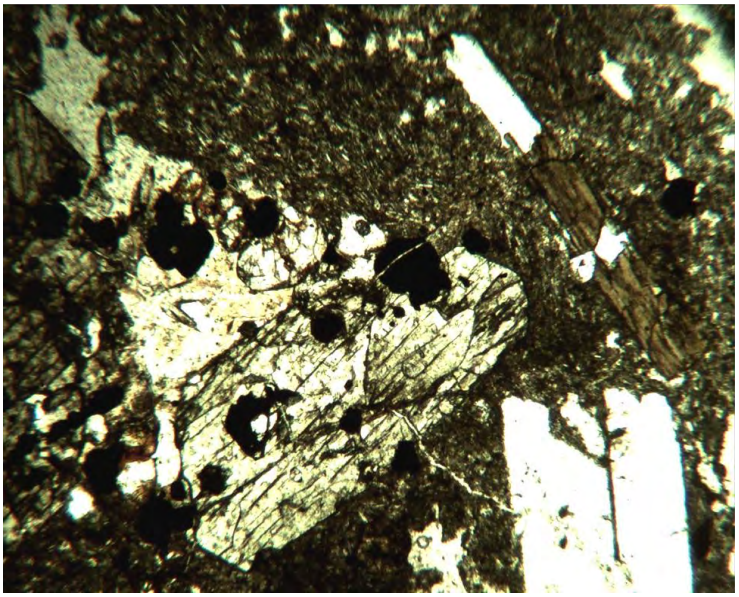

**Fig. 8.4** – Kaersutite phenocryst from ET36 (AAV).

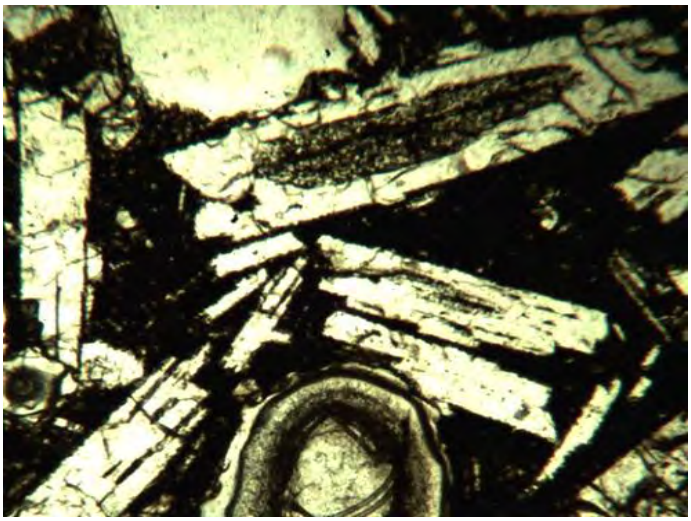

**Fig. 8.5** – Plagioclases phenocrysts from ET52 (Ellittico).

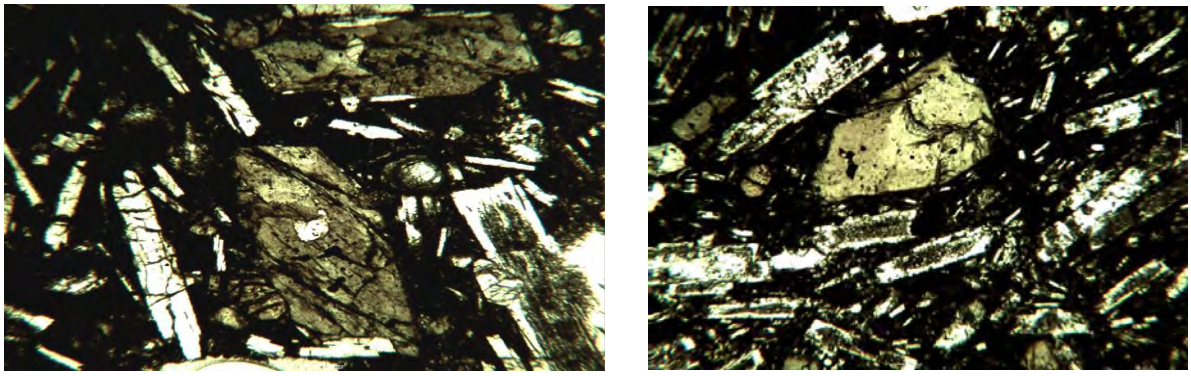

**Fig. 8.6** –Cpx ad plg phenocrysts from a) ET 52 (Ellittico) and b) ET59 (Ellittico).

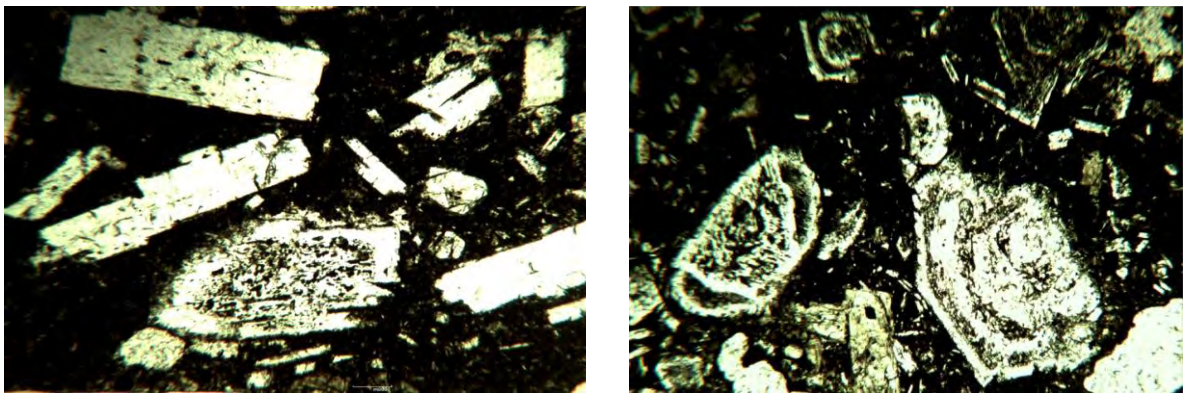

**Fig. 8.7** – a) Plg type 4 (ET15, Recent Mong. Pre-1971) and b) Plg type 5 (ET44, Recent Mong. Post-1971)

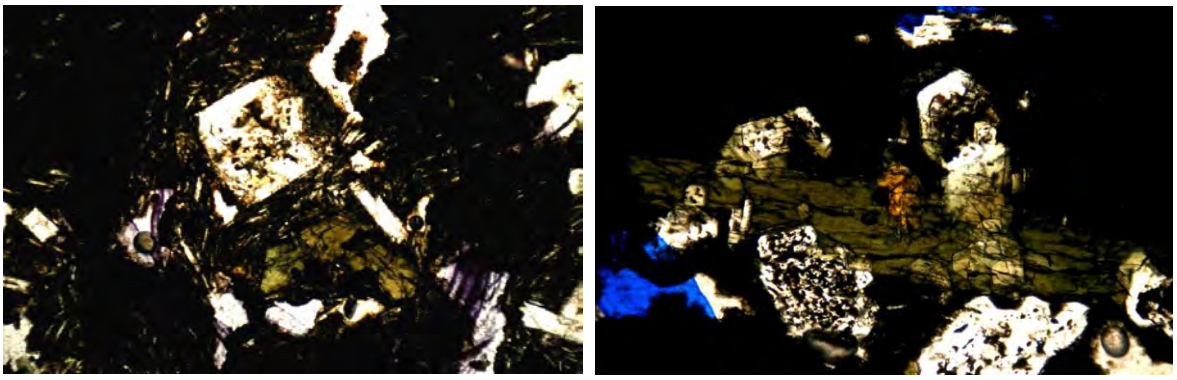

**Fig. 8.8** – a) Plg type 2 and 4, cpx and Ti-mt (ET63, Recent Mong. Pre-1971) and b) Plg 4+6 type and cpx (ET24, Recent Mong. Pre-1971)

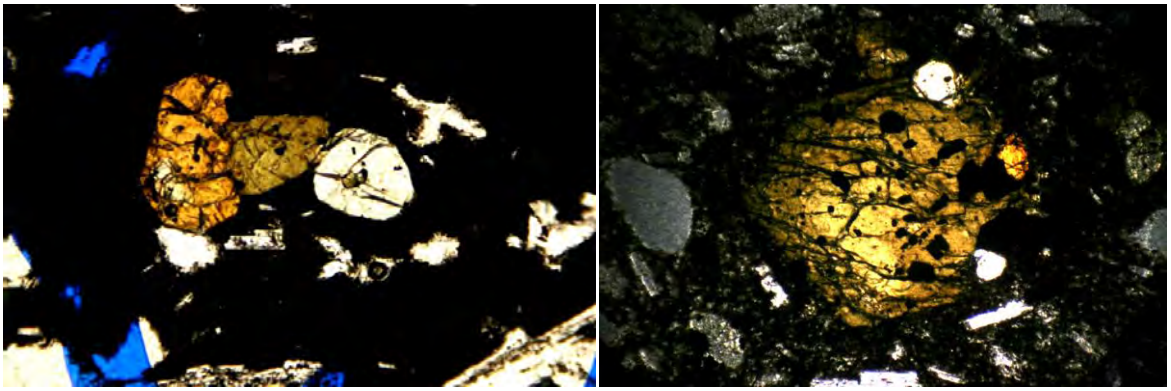

**Fig. 8.9** – a) ET24 (Recent Mong. Pre-1971) and b) ET18 (Recent Mong. Pre-1971)

**Table 3 - Petrographic features of sampled rocks**

| Sample | Period | Mg# | P.I. % | Mineralogical paragenesis | | | | | Plg textures | Plg composition |
|---|---|---|---|---|---|---|---|---|---|---|
| | | | | Plg (%) | Cpx (%) | Ol (%) | Sp (%) | Amph (%) | | |
| ET1 | Thol | 67.93 | 10-15 | 20 | 30 | 50 | 10 | - | - | - |
| ET4 | Thol | 72.38 | 10-15 | 10 | 15 | 65 | 10 | - | - | - |
| ET5 | Thol | 66.72 | 10-15 | - | - | 90 | 10 | - | - | - |
| ET6 | Thol | 68.31 | 10-15 | 10 | - | 80 | 10 | - | - | - |
| ET9 | Thol | 52.36 | 5-10 | 20 | 30 | 40 | 10 | - | - | - |
| ET10 | Thol | 52.45 | 5-10 | - | 10 | 70 | 20 | - | - | - |
| ET14 | Thol | 55.82 | 10-15 | 30 | - | 55 | 15 | - | - | - |
| ET7 | AAV | 29.08 | 5-10 | 90 | - | - | 10 | - | - | Labradorite |
| ET8 | AAV | 30.47 | 5-10 | 90 | - | - | 10 | - | - | Labradorite |
| ET17 | AAV | 46.34 | 30-35 | 55 | 25 | 10 | 10 | - | - | - |
| ET19 | AAV | 40.62 | 35-45 | 80 | 5 | 5 | 10 | - | 4 and 1+4 | - |
| ET32 | AAV | 45.50 | 25-35 | 80 | 10 | 3 | 7 | - | 1 and 6 | Bytownite |
| ET33 | AAV | 49.37 | 35 | 80 | 10 | 3 | 7 | - | - | - |
| ET34 | AAV | 39.44 | 35-45 | 80 | 5 | 5 | 5 | 5 | 1, 5, 7 and 1+5 | - |
| ET35 | AAV | 39.33 | 35 | 75 | 15 | - | 5 | 5 | - | - |
| ET36 | AAV | 34.27 | 35-40 | 60 | 20 | 10 | 5 | 5 | - | - |
| ET37 | AAV | 42.81 | 35-40 | 80 | 5 | - | 10 | 5 | - | - |
| ET38 | AAV | 46.34 | 35-40 | 80 | 15 | 2 | 3 | - | 1, 5, 6, 1+5 and 1+5+6 | - |
| ET39 | AAV | 54.36 | 35-40 | 60 | 30 | 5 | 5 | - | - | - |
| ET40 | AAV | 50.21 | 35-40 | 65 | 15 | - | 5 | 15 | 1, 6 and 1+6 | - |
| ET41 | AAV | 50.67 | 30-35 | 80 | 10 | - | 5 | 5 | - | - |
| ET42 | AAV | 48.78 | 30-35 | 65 | 5 | - | 5 | 25 | - | - |
| ET43 | AAV | 55.26 | 30-35 | 85 | 10 | - | 5 | - | - | - |
| ET46 | AAV | 47.68 | 45 | 80 | 15 | - | 5 | - | 2 and 5 | - |
| ET47 | AAV | 47.35 | 40-45 | 75 | 15 | 5 | 5 | - | - | - |
| ET48 | AAV | 54.62 | 40-45 | 80 | 15 | - | 5 | - | - | - |
| ET49 | AAV | 50.18 | 40-45 | 80 | 15 | - | 5 | - | - | - |

| Sample | Period | Mg# | P.I. % | Mineralogical paragenesis | | | | | Plg textures | Plg compositions |
|---|---|---|---|---|---|---|---|---|---|---|
| | | | | Plg (%) | Cpx (%) | Ol (%) | Sp (%) | Amph (%) | | |
| ASF1 | AAV | 55.19 | 30-35 | 45 | 30 | 20 | 5 | - | - | - |
| ASF2 | AAV | 53.90 | 30-35 | 45 | 30 | 20 | 5 | - | - | - |
| ASF3 | AAV | 55.70 | 30-35 | 45 | 30 | 20 | 5 | - | - | - |
| ASF4 | AAV | 58.27 | 30-35 | 45 | 30 | 20 | 5 | - | 1 and 4+5 | - |
| CAR1 | AAV | 49.18 | 30-35 | 50 | 35 | 10 | 5 | - | 1, 4, 6 and 4+5 | Andesine |
| CAR2 | AAV | 50.28 | 30-35 | 45 | 30 | 20 | 5 | - | 4 and 4+5 | - |
| CAR4 | AAV | 52.46 | 30-35 | 50 | 25 | 20 | 5 | - | - | - |
| ET12 | Ellittico | 42.64 | 30-40 | 70 | 10 | 15 | 5 | - | 1, 4, 7 and 1+4 | Andesine |
| ET13 | Ellittico | 36.21 | 40 | 90 | - | 5 | 5 | - | 4 and 7 | Labradorite |
| ET28 | Ellittico | 51.20 | 35 | 60 | 20 | 15 | 5 | - | - | - |
| ET31 | Ellittico | 28.47 | 30-35 | 85 | 5 | 3 | 7 | - | - | - |
| ET50 | Ellittico | 50.47 | 50 | 70 | 10 | 15 | 5 | - | - | - |
| ET51 | Ellittico | 51.17 | 40-50 | 50 | 25 | 20 | 5 | - | 2, 3 and 7 | - |
| ET52 | Ellittico | 50.93 | 40-50 | 60 | 10 | 25 | 5 | - | 2, 3 and 7 | - |
| ET53 | Ellittico | 47.56 | 35-40 | 75 | 10 | 10 | 5 | - | 5 and 6 | - |
| ET54 | Ellittico | 48.13 | 35-40 | 70 | 10 | 15 | 5 | - | 4, 5 and 7 | - |
| ET55 | Ellittico | 48.60 | 35-40 | 65 | 10 | 20 | 5 | - | 5 and 6 | - |
| ET56 | Ellittico | 47.53 | 35-40 | 70 | 10 | 15 | 5 | - | 5 and 6 | - |
| ET57 | Ellittico | 47.53 | 35-40 | 75 | 10 | 10 | 5 | - | 1 and 5 | - |
| ET58 | Ellittico | 55.36 | 35-40 | 60 | 15 | 20 | 5 | - | - | - |
| ET59 | Ellittico | 51.37 | 35-40 | 60 | 15 | 20 | 5 | - | - | - |
| ET60 | Ellittico | 44.39 | 10-15 | 60 | 10 | 25 | 5 | - | 1, 4, 5, 6, 1+5 and 1+6 | Andesine |
| ET61 | Ellittico | 29.94 | 10-15 | 90 | 5 | - | 5 | - | 1, 3 and 4 | - |
| ET62 | Ellittico | 38.94 | 5-10 | 85 | - | 10 | 5 | - | 2, 4, 5 and 6 | Labradorite |
| ET63 | Ellittico | 31.62 | 10 | 90 | 5 | - | 5 | - | - | - |
| ET2 | Recent Mong. | 47.38 | 25-35 | 60 | 25 | 10 | 5 | - | 3, 4 and 7 | Andesine |
| ET3 | Recent Mong. | 48.46 | 25-35 | 60 | 25 | 10 | 5 | - | 3 | Andesine |
| ET11 | Recent Mong. | 38.35 | 25-35 | 50 | 30 | 15 | 5 | - | - | - |
| ET15 | Recent Mong. | 43.22 | 35-40 | 60 | 20 | 15 | 5 | - | 4, 5, 6 and 7 | Labradorite |

| Sample | Period | Mg# | P.I. % | Mineralogical paragenesis | | | | | Plg textures | Plg compositions |
|---|---|---|---|---|---|---|---|---|---|---|
| | | | | Plg (%) | Cpx (%) | Ol (%) | Sp (%) | Amph (%) | | |
| ET16 | Recent Mong. | 49.47 | 35-40 | 55 | 30 | 10 | 5 | - | - | - |
| ET18 | Recent Mong. | 48.49 | 35-40 | 60 | 20 | 15 | 5 | - | - | - |
| ET20 | Recent Mong. | 43.13 | 25-30 | 55 | 10 | 30 | 5 | - | 4 and 7 | Andesina |
| ET21 | Recent Mong. | 47.85 | 25-30 | 50 | 25 | 20 | 5 | - | - | - |
| ET22 | Recent Mong. | 47.53 | 30-35 | 50 | 30 | 15 | 5 | - | 2, 5, 6, 7, 5+7 and 6+7 | Labradorite |
| ET23 | Recent Mong. | 47.88 | 35 | 70 | 10 | 15 | 5 | - | 4 and 7 | - |
| ET24 | Recent Mong. | 35.89 | 35-40 | 75 | 15 | 5 | 5 | - | 1, 4, 5 and 1+6+7 | - |
| ET25 | Recent Mong. | 41.37 | 25 | 80 | 5 | 5 | 10 | - | 4 and 7 | - |
| ET26 | Recent Mong. | 48.15 | 25-30 | 45 | 45 | 5 | 5 | - | - | - |
| ET27 | Recent Mong. | 38.36 | 25-30 | 75 | 5 | 15 | 5 | - | 2, 4, 6 and 7 | Labradorite |
| ET29 | Recent Mong. | 49.22 | 35-40 | 45 | 20 | 30 | 5 | - | 1, 4 and 1+4 | Labradorite |
| ET30 | Recent Mong. | 37.40 | 35 | 90 | 5 | 3 | 2 | - | 1, 4, 5, 6, 1+5 and 4+6 | - |
| ET44 | Recent Mong. | 47.47 | 30 | 60 | 25 | 10 | 5 | - | 1, 2, 5 and 1+5 | - |
| ET45 | Recent Mong. | 49.61 | 30 | 35 | 40 | 20 | 5 | - | - | - |
| ET64 | Recent Mong. | 39.22 | - | - | - | - | - | - | - | - |

# 9. WHOLE-ROCK GEOCHEMISTRY

## 9.1 MAJOR ELEMENTS

All lavas sampled in this work were plotted together with published data for major elements in a Total Alkali Silica diagram (Fig. 9.1.1) (Appendix A). Two main trends are observable, a first one tholeiitic ($SiO_2$ ranging from 47.5 to 53 wt% and alkalies from 2.43 to 4.87 wt%) and a second one alkaline that comprises AAV, Ellittico and Recent Mongibello products. Lavas from Recent Mongibello are the most primitive and are classified as hawaiites and mugearites. During the Ellittico and AAV periods the most evolved products were emitted because magma was ponded in shallow reservoirs and had given rise to evolved benmoreites and trachytes. AAV range in silica from 47.5 to 60.5 wt% and in $K_2O+Na_2O$ from 4.25 to 9.51 wt%. Ellittico products vary between 47.9 and 64.5 wt% in $SiO_2$ and 2.97 and 10.8 wt% in alkalies. Recent Mongibello lavas have less $SiO_2$ (from 47.4 to 55.1 wt%) and about the same content in alkalies (3.87 – 9.40 wt%) of earlier phases.

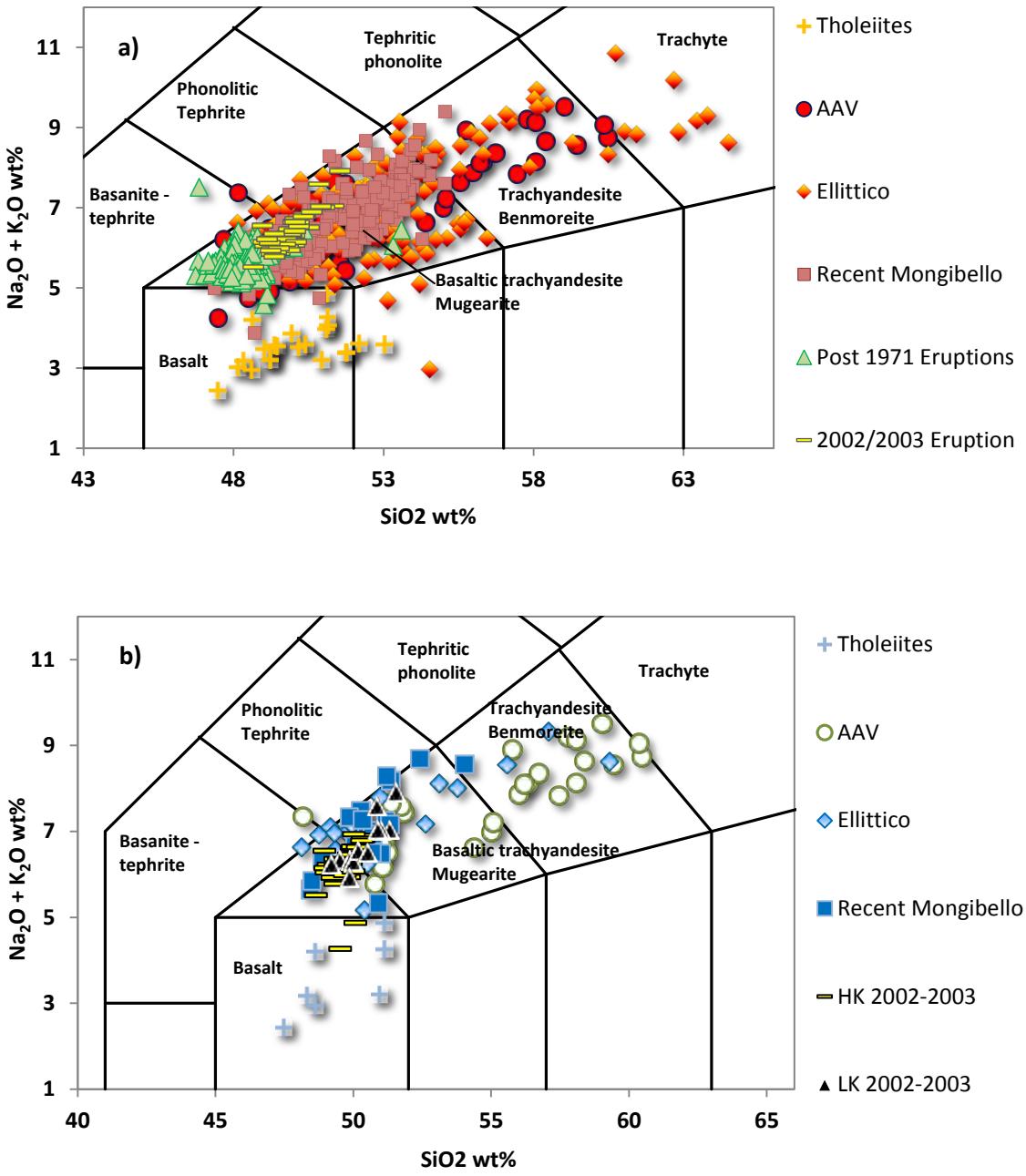


**Fig. 9.1.1** - Total Alkali Silica of Mt. Etna products (le Maitre, 1989); Figure a) literature data and b) analyzed samples; HK (high content in K) and LK (low content in K) products from Giacomoni et al. (2012).

$Na_2O$ vs $K_2O$ and $K_2O/Na_2O$ vs $K_2O$ diagrams point out the presence of two distinct alkaline trends, a first one sodic and second one potassic. Samples from AAV period are among the most evolved terms but always show a sodium affinity (Fig. 9.1.2a and 9.1.2b). In the last decade a lot of authors (Gasperini et al. 2002; Schiano et al. 2001; Tonarini et al. 2001;

Armienti et al. 2004; Clocchiatti et al. 2004; Viccaro and Cristofolini 2008) observed a shift from sodic (Hawaiites, mugearites, benmorites and trachytes) to potassic alkaline terms starting from the 1971 eruption. This is shown in Fig. 9.1.2a and 9.1.2b, where most of the post-1971 products fall in the K-alkaline series (from 1.45 to 2.27 wt% in K) (Trachybasalts and basaltic trachyandesites). Further, Fig. 9.1.3a and 9.1.3b, evidence this distinction within more recent lavas that have higher contents in K (up to 1% in range) than ancient ones at comparable degree of evolution (represented by $SiO_2$ wt%). Many authors tried to justify this K-enrichment (that could not be related to simple crystal fractionation) suggesting several models that failed to explain the phenomenon satisfactorily. However several lavas from, Ellittico and Pre-1971 Recent Mongibello are classified as potassic terms (Fig. 9.1.2a and b) indicating that this shifting is not prerogative of the last 40 years (Ferlito and Lanzafame 2010). Plotting only Ellittico (Fig. 9.1.4a) or Recent Mongibello lavas (Fig. 9.1.4b) in a $K_2O$ – $Si_2O$ wt% diagram it is possible to distinguish a common fractionation trend with several impulses towards potassium rich terms, as already noticed by Ferlito and Lanzafame (2010). They started from the assumption that the K-enrichment during differentiation follows this formula $\Delta K_2O/\Delta SiO_2$ where $\Delta$ is the difference between the maximum and minimum values for potassium and silica respectively. In the computed differentiation $\Delta K_2O/\Delta SiO_2$ have to be <0.2. Significantly, the K increment for most of the rocks of Mongibello follows a characteristic low K trend ($K_2O$ max 1.9 wt%; $\Delta K_2O/\Delta SiO_2$~0.1–0.2, Fig. 9.1.4a and 9.1.4b), driven by crystal fractionation of mafic phases. However, a good percentage of the recent Mongibello and Ellittico rocks display a high K trend ($K_2O$ max 2.9 wt%; $\Delta K_2O/\Delta SiO_2$~0.4–0.6, Fig. 4a and b), too high to be explained by simple fractional crystallization. In literature a lot of analyses on post-1971 products are statistically outnumbered with respect to the three more ancient periods. This could be the reason for the apparent lack of K-alkaline products in the previous Etnean volcanological stages.

In chapter "Melting modelling" an hypothesis to explain the cyclic shift to K-terms in the emitted lavas will be proposed.

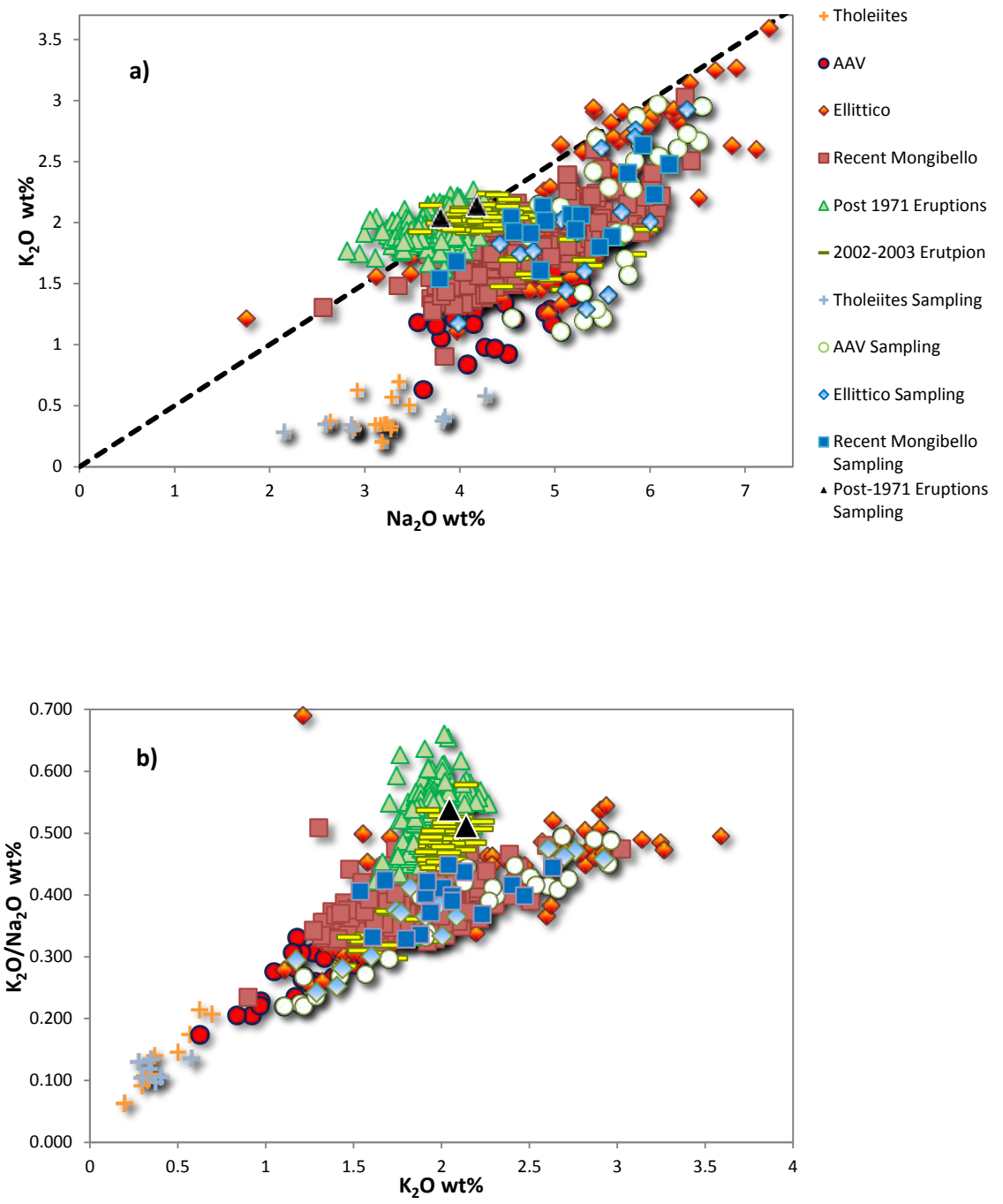


**Fig. 9.1.2** - a) $K_2O$ vs $Na_2O$ and b) $K_2O/Na_2O$ – $K_2O$ Archer Diagram for Mt. Etna products. Legend as in fig. 9.1.1.

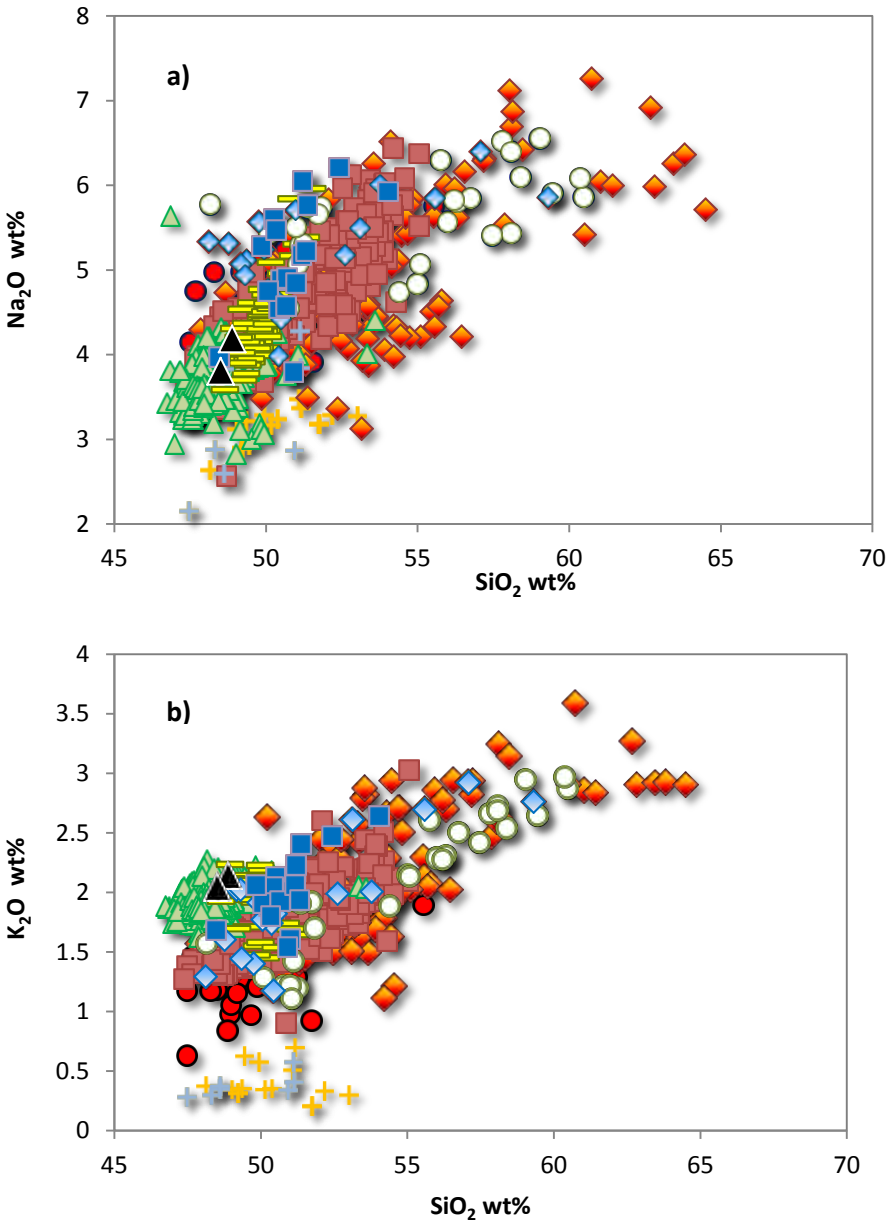


**Fig. 9.1.3** - a) $Na_2O$ vs $SiO_2$ and b) $K_2O$ vs $SiO_2$ diagrams. Symbols as in fig. 9.1.1.

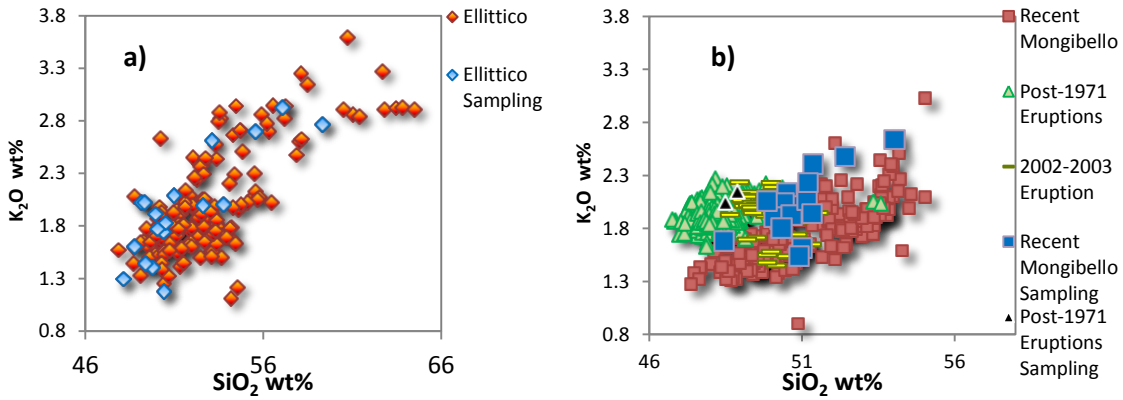


**Fig.9.1.4** - $K_2O$ vs $SiO_2$ diagram for a) Ellittico and b) Recent Mongibello.

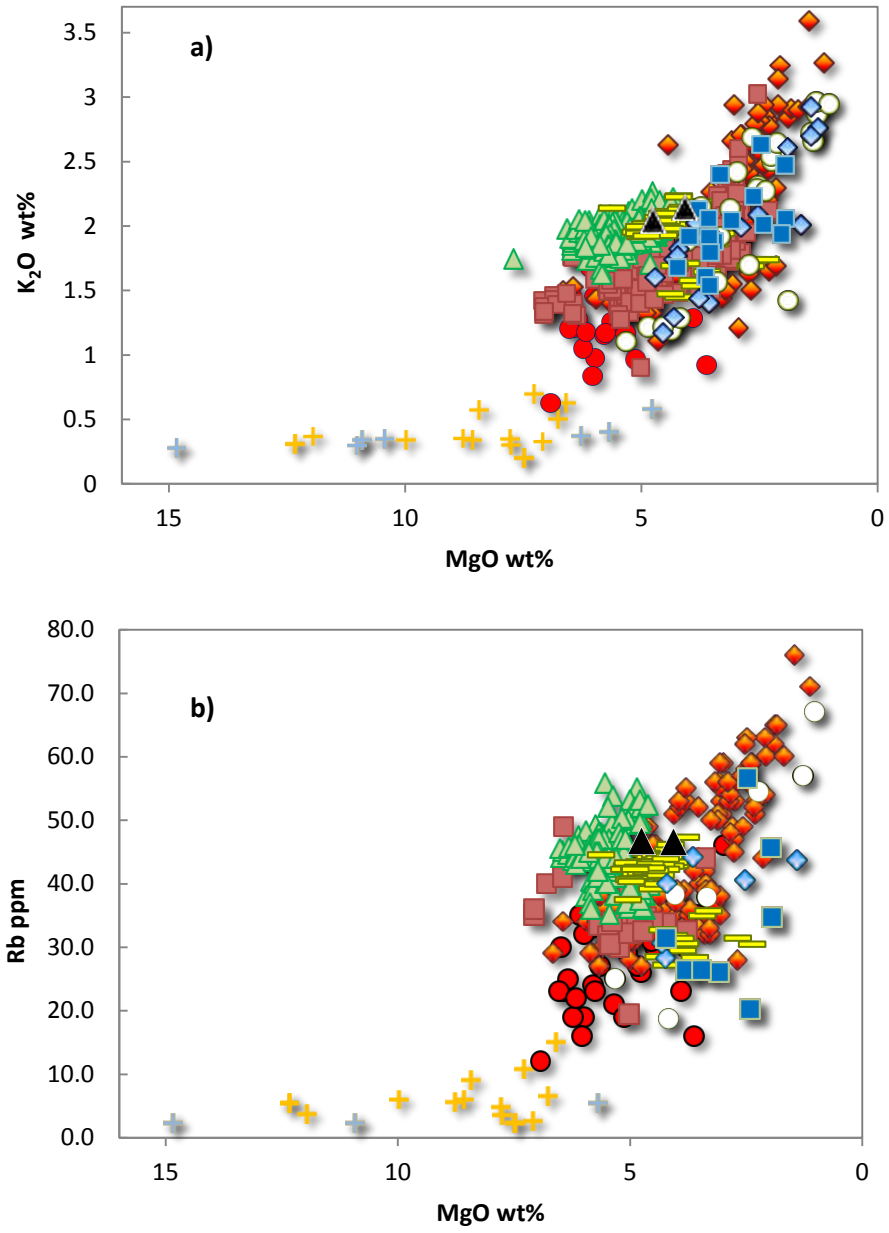


**Fig. 9.1.5** - MgO vs $K_2O$, and Rb (ppm) variation siagrams (Legend as in fig. 9.1.1)

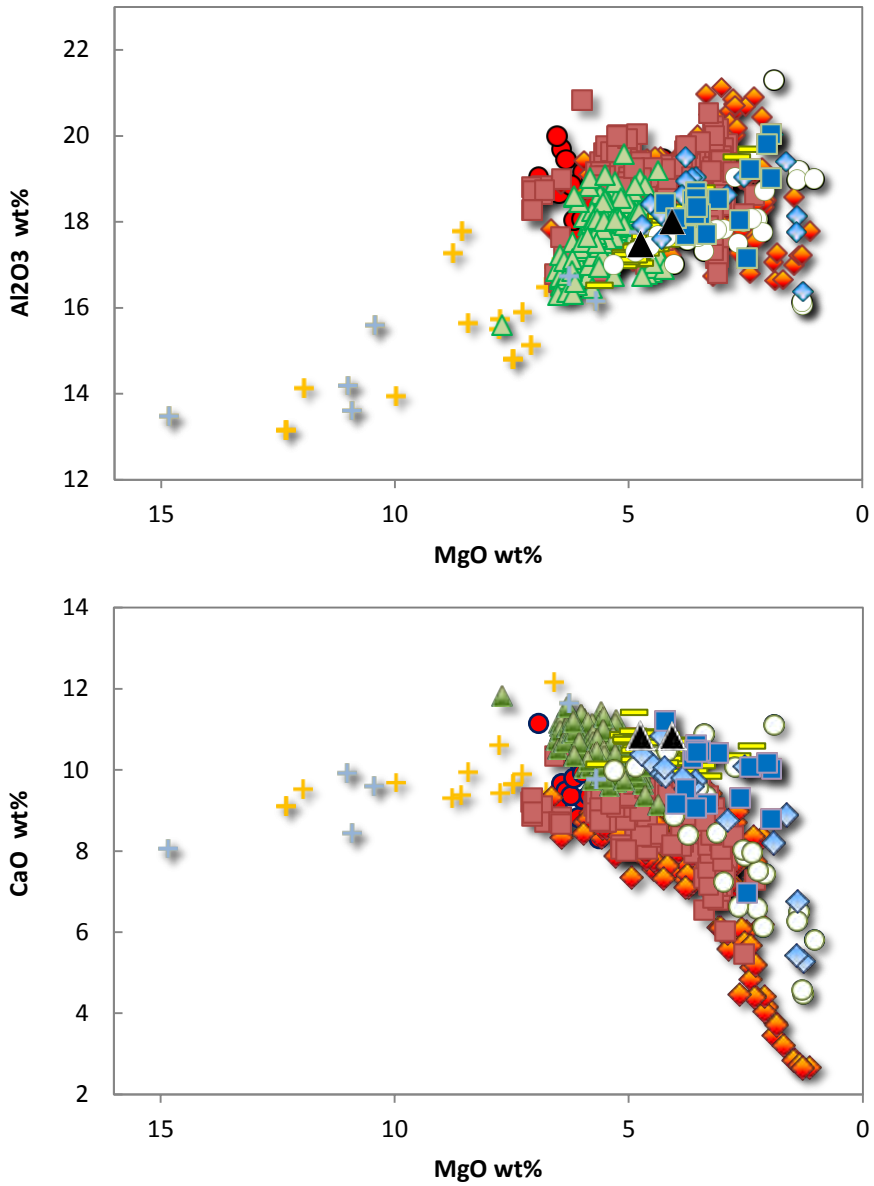


**Fig. 9.1.6** – MgO vs $Al_2O_3$ and CaO variation diagrams (Legend as in fig. 9.1.1)

MgO wt% tends to increase with time from Ellittico to the most recent products (Fig. 9.1.5 and 9.1.6), a shift that has been noticed in recent erupted lava by Metrich et al. (2004), Ferlito et al. (2010), Ferlito and Lanzafame (2010) and Giacomoni et al. (2012) and related to the rising of new primitive magmas into the Mt. Etna shallow feeding system. In the variation diagram MgO wt% was preferred respect to $SiO_2$ or Mg# as differentiation index because it displays better the differences for each evolutionary stage.

In Fig. 9.1.5 and 9.1.6, MgO wt% compared to $K_2O$, $Al_2O_3$ and CaO wt% and Rb (ppm) show again the clear distinction between the tholeiitic and alkaline Etnean products. The first ones

are more primitive with a MgO content varying from 4.77 to 14.8 wt% and with constant K-concentrations. The alkaline suites display primitive magmas (up to 7.70 wt% in MgO) with different contents in $K_2O$ wt% that increase from AAV to Ellittico and Recent Mongibello lavas. The differentiated terms are instead widely enriched in K, without the presence of an evident trend from ancient to recent products. For alumina a linear trend without big differences in the three alkaline periods can be observed. AAV analyses from literature are less differentiated than lavas from this work and, post-1971 products seem the most primitive of the alkaline suites (Fig. 9.1.5 and 9.1.6). MgO vs CaO wt% displays a great depletion in Calcium for Ellittico and several AAV rocks that can be related to the massive and polybaric crystallization of plagioclase in the open conduit system (Ferlito and Lanzafame, 2010 and reference therein) (Fig. 9.1.6). In Fig. 9.1.6 the higher CaO and lower $Al_2O_3$ contents for Post-1971 products with comparable MgO values is evident. This could suggest the participation of a greater quantitative of clinopyroxene in the partial melting of the Etnean mantle source. This object will be discussed In the "Fractionation modeling" chapter where most primitive etnean analyses will be compared to melt inclusions data and to "reconstructed primary magmas" for each period.

$Na_2O$ wt% in Fig. 9.1.7 shows a trend similar to the $K_2O$ vs $SiO_2$ diagram with a marked enrichment towards most evolved lavas. However, for the highest MgO wt% values, a decreasing in $Na_2O$ content from AAV to Ellittico and Recent Mongibello (pre- and post-1971) is evident with a specular behavior respect to $K_2O$ wt% (Fig. 9.1.3b and 9.1.5). FeO and $TiO_2$ wt% (Fig. 9.1.7), decrease with the proceed of the differentiation and subsequently the crystallization of Ti-magnetite that is the mineralogical phase (for Etnean paragenesis) with the highest concentrations in iron and titanium. A little difference is represented by the more marked variation of FeO respect to $TiO_2$ that decrease more slightly towards the evolved products (from both AAV and Ellittico phases).

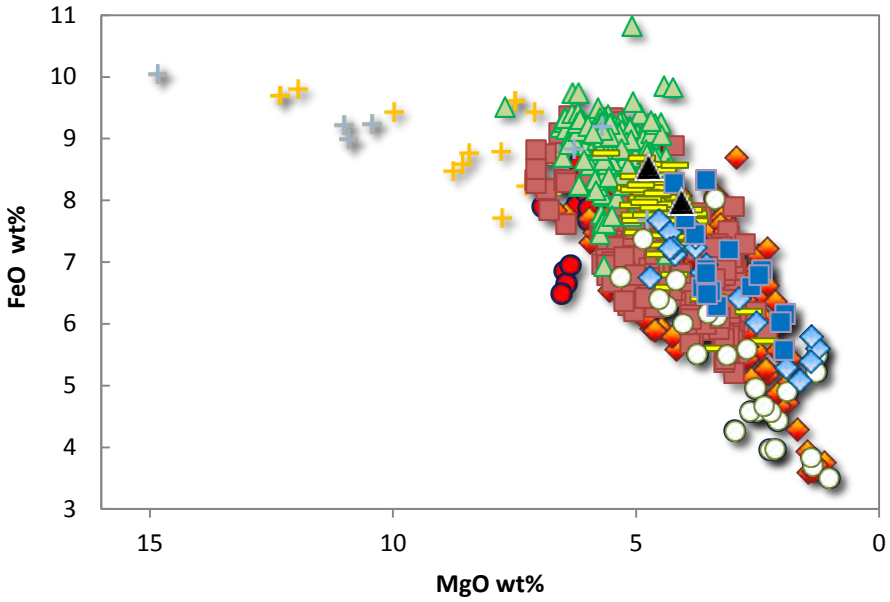
11
10
9
8
7
6
5
4
3
FeO wt%
15
10
5
0
MgO wt%

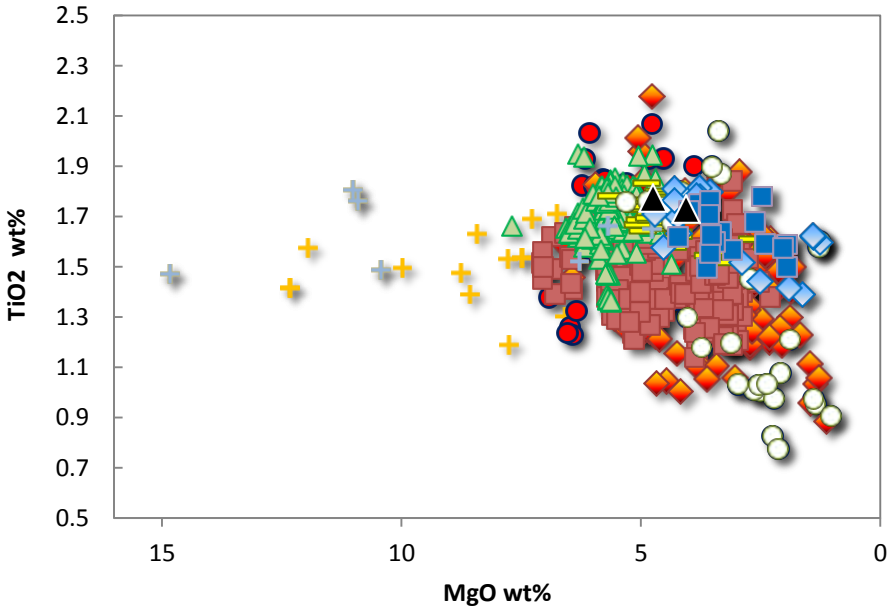
2.5
2.3
2.1
1.9
1.7
1.5
1.3
1.1
0.9
0.7
0.5
TiO2 wt%
15
10
5
0
MgO wt%

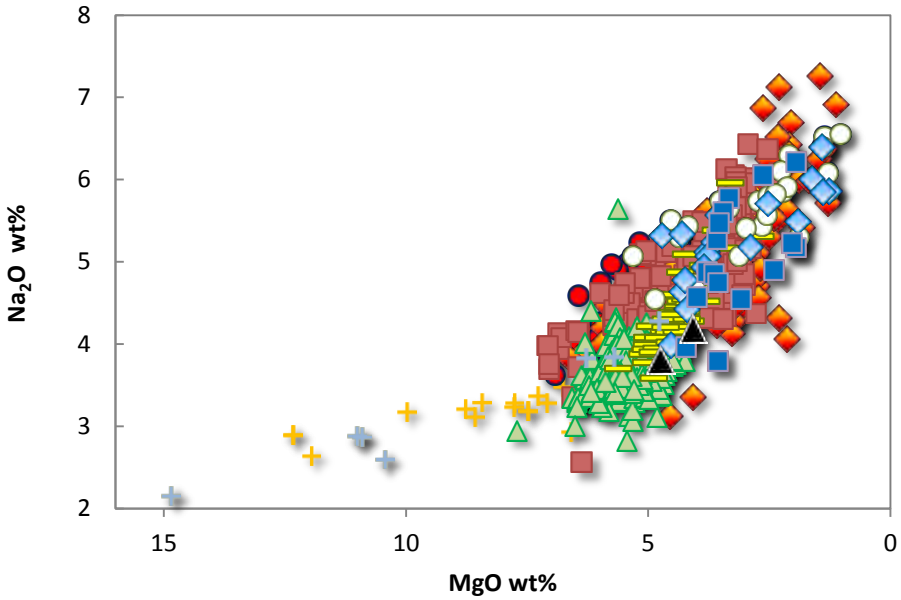


**Fig. 9.1.7** – MgO vs FeO, $TiO_2$ and $Na_2O$ variation diagrams (Legend as in fig. 9.1.1)

## 9.2 TRACE ELEMENTS

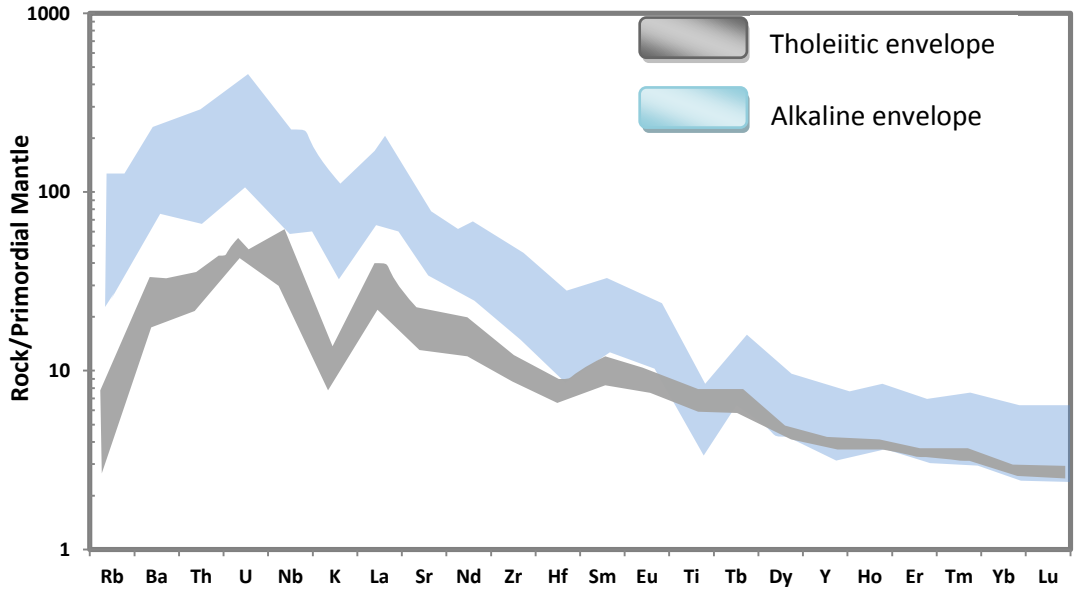


**Fig. 9.2.1** – Incompatible element patterns of sampled etnean products normalized to primordial mantle (Sun and McDonough, 1989)

Incompatible element patterns normalized to primordial mantle compositions for mafic rocks (Sun and McDonough, 1989) are very different from other volcanites of the central-southern Italy (Peccerillo, 2005).

In Fig. 9.2.1, envelopes of the analyzed samples (representative rocks of each magmatic suite) for both tholeiitic (grey area) and alkaline types (blue area) show a marked upward convexity with positive spikes for Th, U and La and negative in Rb, K, Hf, Ti and Y. The depletion in Hf and Ti is not so frequent in Na-alkaline magmas from intraplate geodynamic settings (Wilson 1989). These anomalies are typical of the Etnean analyses present in literature, but in Fig. 9.2.3 a comparison between pre- and post-1971 lavas shows how the K-alkaline terms are instead enriched in Rb, K and other LILE.

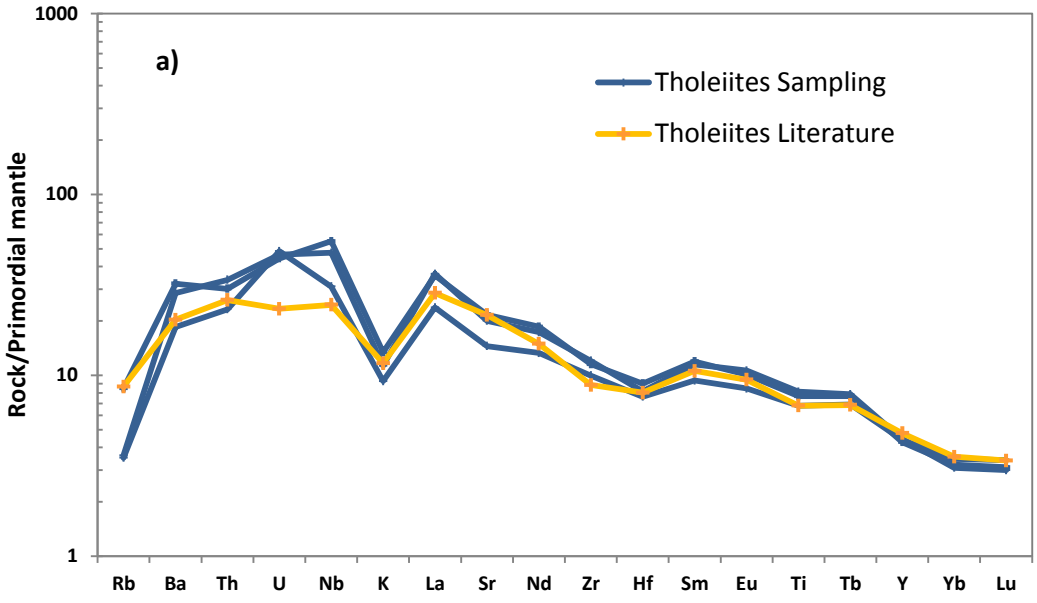


**Fig. 9.2.2a** – Comparison between tholeiitic rocks incompatible elements.

Tholeiites from literature and (Fig. 9.2.2a) sampling lavas match well in similar trends and show the previous mentioned features but with less marked negative anomalies in Hf and Ti and a positive one in Nb. Spider diagrams from Armienti et al. (2004) have Th and U absolute values lower than those of the lavas of the present work.

AAV patterns, typical of a Na-alkaline intraplate magmatism, are more fractionated for sampled lavas respect to the bibliographic ones (Fig. 9.2.2b). These trends reflect what shown in variation diagrams with literature data more primitive than this work products.

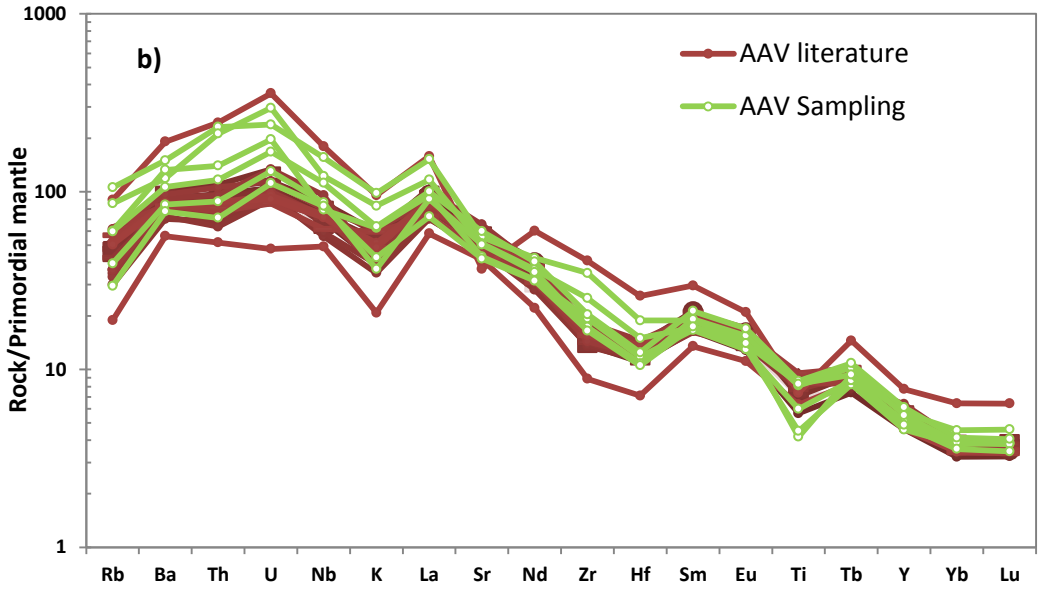


**Fig. 9.2.2b** – Comparison between AAV rocks incompatible elements.

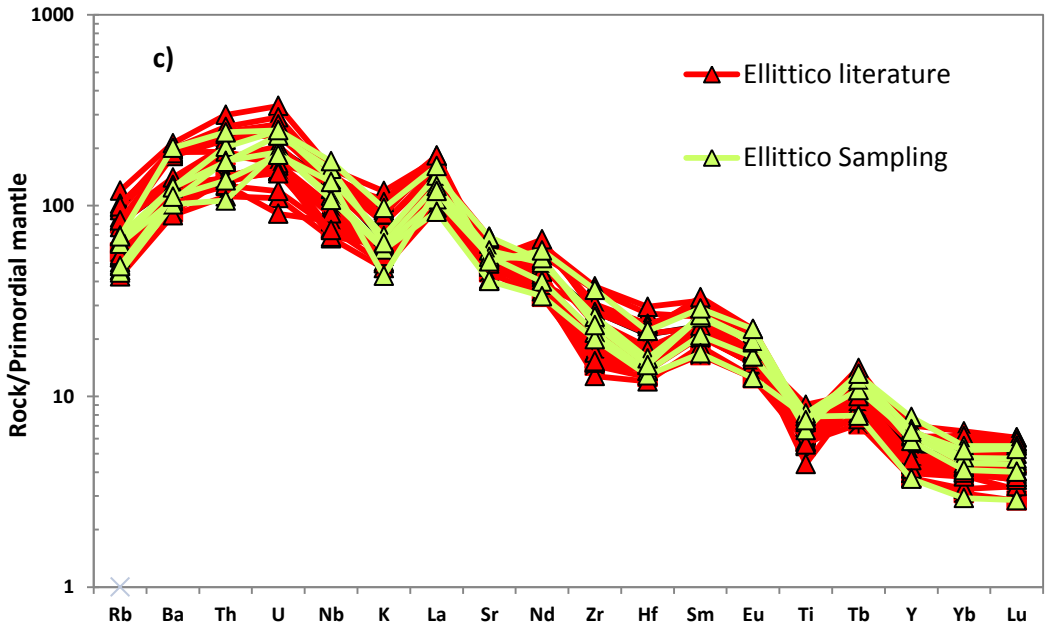


**Fig. 9.2.2c** – Comparison between Ellittico rocks incompatible elements.

Ellittico lavas display the same trend of AAV period. Being the most evolved terms emitted by Mt. Etna these products show the highest absolute values in trace elements concentrations (Fig. 9.2.2c; Appendix A).

Recent Mongibello pre-1971 products have similar patterns to AAV and Ellittico phases but less fractionated (Fig. 9.2.2d). In Fig. 9.2.3, the comparison between post-1971 Recent Mongibello data and all alkaline pre-1971 products (that show common geochemical features) points out how the recent eruptions have a predominantly different imprint from the older ones. K-alkaline lavas emitted from 1971 eruption, and cyclically during AAV and Ellittico

periods, display positive anomalies in Rb, and K and negative in Ba, Th and U. The enrichment in K, observed in spider diagrams (trace elements) and Archer diagrams (major elements), will be further discussed in the "Melt modelling" chapter.

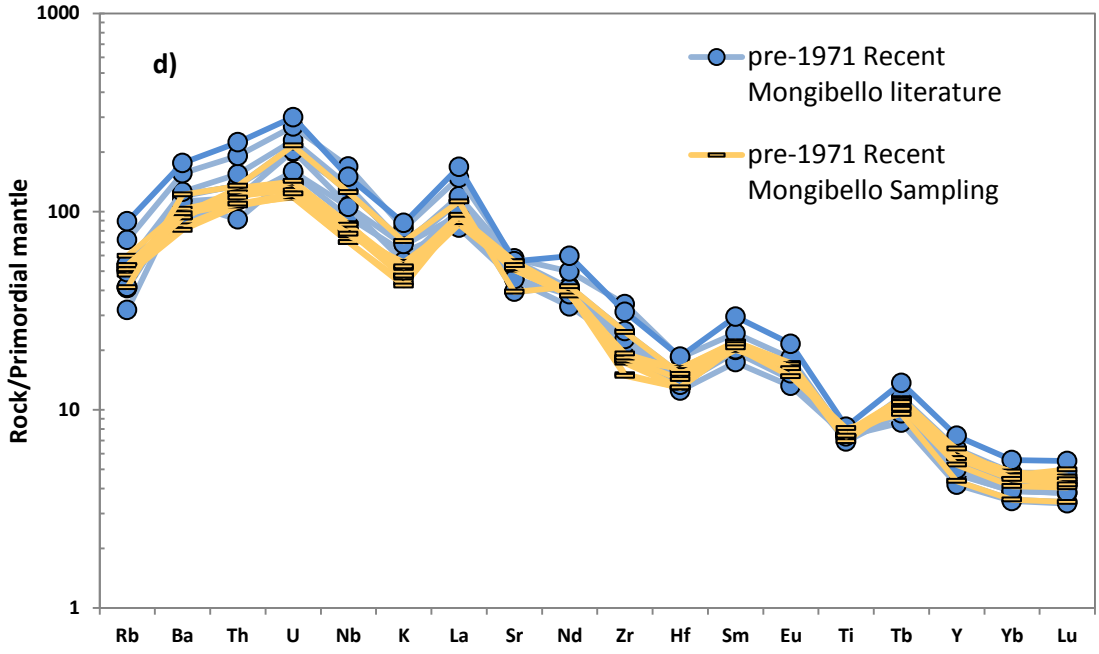


**Fig. 9.2.2d** – Comparison between Recent Mongibello, pre-1971 rocks incompatible elements.

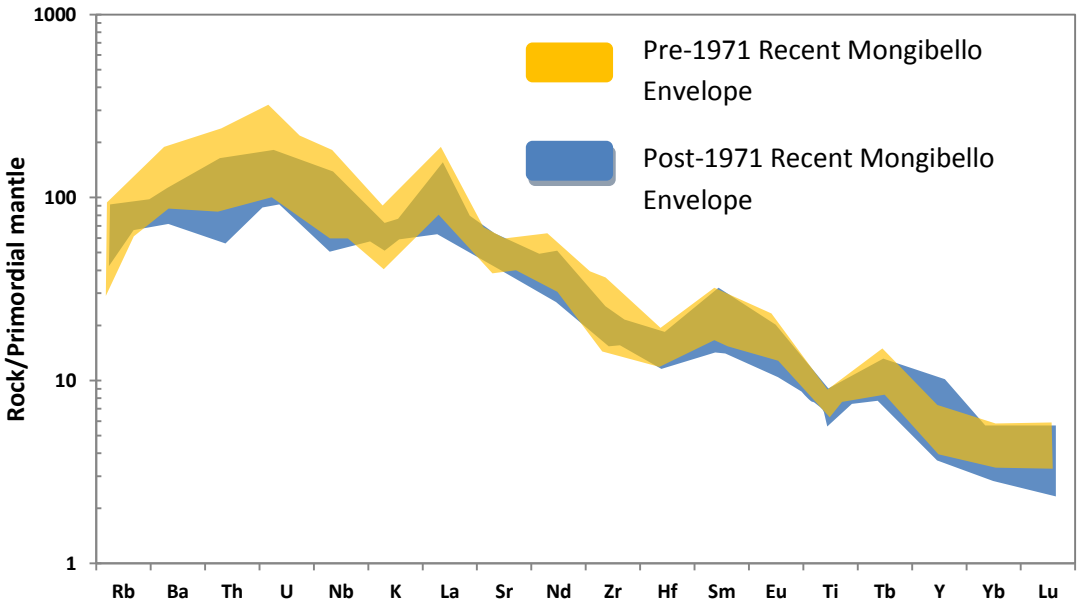


**Fig. 9.2.3 -** Comparison between pre-1971 and post-1971 Recent Mongibello trace elements envelopes.

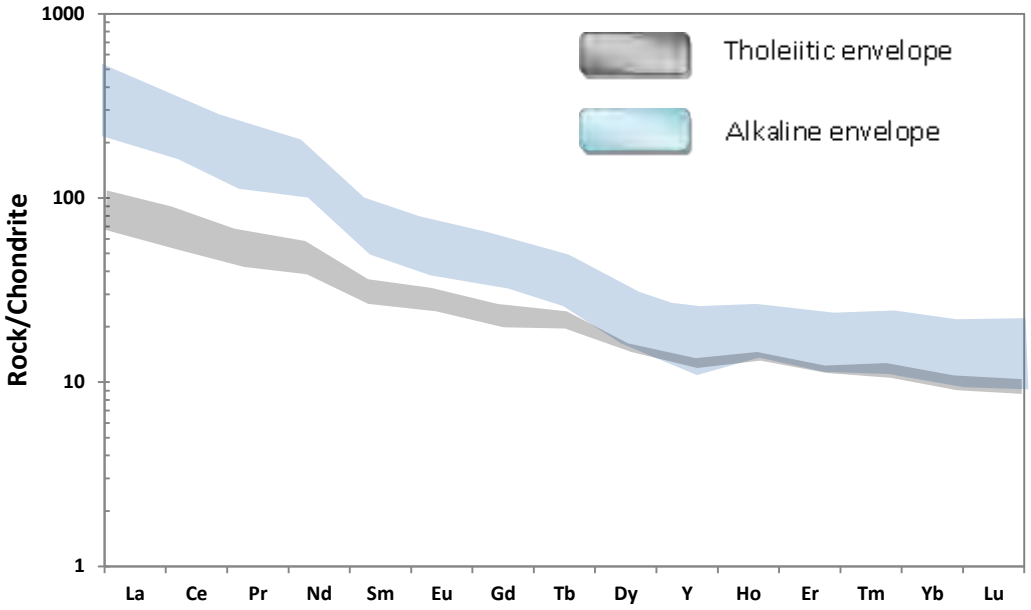


**Fig. 9.2.4.** – Rare earth element patterns of sampled etnean products normalized to chondrite

Ree patterns are fractionated for all rocks, but tholeiites display lower Yb/La ratios than alkaline products. Fig. 9.2.4 shows two distinct alkaline trends, the first one with high LREE/HREE ratios represented by Recent Mongibello lavas (both pre- and post-1971), and the second one identified by AAV and Ellittico products that reach the highest values related to theirs differentiation degree.

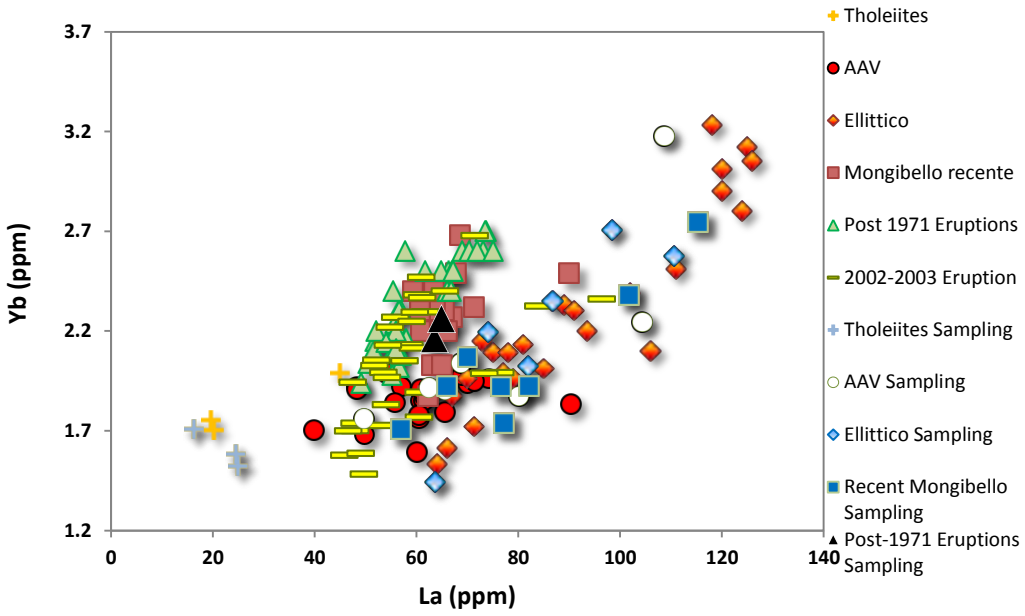


**Fig. 9.2.5** – Yb vs La (ppm) for sampled rocks and bibliographic data.

## 10. IN-SITU GEOCHEMISTRY

A total of almost 700 points analyses were taken by means of Electron Microprobe (chapter "Sampling and analytical methods") from 16 selected thin sections (about 80μ-thick) representative of the petrological and geochemical features of the four evolutionary period of Mt. Etna

- 2 *Tholeiitic* samples (ET4 and ET9)
- 5 samples for *AVV* phase (ET36, ET38, ASF1, ASF4 and CAR1)
- 3 *Ellittico* lavas (ET52, ET59 and ET63)
- 6 Recent Mongibello samples (ET15, ET16, ET18, ET24 for pre-1971; clinopyroxenes from L2 and L5 for post-1971, Giacomoni et al. 2012)

Most primitive and differentiated lava samples were selected to reproduce the complete fractionation trends.

For each samples olivine, clinopyroxene, plagioclase and spinels phenocrystals were analyzed (Appendix B). They were chosen by dimensions, degree of alteration, the presence of zonings or the absence of fractures and inclusions of secondary mineralogical phases. For plagioclase and clinopyroxene several profiles from cores to rims, at a constant step were made. Some samples from AAV, showing abundant and zoned clinopyroxene (up to centimetric) phenocrysts, were studied in detail distinguishing the observed texture and their compositional variation along the crystal sections.

### *Tholeiites*

Olivine phenocrysts have a forsteritic content varying from 77.3 to 84.4 (Fig. 10.1a) and subsequently are the most primitive of the entire Etnean evolutionary cycle (Fig. 10.1a and 10.1b). In Fig. 10.2a, b, c two main compositions are shown: i) Primitive group (MgO from 42,5 and 46 wt%) with low Fayalite contents (down to 15.1 %) and NiO ranging between 0,19 and 0,3 wt%; ii) More evolved group with higher Fa wt% values (up to 22) and more or less the same Ni wt% concentration of the previous one (Fig. 10.2). Clinopyroxene phase is not found in these lavas. Labradoritic plagioclases have quite constant Anorthite contents, ranging from 51.3 to 61.7 % (Fig. 10.5), and most of them show low concentrations in FeO (0.4 – 0.9

wt%; Fig. 10.6a). Their An content is less primitive than that in plagioclase from AAV, Ellittico and Recent Mongibello. They seems to follow a different trend (together with same sample from AAV and Ellittico) from the majority of Recent Mongibello, and some of AAV and Ellitico plagioclases (Fig. 10.6a). The same features are displayed in Fig. 10.6b with a little difference represented by the higher tholeiitic plagioclase $SiO_2$ values at similar anorthitic contents.

Tholeiitic oxides are classified as Cr-Spinels for their elevated $Cr_2O_3$ (33.2-34.4) and $Al_2O_3$ wt% (25.2-26.7) and low FeO (24.9 -27.7) and $TiO_2$ (1-1.14) wt% contents (Fig. 10.7).

***AAV***

Fig. 10.1a, b and 10.2 show two main olivine populations. One evolved that fits well (for FeO and NiO wt%) with most of the phenocrysts from the alkaline suites (MgO from 38.1 to 36 wt% and Fo from 73.2 to 71) and another one with primitive features revealed by higher magnesium values (42 – 42.2 wt% and Fo = 79.5%). This second group plots between the primitive tholeiitic and the evolved alkaline olivines suggesting an intermediate composition that could represents the missing link for these two magmatic series. Eventually Fig. 10.2a identifies up to three different compositions, one of them with anomalous low CaO values (up to 0.2 wt%). All variation diagram for clinopyroxenes (from salite to augite, Fig. 10.3) evidence two distinc trends (Fig. 10.4). The primitive one, with Mg# varying from 86.2 to 79.2, have higher contents in $Al_2O_3$, $TiO_2$, $Na_2O$ and CaO wt% whereas the second evolved one shows similar values but with lower Mg# (78.7 – 71.9). This is aligned with some pre-1971 Recent Mongibello Cpx defining an unique and evident trend (Fig. 10.4). Two variation diagrams were developed for plagioclases (from andesine to bytownite, Fig. 10.5) with An% vs FeO and $SiO_2$ wt%. In fig. 10.5 and 10.6b is easy to realize how phenocrysts from AVV period are the most evolved in the evolutionary history of Mt. Etna (up to 56.7 wt% in $SiO_2$ and only 42.7% of anorthite). FeO ranging from 0,43 to 0,89 is typical of plagioclases literature analyses (Viccaro et al., 2010 and reference therein) (Fig. 10.6a). Oxides are classified as Ti-magnetites (as well as Ellittico and Recent Mongibello spinels). They range in MgO from 2.77 to 5.76 wt% showing very low $Cr_2O_3$ (Fig. 4a) and $Al_2O_3$ (1.36 - 6.15 wt%) (Fig. 10.7a and c) and high FeO (62.5 – 79.6 wt%) and $TiO_2$ (up to 24.5 wt%) (Fig. 10.7b and d).

***Ellittico***

Olivines from Ellittico display two distinct trends (Fig. 10.1 and 10.2) that remark the situation showed for AAV phenocrysts. One evolved trend (Fo from 78.4 to 80.6%, fig. 10.1a) with high tenors in FeO, CaO and low in NiO wt% and another one more primitive (70.1 - 74.7 Fo%; Fig. 10.1a) with intermediate values (FeO, CaO and NiO wt%) between tholeiites and the differentiated group (Fig. 10.2). All clinopyroxenes, of salitic composition (Fig. 10.3), plot in a single trend and are among the most differentiated of the alkaline suite ranging in Mg# from 71 to 77.4 (Fig. 10.4). These values are comparable with some clinopyroxenes of AAV and Recent Mongibello suites. Plagioclase, prevalently labradoritic (Fig. 10.5), reflects the same trend shown for AAV crystals, with a wide anorthitic range (44.9 – 84.5%) and two main groups with different primary FeO wt% (Fig. 10.6a). Ti-magnetites have composition similar to the other alkaline suite oxides, with high FeO, and $TiO_2$ wt% (11.7-16.1) and low $Al_2O_3$ wt% values (3.47 – 5.97) (Fig. 10.7).

***Recent Mongibello***

Olivines from pre-1971 Recent Mongibello lavas plot in a single differentiated trend (Fig. 10.1), fitting well with most of AAV and Ellittico phenocrysts. There is not evidence of an intermediate group joining the most differentiated terms to the tholeiitic ones as displayed for the previous described alkaline series (Fig. 10.2). Fo% and MgO wt% vary from 67.4 to 75 and from 34.2 to 39.1 respectively (Fig. 10.1 and 10.2). For clinopyroxenes (from salite to augite, Fig. 10.3) phenocrysts from both pre- and post-1971 products (2002-2003 eruption) wew analyzed. The older series show two distinct trends, well comparable with those observed for AAV terms, even if less differentiated. The primitive alignment, have an Mg# varying from 86.3 to 89.1%, and represents the onset of a common trend with several AAV phenocrysts (more fractionated) for all displayed elements (Al, Ca, Na and Ti; Fig. 10.4). The evolved terms plot with most of all other alkaline Cpx, except for few crystals showing anomalous low CaO wt% contents (17.5 – 18.6) that normally ranges from 20.4 to 22.5 wt% (Fig. 10.4b). Clinopyroxenes from post-1971 lavas are represented by two totally distinct

populations. 1) Phenocrysts with relatively primitive features following the typical trend observed for most of AAV, Ellittico and pre-1971 Recent mongibello Cpx; 2) Evolved terms (Mg# down to 61.7%) fitting in single trend that maintains higher CaO, and lower $TiO_2$, $Na_2O$ wt% (Fig. 10.4) than the "primitive trend". Recent Mongibello plagioclases are the most anorthitic of the entire alkaline suite ranging from 55.5 to 87.6% (labradorite – bytownite, Fig. 10.5) and displaying constant FeO values (0.61-0.82 wt) (Fig. 10.6a). Oxides are Ti-magnetites as well as the other alkaline phenocrysts, with comparable values in $Cr_2O_3$, FeO, $Al_2O_3$ and $TiO_2$ (Fig. 10.7).

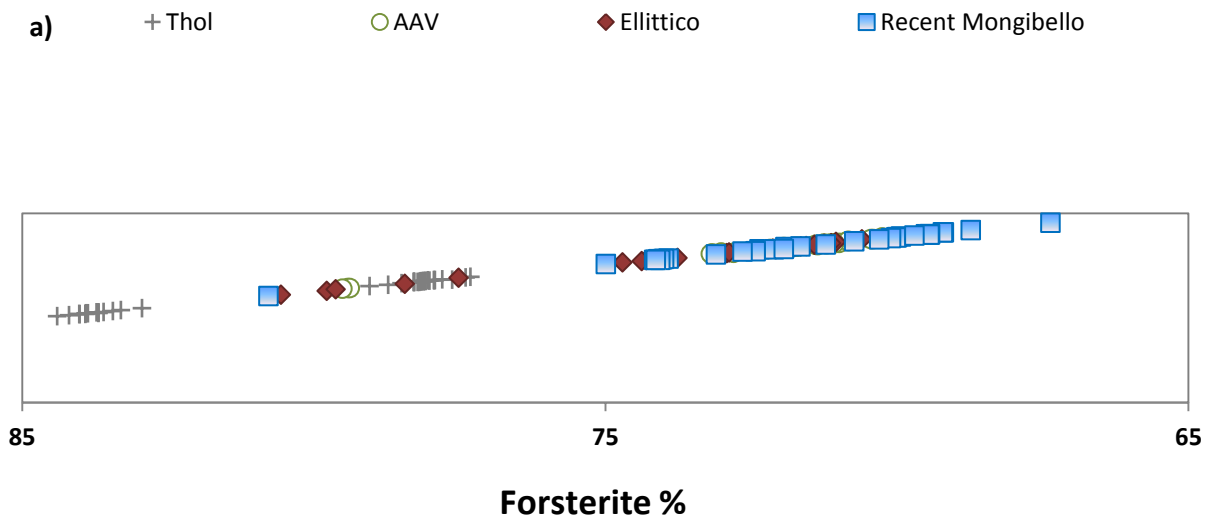

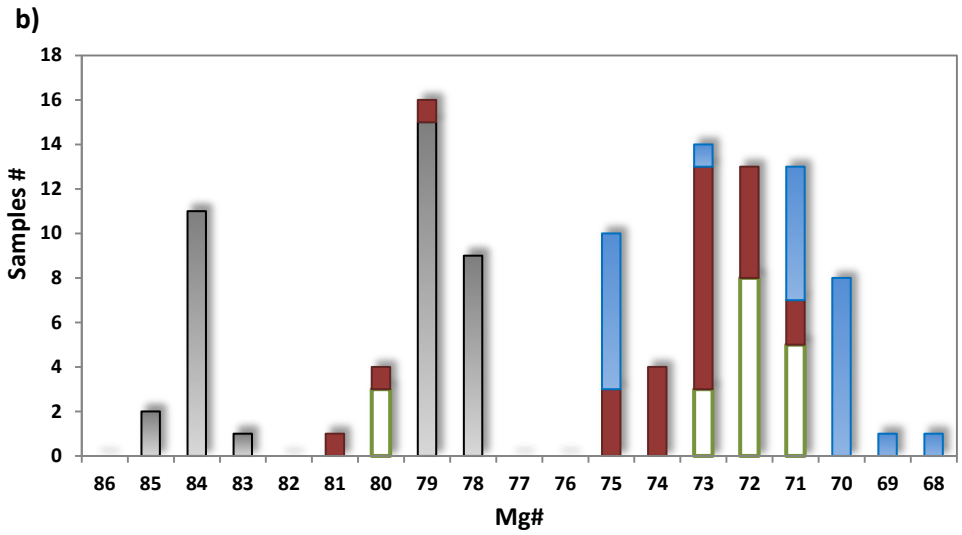


**Fig. 10.1** – a) Forsteritic contents and b) Statistical distribution of Mg# values for olivine phenocrysts from the four evolutionary periods.

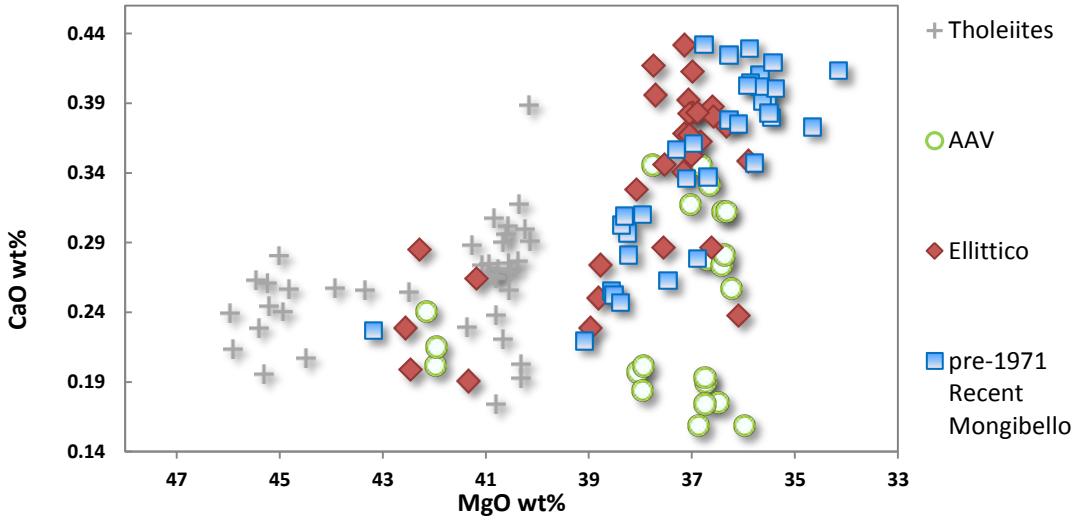

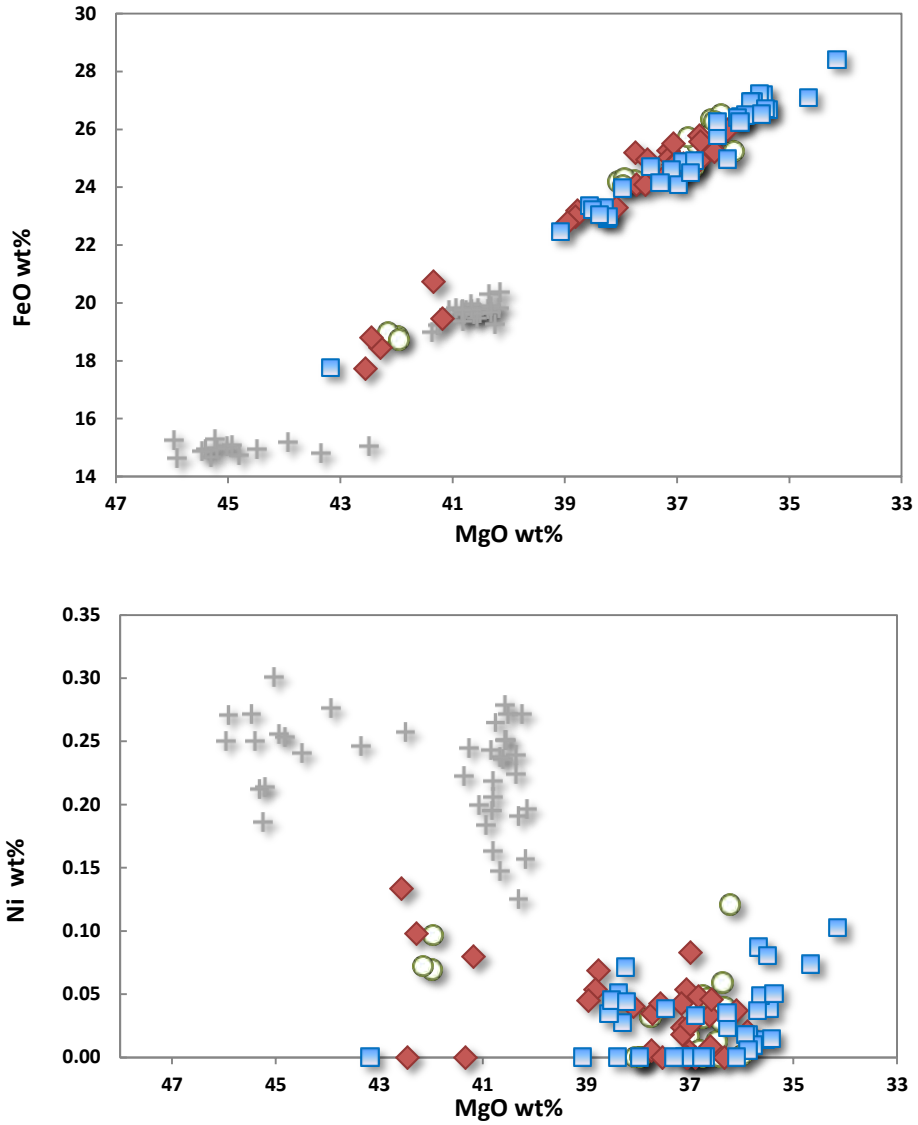


**Fig. 10.2** – MgO vs CaO and FeO and NiO wt% of Mt. Etna olivine phenocrysts.

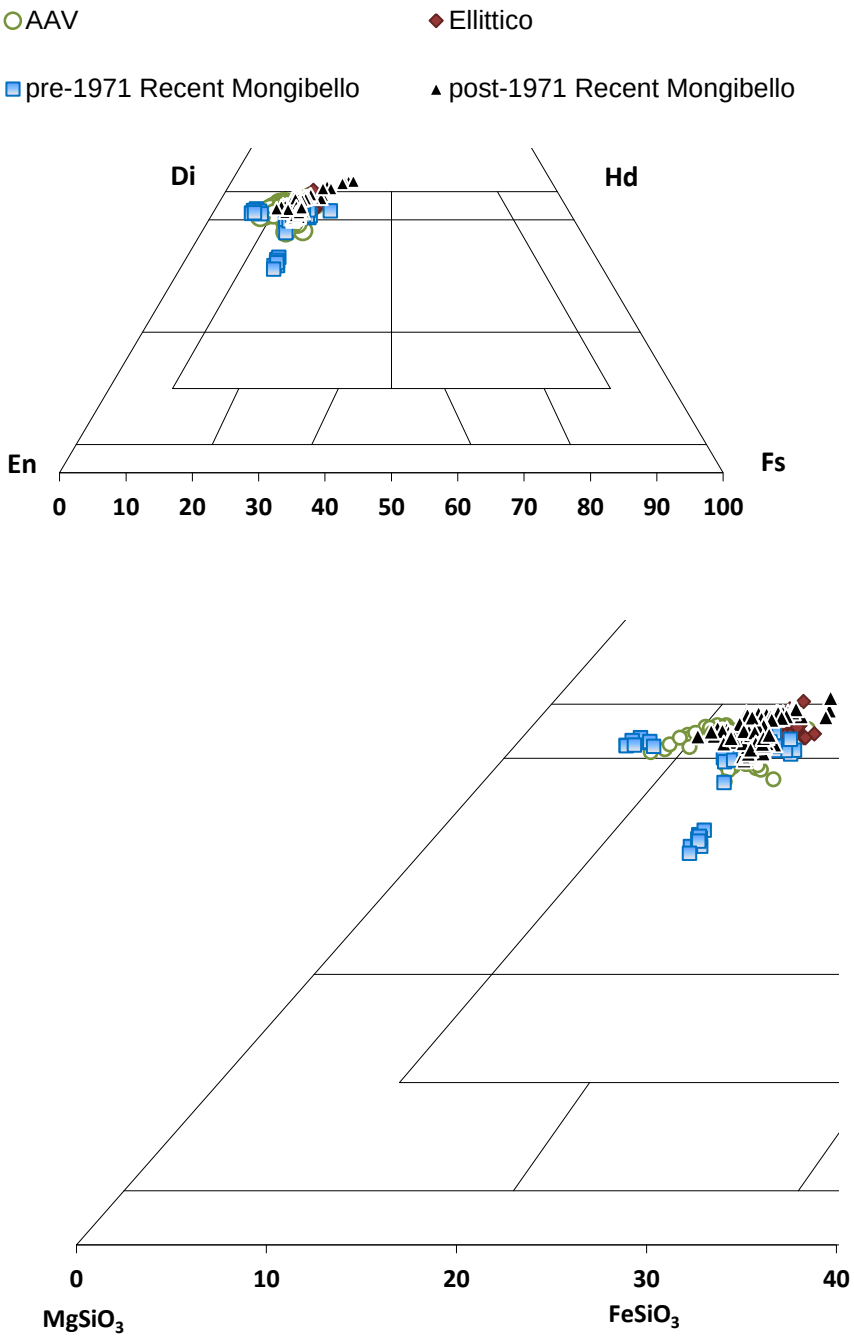


**Fig. 10.3** – Classification diagrams of Mt. Etna clinopyroxenes. (Morimoto and Kitamura, 1983)

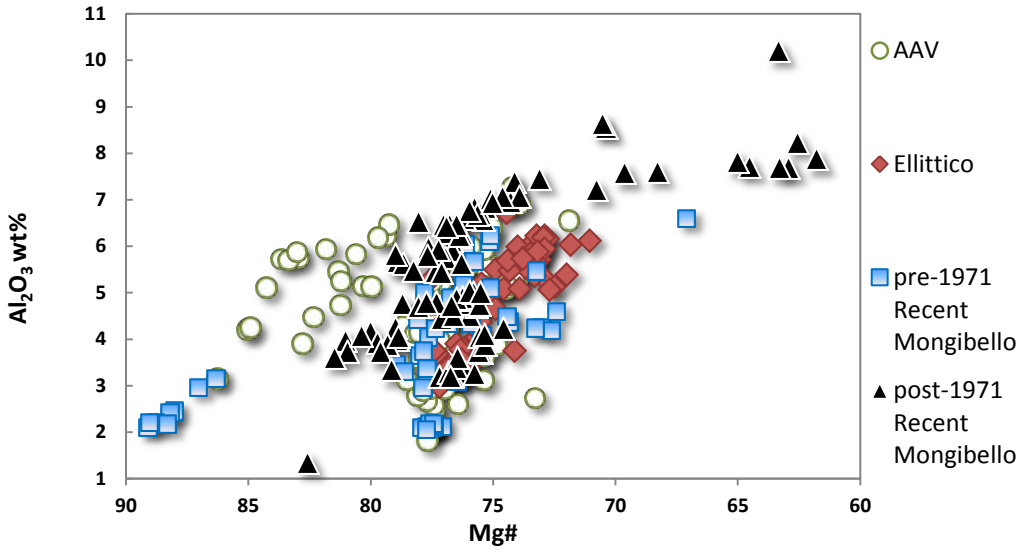
11
10
9
8
7
6
5
4
3
2
1
$Al_2O_3$ wt%
90
85
80
75
70
65
60
Mg#
AAV
Ellittico
pre-1971 Recent Mongibello
post-1971 Recent Mongibello

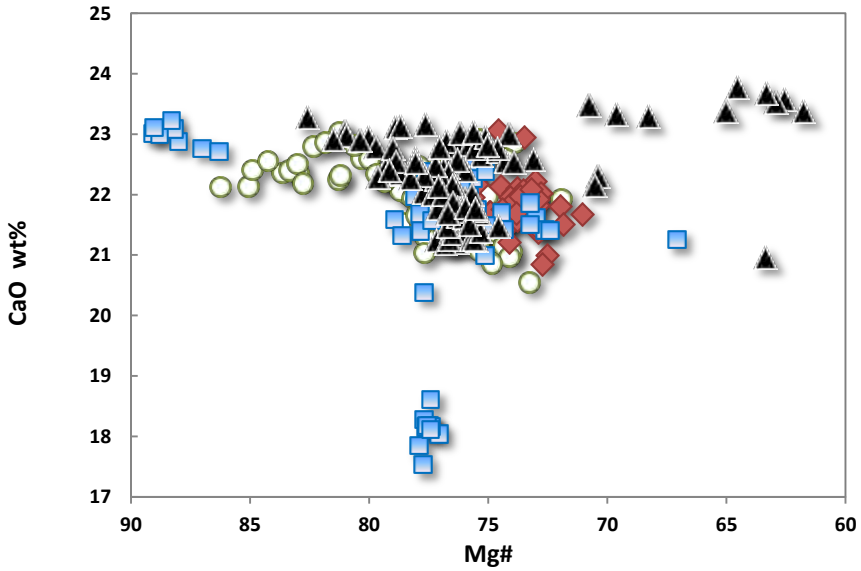
25
24
23
22
21
20
19
18
17
CaO wt%
90
85
80
75
70
65
60
Mg#

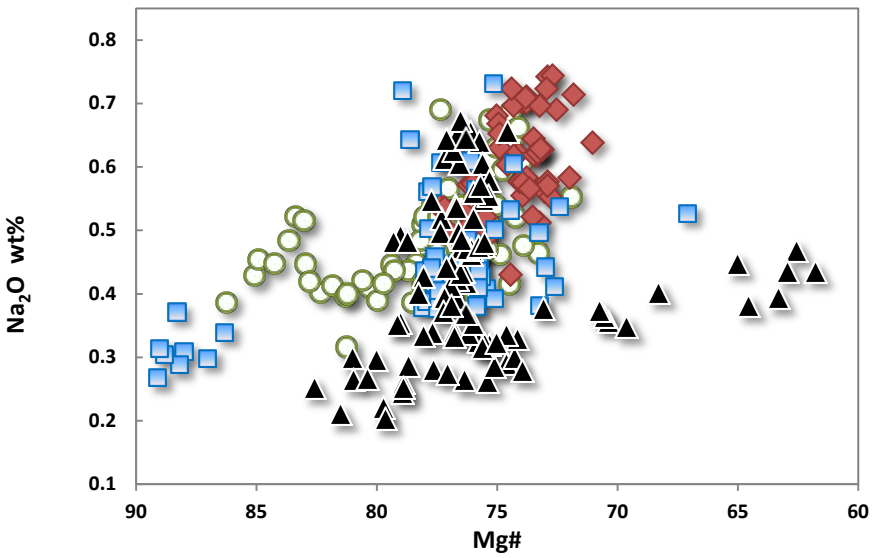


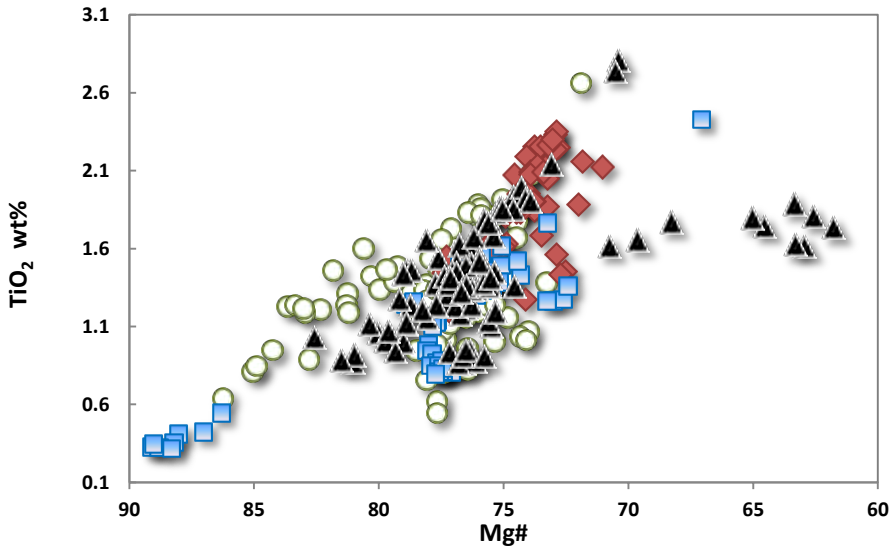


**Fig. 10.4** – Mg# vs $Al_2O_3$, CaO, $Na_2O$ and $TiO_2$ of Etnean clinopyroxene phenocrysts.

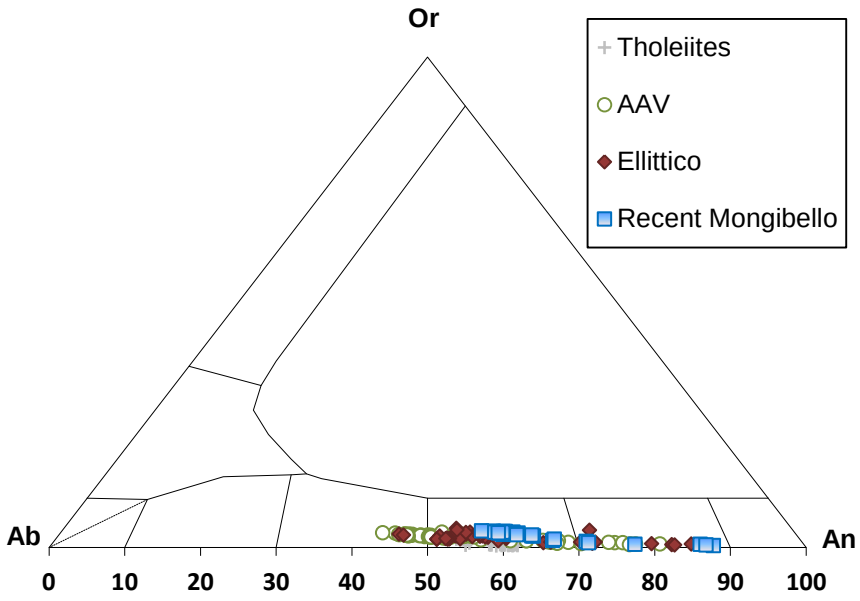


**Fig. 10.5** - Classification diagram of Mt. Etna plagioclases.

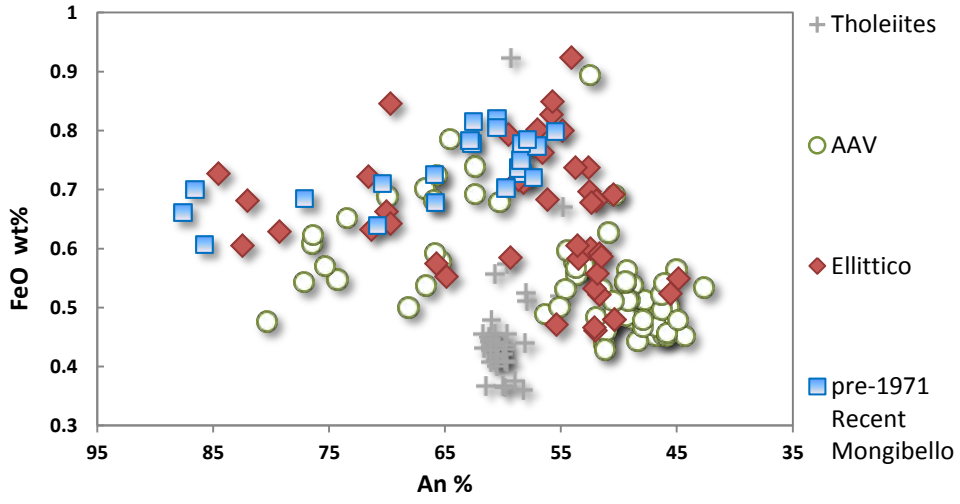

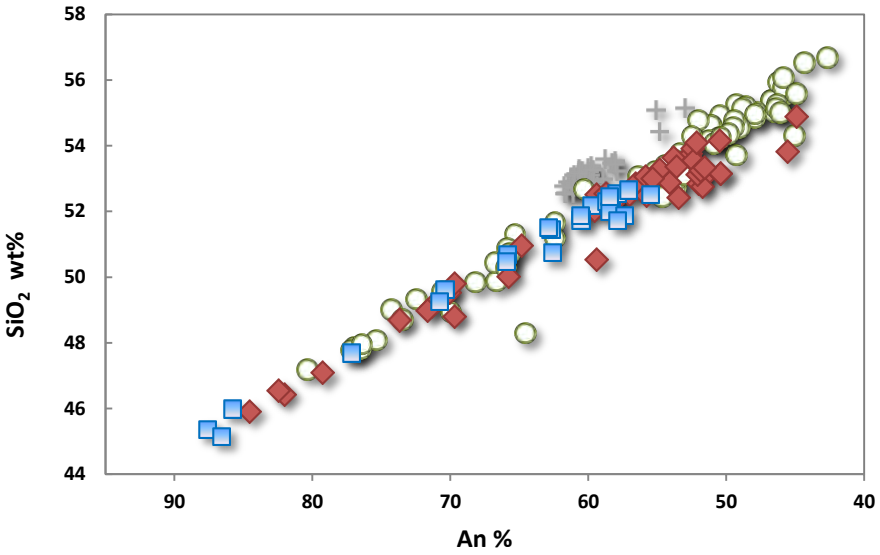


**Fig. 10.6** – An% vs FeO and $SiO_2$ wt% of Mt. Etna plagioclase phenocrysts.

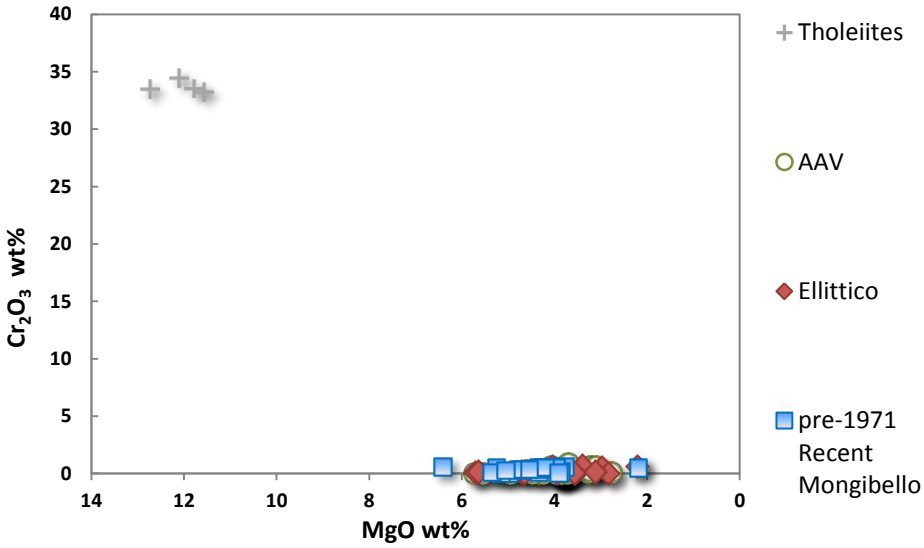

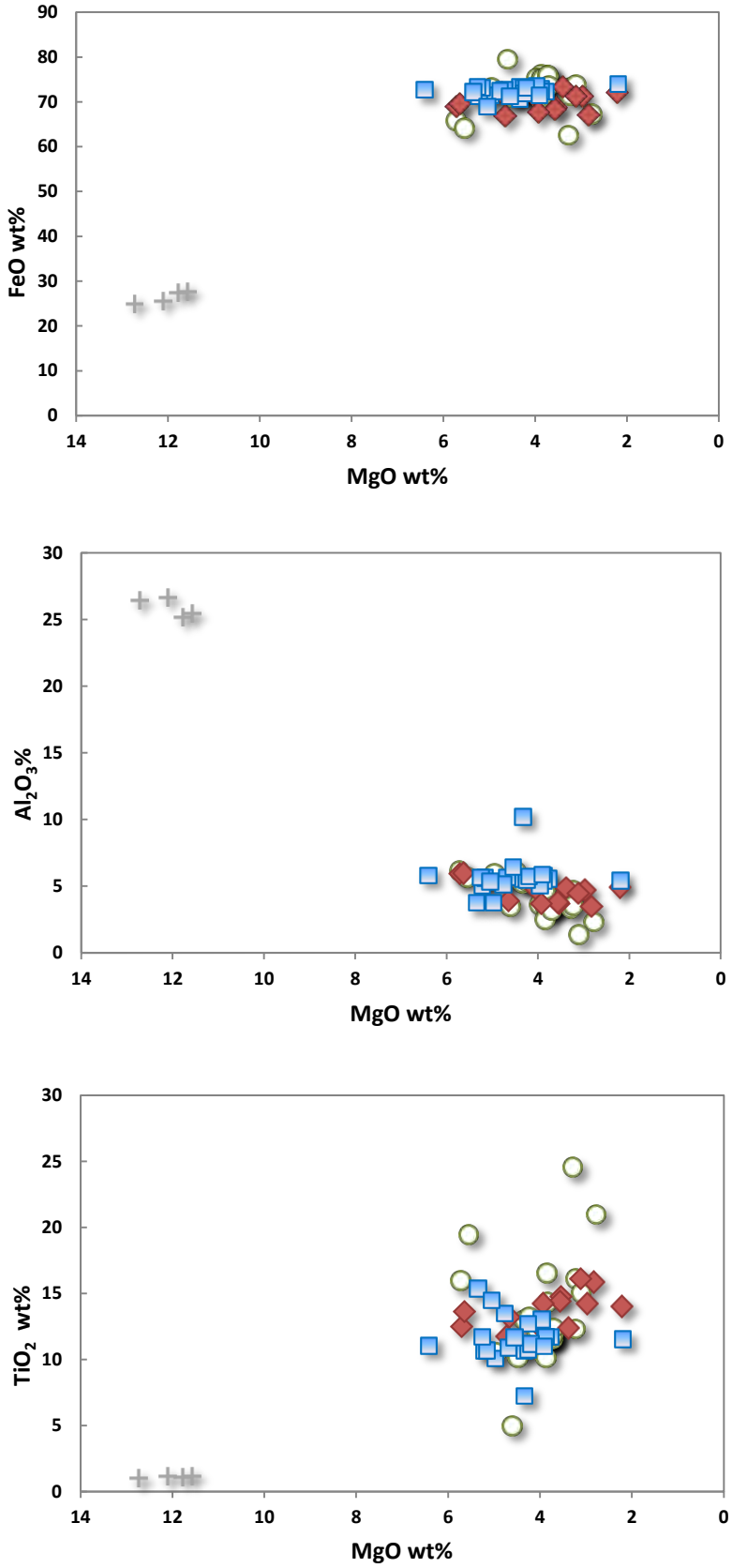


**Fig. 10.7** – MgO Vs $Cr_2O_3$, FeO, $Al_2O_3$ and $TiO_2$ wt% of Etnean oxides phenocrysts.

# 11. FRACTIONATION MODELING

In chapter "Gases and melt inclusions" the actual knowledge on Mt.Etna primitive magmas was exposed derived from the "direct" study of melts trapped during olivine phenocrysts growth. They give us important information on the original magma compositions produced by the mantle partial melting. Several works published both major element and volatiles contents which nevertheless are quite different and do not converge in a unique and reliable magma composition. An alternative method to obtain the primary magmas features (used in this work) is represented by the development of backward fractionation models (an "indirect method") that, starting from real and primitive analyzed magmas, allow to reconstruct the "primary" and un-fractionated compositions. In this work two different kind of fractionation models are presented with the aim of, i) describing the differentiation processes of each Etnean magmatic series and ii) reconstructing primary melts and compare them with bibliographic data. They were modeled by means of major and trace element mass balance calculations using major element whole rock and in situ mineralogical phases analyses (olivine, clinopyroxene, plagioclase and spinel; Appendix A and B**).** The least differentiated samples were chosen, on the basis of $SiO_2$, MgO contents, and Mg# values, and used as starting melt for both backward fractionation modelling. The fractionation was extended until the magma did not result in equilibrium with mantle olivine with Fo about 87%. They were then used for modeling whole-rock trace element contents for the parental magma, using Rayleigh fractionation model (and relative Kd downloaded from the GERM database, http://earthref.org/GERM/). Mineral proportions and total amount of fractionated material were then used to calculate the trace element contents of the differentiated magma. Composition of the resulting melt was calculated according to the following formula: $C_l = C_0 \text{ X } F^{(D-1)}$, where Cl is the calculated composition of the resulting melt, $C_0$ is the composition of the starting melt, F is the residual melt percentage, and D is the total weighted partition coefficients (Shaw, 1970).

## 11.1 MAJOR ELEMENTS FRACTIONATION MODELING

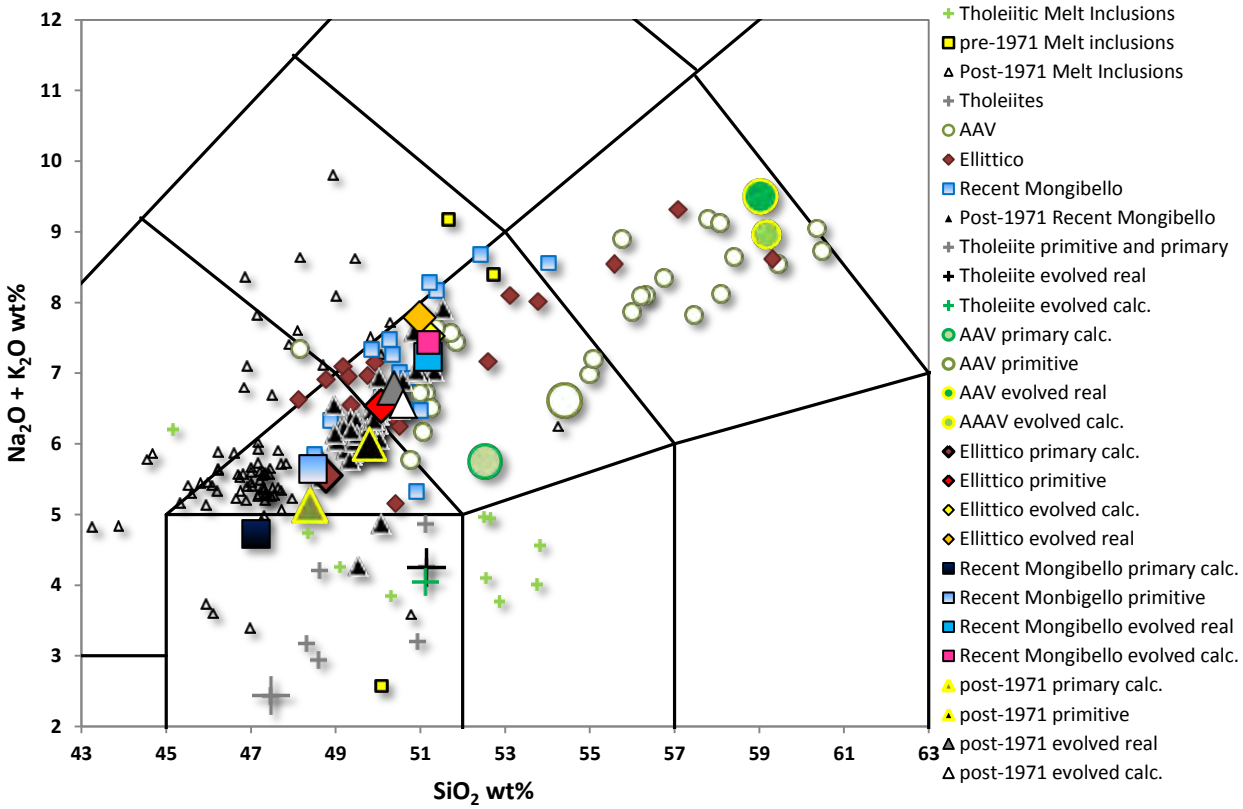


**Fig. 11.1.1** – TAS diagram of modeled and analyzed samples and melt inclusions from bibliography (Kamenetsky and Clocchiatti, 1996; Del Carlo and Pompilio, 2004; Metrich et al., 2004; Spilliaert et al., 2006; Collins et al., 2011).

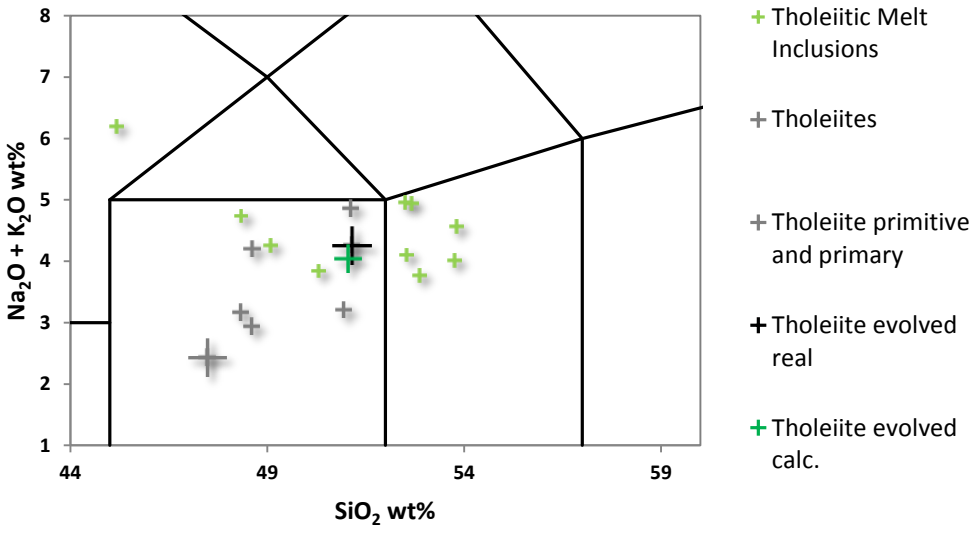

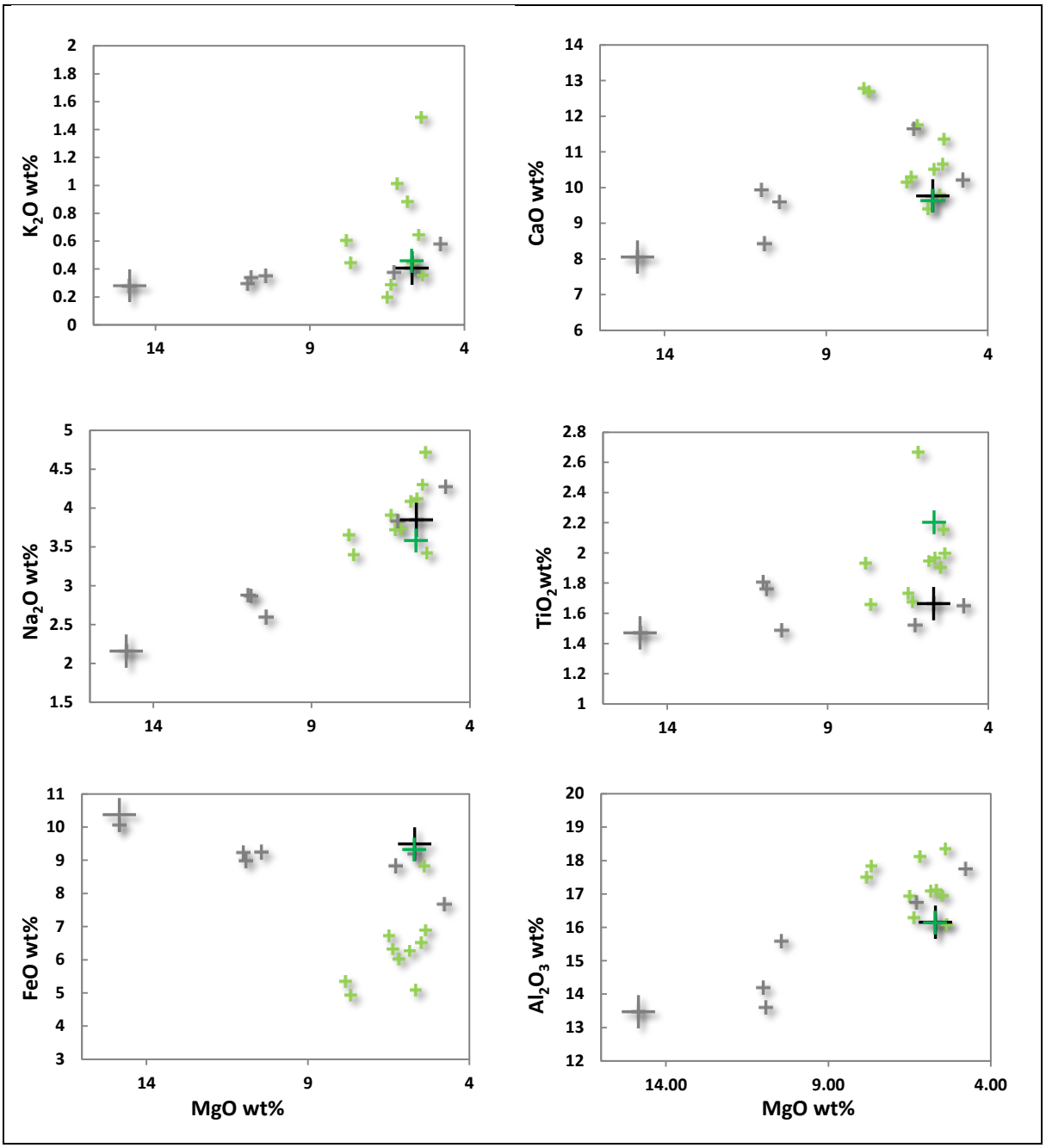


**Fig. 11.1.2** – a) TAS and b) variation diagrams for tholeiitic samples.

***Tholeiites***

Several Tholeiitic lavas from this work have such a high Mg# that they could be considered as "primary" magmas. For this reason the sample ET4 (Mg# = 72.38%), used as starting magma for the differentiation modeling, represents a primary and un-fractionated composition, generated directly by the partial melting of the Etnean mantle source. The degree of primitivity of this sample is higher than that obtained from melt inclusions (Kamenetsky and Clocchiatti, 1996). In Fig. 11.1.2 the Tholeiitic fractionation is shown that hypothesizes the crystallization of 27.08% Ol, 13.94% Cpx, 28.91 Opx, 14.69 Plg and 15.39 Spinel for a total amount of 53.1% Gabbroic material (Table 4 and 5). Calculated Data obtained by means of two steps Rayleigh fractionation models (from ET4 to the intermediate composition ET6 and from ET6 to the evolved end member ET9) fit well with real compositions ($0.3 < r^2 < 0.69$). All variation diagrams display a single differentiation trend with lower $TiO_2$ and higher FeO contents respect to MI from Kamenetsky and Clocchiatti (1996).

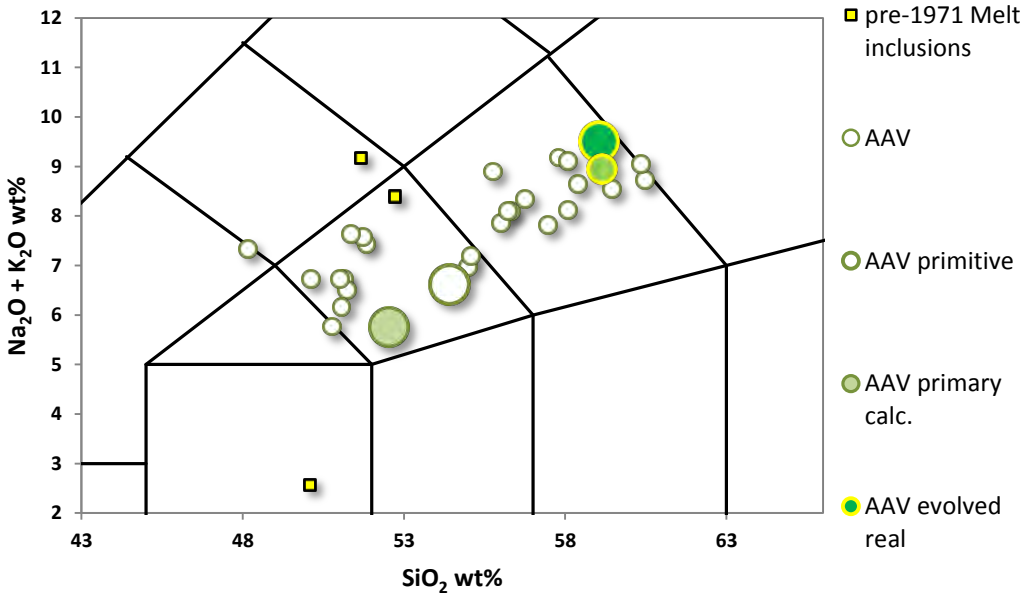

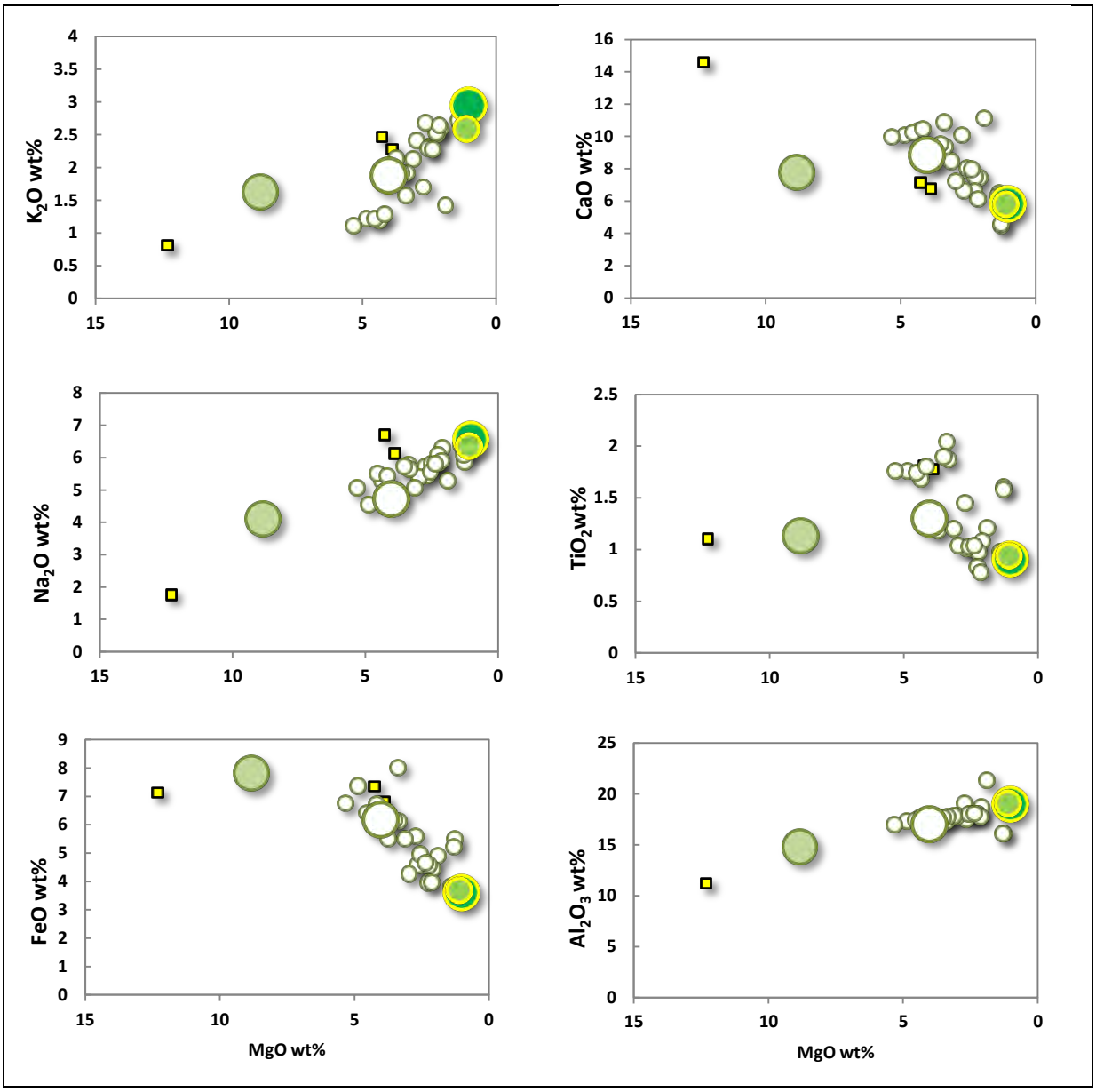


**Fig. 11.1.3** – a) TAS and b) variation diagrams for AVV samples.

*AAV*

Differently, AAV series was modeled by means of backward and direct fractionation models. Starting from sample ET39 (Mg# = 54.36%) was reconstructed a primary composition (Mg#= 63.89%) removing a total percentage of 15% formed by 96.9% Ol and 3.1 Cpx in two fractionation stages. The direct fractionation model hypothesizes the addition of 28.09% of gabbroic material represented by 6.91% Ol, 55.38 Cpx, 24.92 Plg and 12.8 Ti-Mt to reach the most evolved term ET36 (Mg# = 34.27%) (Table 4 and 5). The primary calculated magma seems to follows a realistic trend although the scarcity of alkaline pre-1971 melt inclusions analyses. For each Archer diagram the evolved real and calculated arrival magmas are well comparable ($r^2$ = 0.51; Fig. 11.1.3). Overall it possible to define a complete differentiation model that startes from the reconstructed primary magmas and arrives to the most evolved one providing a total amount of 43.1% of fractionated material composed by 48.5% Ol, 22.8% Cpx, 15.5% Plg and 13.1% Ti-Mt (Table 4).

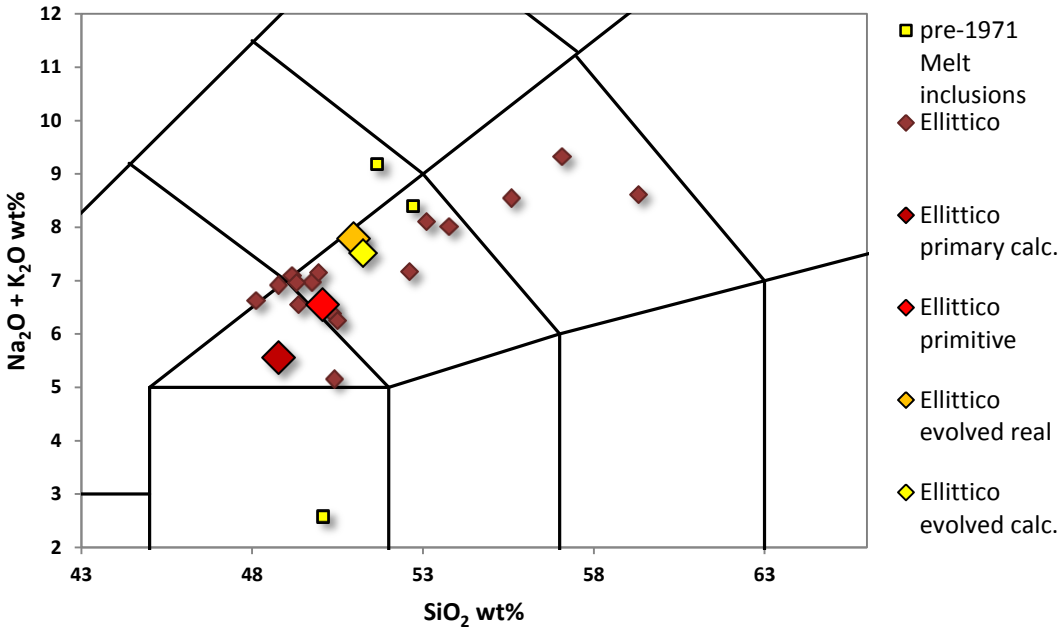

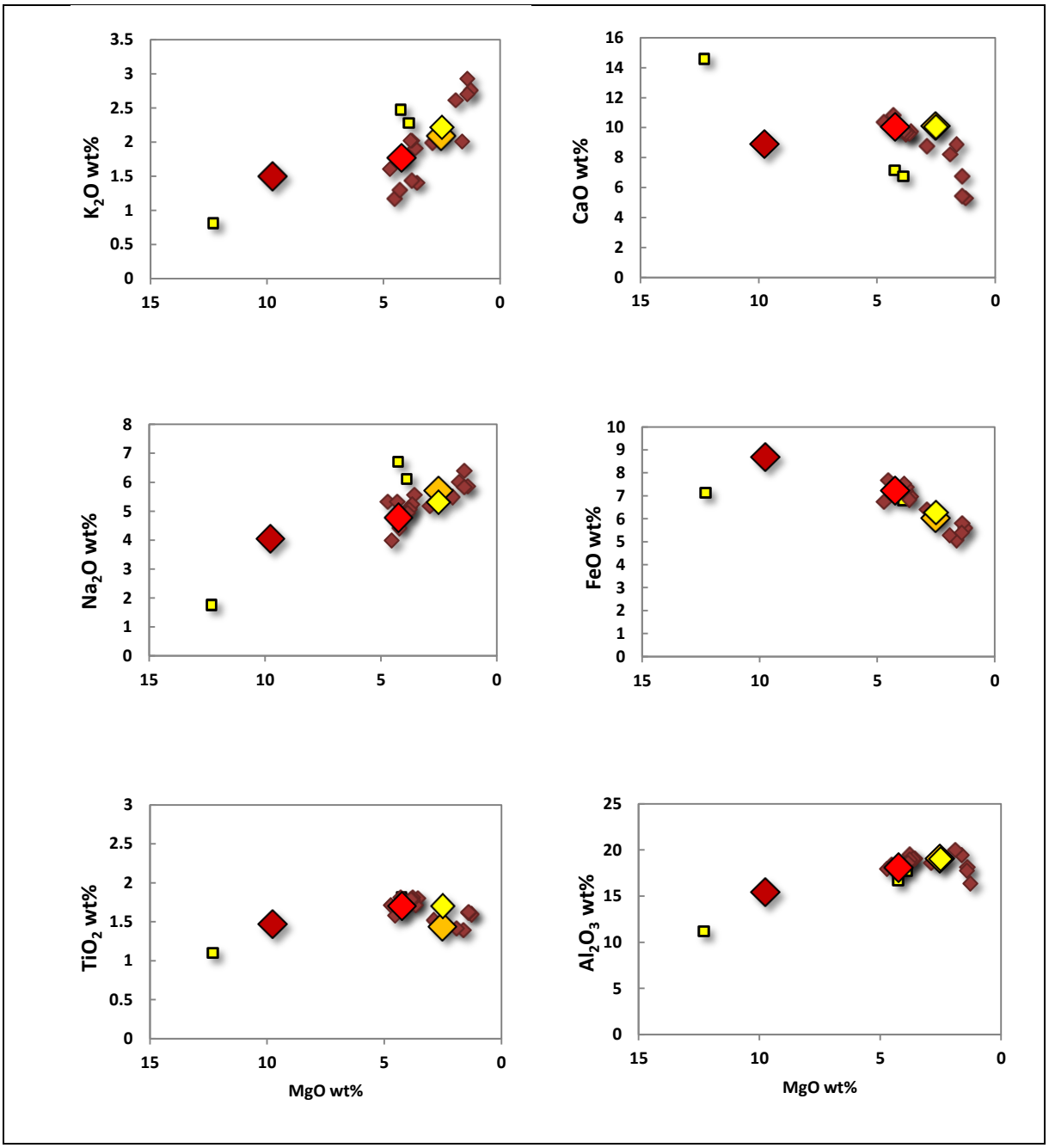


**Fig. 11.1.4** – a) TAS and b) variation diagrams for Ellittico samples.

***Ellittico***

The Ellittico fractionation trend showed in Fig. 11.1.1 is similar to pre- and post-1971 Recent Mongibello ones. The primitive composition is represented by sample ET52 with an Mg# = 50.93%, from which it was reconstructed the primary melt adding 18% of material (89.96% Ol and 13.04 Cpx). In this case, the fractionation of abundant clinopyroxene respect to AAV and Recent Mongibello models is proposed (Table 4 and 5). The direct differentiation model, from the primitive to the evolved term (ET12 represents the evolved end-member with Mg# = 42.62%), supposes the separation of 18.45% Ol, 25.95% Cpx, 47.97% Plg and 7.63% Ti-Mt for a total amount of 22.93% of fractionated, gabbroic material (Table 4). The complete differentiation process, from the primary calculated composition to the real evolved term, was obtained with 40.93% of fractionated material composed by 52.2% Ol, 19.7% Cpx, 16.7% Plg and 11.4% Ti-Mt. Variation diagrams displays a well defined evolution trend and the primary reconstructed magma seems to follow it representing the starting melt composition (Fig. 11.1.4). The evolved real and the calculated compositions are always well comparable ($r^2$ = 0.57; Table 5)

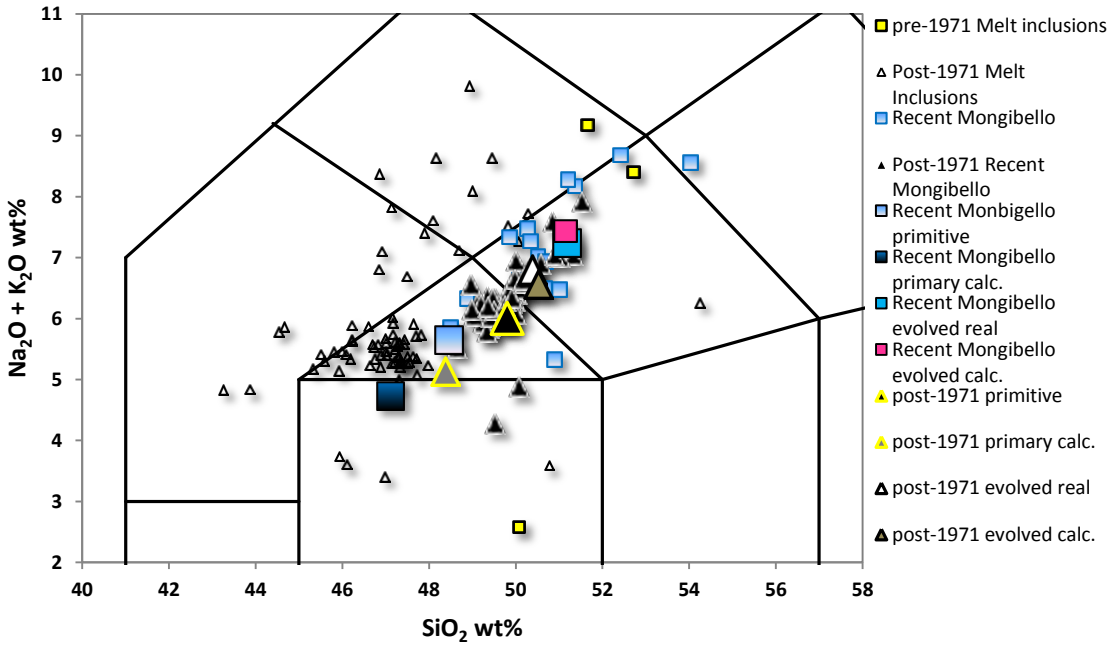

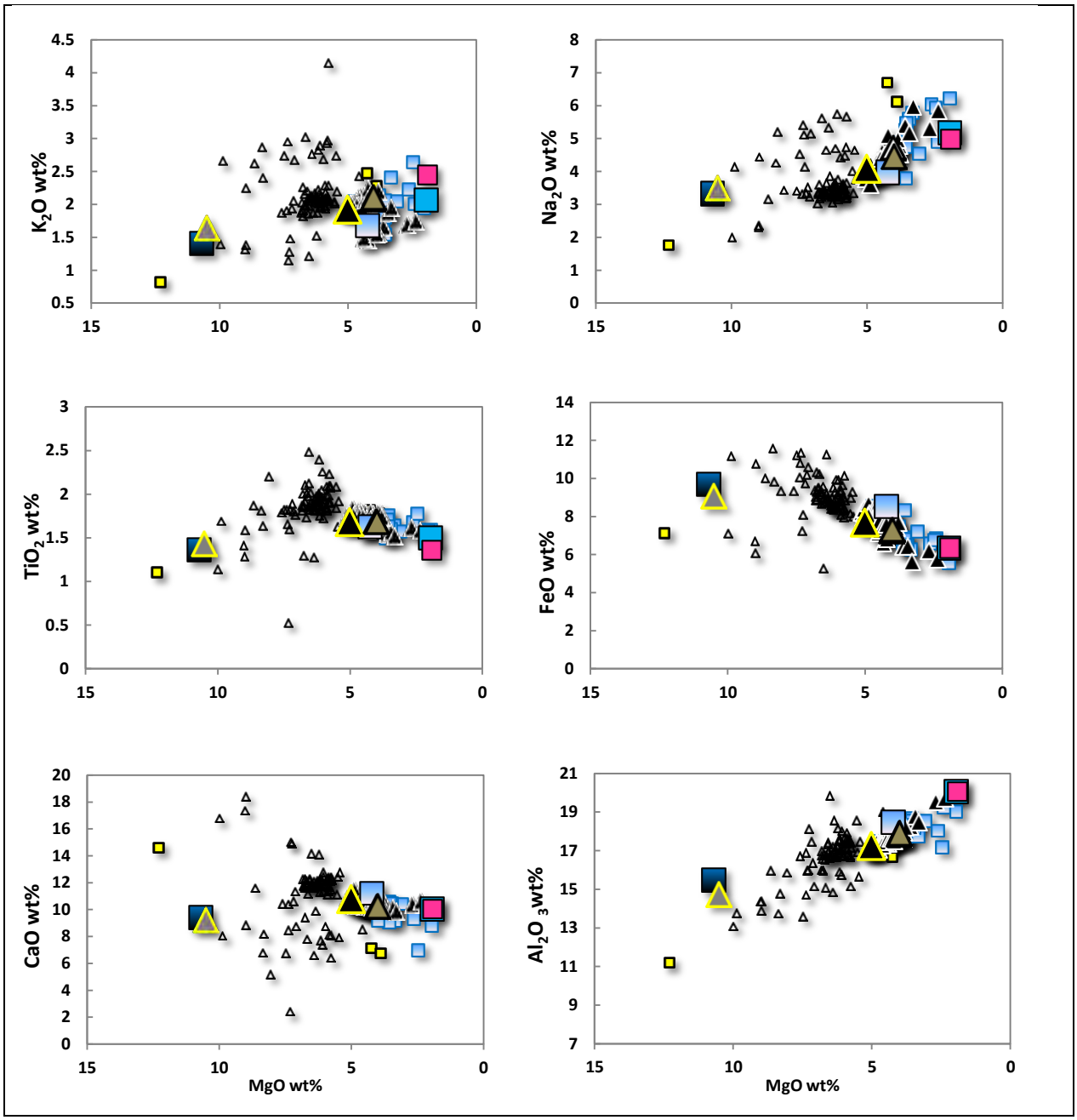


**Fig. 11.1.5** – a) TAS and b) variation diagrams for pre- and post-1971 Recent Mongibello samples.

***Recent Mongibello***

Recent products were distinguished in pre- and post-1971 trying to find any differences between these two series. Pre-1971 suite starts from ET22 sample (Mg# = 55.33%) and reaches a primary reconstructed term (Mg# = 66.24%), adding 19% of material totally made up of olivine (100%). The direct differentiation model hypothesizes the fractionation of 6.63% Ol, 36.37% Cpx, 42.82% Plg and 14.17% Ti-Mt for a total amount of 33.16%. Overall the complete model supposes the fractionation of 52.16% of gabbroic material composed by 47.2% Ol, 18.7% Cpx, 19.9% Plg and 14.2% Ti-Mt. Post-1971 lavas (2002-2003 eruption) show percentages similar to that of pre-1971 ones. From Bg1, the primitive real magma (53.67%), is possible to obtain a primary composition (Mg# = 67.28%) adding 17% of material (olivine = 100%). Adding the percentage related to the direct fractionation (from Bg1 to Pm2 from Giacomoni et al. 2002), the complete model hypothesizes the fractionation of 26.11% gabbroic material formed by 77.8% Ol, 8.3% Cpx, 6.7% Plg and 7.2% Ti-Mt. The difference in relative percentages between pre- and post-1971 models is due to the degree of evolution of the chosen arrival samples (Pm2, Mg# = 49.77 and ET24, Mg# =35.18) (Table 4 and 5).

TAS diagram (Fig. 10.1.5) do not displays great differences between pre-and post-1971 suites, with primary, calculated magmas that show similar features. They also fit well with some melt inclusions analyses (post-1971 eruption) from Kamenetsky and Clocchiatti (1996), Del Carlo and Pompilio (2004), Metrich et al. (2004) and Spilliaert et al. (2006). Data from Collins et al. (2011) show anomalous high concentrations in alkaline elements.

$K_2O$ vs MgO wt% evidence two distinct alignments: i) The Low-K (low potassium contents) trend typical of pre-1971 Recent Mongibello and of same post-1971 eruptions (2002-2003 eruption, NE-Rift, Ferlito et al. 2010 and Giacomoni et al. 2012) and b) the High-K (high potassium contents) that, how displayed in this work and in Ferlito and Lanzafame (2010), is prevalent in post-1971 eruptions and in some AAV, Ellittico and pre-1971 eruptive events (Fig. 10.1.5). The two reconstructed primary end-members have 1.41 and 1.64 $K_2O$ wt% respectively, with a difference in the original content of about 0.25. Melt inclusions reflect the just mentioned situation except for Collins et al. (2011) data, that show too high $K_2O$ wt% values for the same degree of primitivity. In the other variation diagrams, primary reconstructed magmas represent realistic composition for the Etnean differentiation trends. The calculated values obtained by direct fractionation models are very similar to the real arrival magmas.

Avarage fractionation modeling percentages from the primary (real for tholeiites and reconstructed for alkaline series) to the evolved compositions (Table 4) show similar relative proportions for phases of the alkaline suites. Tholeiites are the most primitive and include the separation of orthopyroxene and Cr-spinel.

AAV, Ellittico and pre-1971 Recent Mongibello display similar amount of fractionated gabbroic material without considerable difference in the relative percentages of the mineralogical phases. Separated olivine ranges from 47.2 to 52.2%, clinopyroxene from 18.7 to 22.8%, plagioclase from 15.5 to 19.9% and Ti-Mt from 11.4 to 14.2%. Post-1971 model is quite different because the arrival magma (Pm2 from 2002-2003 Eruption, Giacomoni et al. 2012) is less differentiated with a Mg# of 49.8%.

| | **Thol.** | **AVV** | **Ellittico** | **pre-1971** | **post-1971** |
|---|---|---|---|---|---|
| **Mg#** | **72.4 - 52.4** | **66.8 - 34.3** | **66.6 - 42.6** | **66.2 - 35.9** | **67.3 - 49.8** |
| **Ol** | 27.1 | 48.5 | 52.2 | 47.2 | 77.8 |
| **Cpx** | 13.9 | 22.8 | 19.7 | 18.7 | 8.3 |
| **Opx** | 28.9 | - | - | - | - |
| **Plg** | 14.7 | 15.5 | 16.7 | 19.9 | 7.2 |
| **Sp** | 15.4 | 13.1 | 11.4 | 14.2 | 6.7 |
| **Tot** | 100 | 100 | 100 | 100 | 100 |
| **Tot fraz. %** | **53.1** | **43.1** | **40.9** | **52.16** | **26.1** |

**Table 4 –** Summary of the complete fractionation models (from the primary reconstructed magma to the evolved term) for each Etnean evolutionary period.

## 11.2 TRACE ELEMENTS FRACTIONATION MODELING

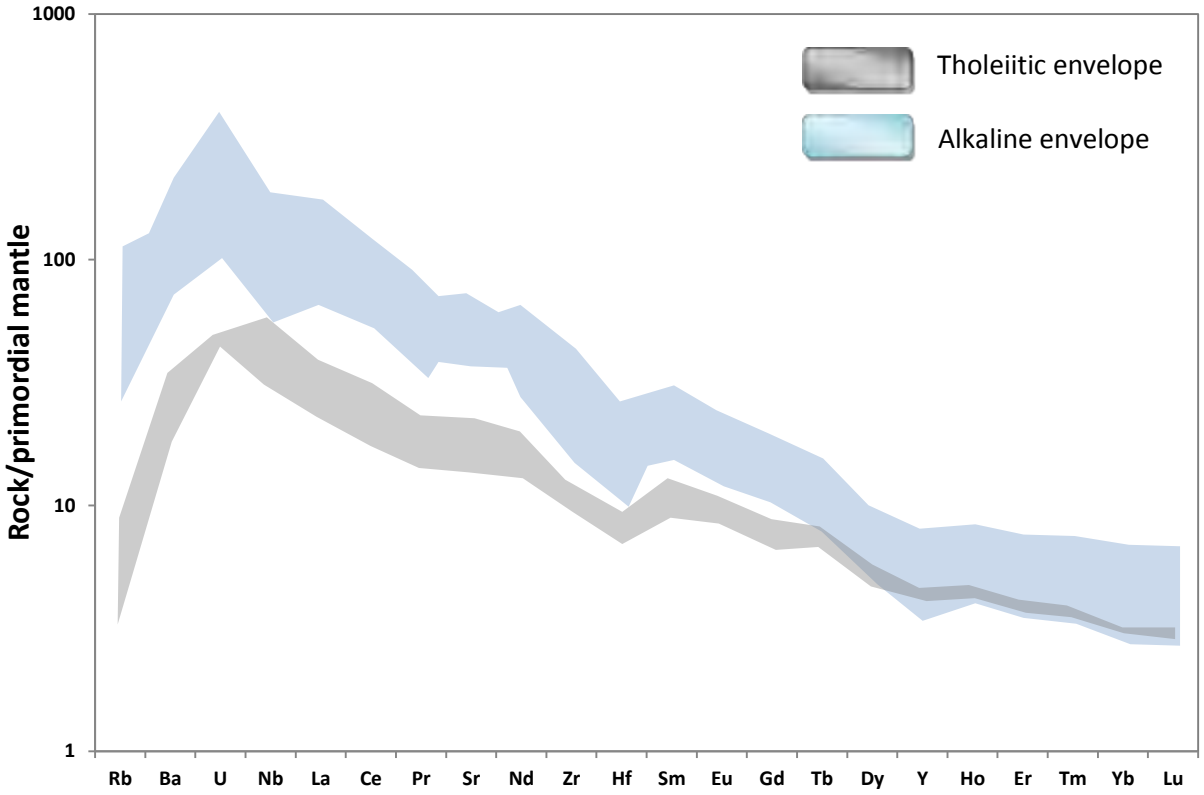


**Fig.10.2.1 –**Trace element patterns of primary (reconstructed), primitive (real) and evolved (real and calculated) magmas

Trace elements fractionation modeling was performed for both backward and direct models starting always from the primitive real magma. Direct mass balance fractionation models took into account the following formula $C_l=C_0*F^{(D-1)}$ (explanations in chapter 10.1) and Kd for olivine, clinopyroxene, orthopyroxene plagioclase and spinel were selected from GERM Database (http://earthref.org/GERM/) referring mainly to Villemant et al. (1981), Wood and Trigila (2001), Adam and Green (2006) and Aigner-torres et al. (2007). "F", the residual melt percentage and "D", the total weighted partition coefficients, were calculated using the values obtained from major elements fractionation models. For backward fractionations always Rayleigh mass balance fractionation models were used but starting from known $C_l$ values (primitive real magmas) and with $C_o$ as incognita. In this case $C_o$ represents the primary, undifferentiated composition. Fig. 10.2.1 summarizes all trace elements patterns obtained for each Etnean magmatic series. Observing the diagram is evident the usual distinction between tholeiitic and alkaline terms, specially for the different degree of fractionation shown. Because

the difficulties to distinguish the modeled compositions, each magmatic series well be discussed and described separately.

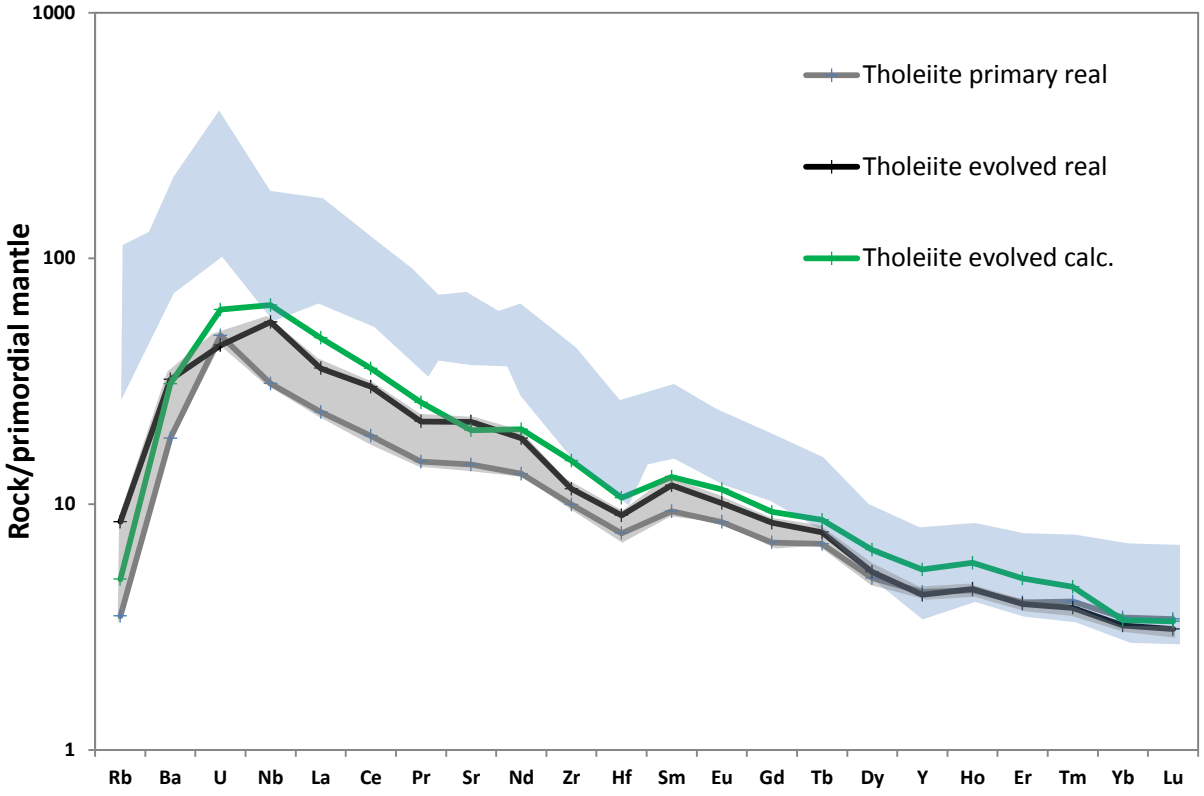

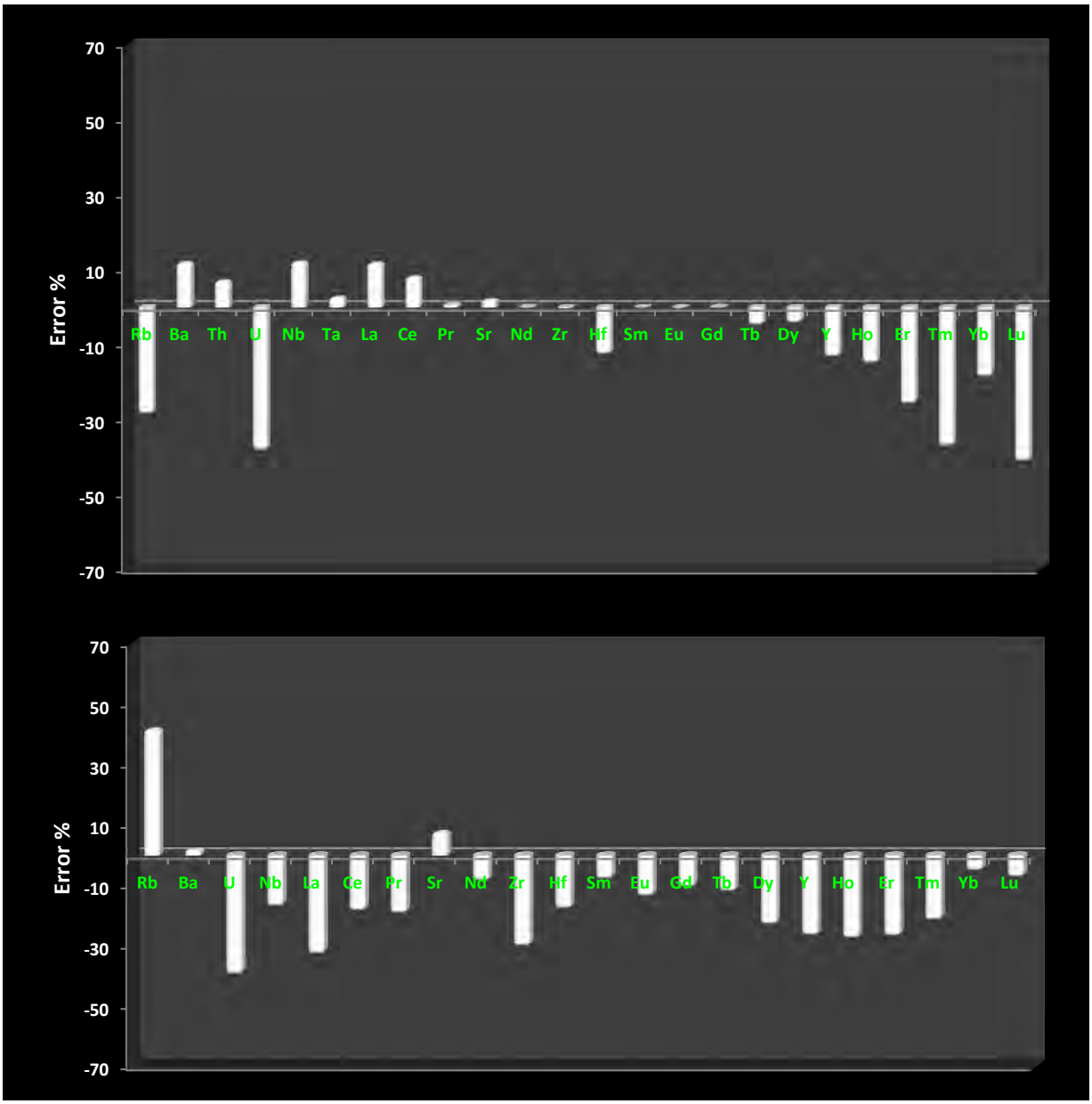


**Fig. 10.2.2 –** a) Trace Element patterns of Tholeiites and b) histograms of error percentages from fractionation models (From ET4 to ET6 and from ET6 to ET9).

### *Tholeiites*

Tholeiitic modeling starts from ET4, that represents a primitive and primary magma with 72.38% Mg# (Table 4 and 5), which correspond to an equilibrium olivine = 89.7%. For this reason it didn't necessitate of a backward mass balance calculation but only of a direct one to reach the evolved term ET9 (it was developed by using an intermediate step, from ET4 to ET6 and from ET6 to ET9, with the aim to obtain a better representation of the complete fractionation). In Fig. 10.2.2a the comparison between trace element patterns of the arrival magmas, both real and calculated are compared. The modeled data fit quite well with the real composition except for Rb, U, La, Zr and some REE. Blue and grey areas include all analyzed

samples distinguished between tholeiitic and alkaline products. Fig.10.2.2b evidences low average error percentages of the modeled data except for previous mentioned elements that reach 41.6%. These error percentages are in absolute value the lowest obtained by numerous combinations between Kd values from GERM database.

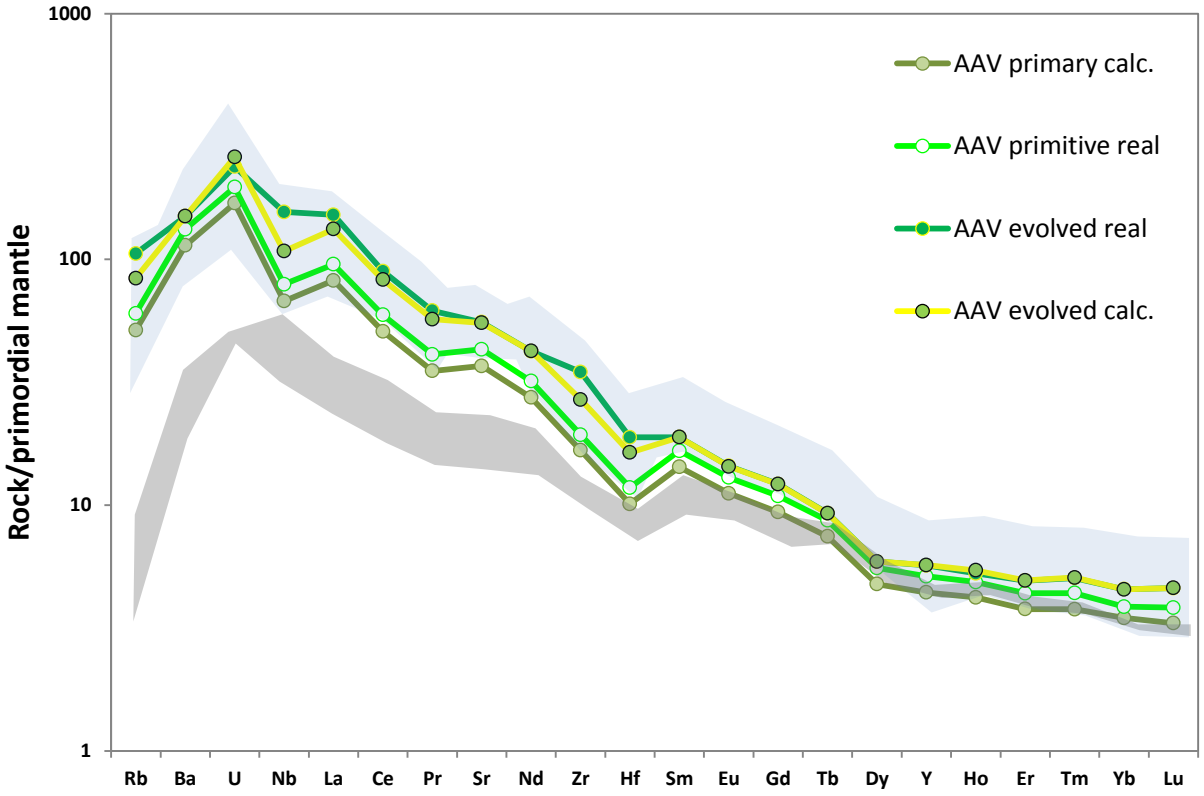

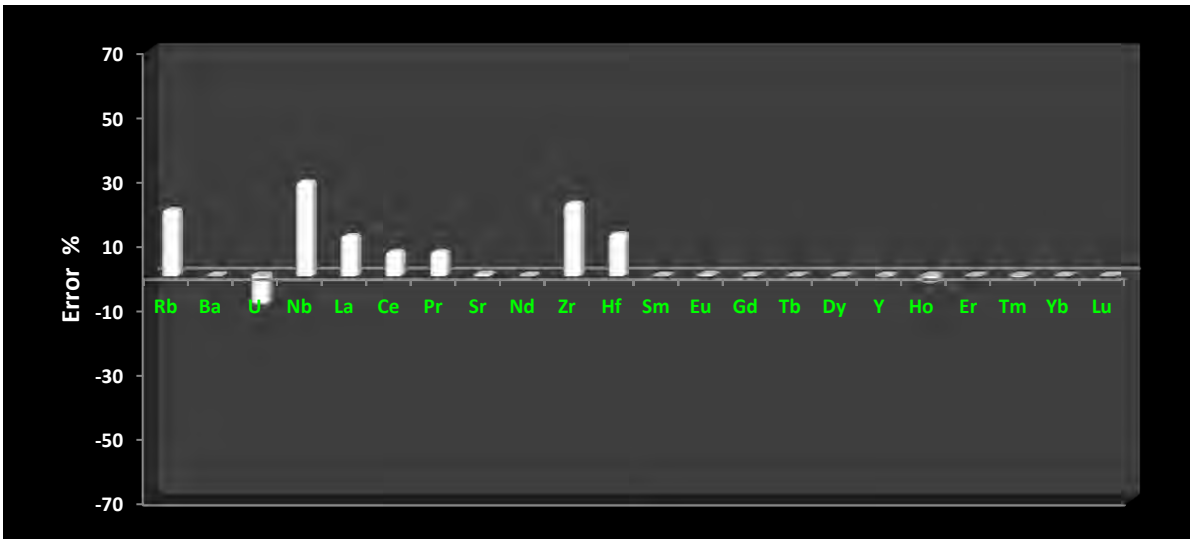


**Fig. 10.2.3 –** a) Trace Element patterns of AVV lavas and b) histogram of error percentages from fractionation models.

### *AAV*

AAV models show a primary reconstructed magma that plots at the base of the alkaline envelope and follows the primitive real sample (ET39, Mg# = 54.36%) pattern (Fig. 10.2.3a). Evolved real (ET36) and calculated terms (ET 36 calc., Table 6 and 7) are very similar, proving the goodness of Rayleigh mass balance fractionation models: within the set of 22 trace elements the largest difference is noted for Nb, Zr and Rb (29.4, 22.7 and 20.7% respectively) (Fig. 10.2.3b). Calculated values have concentration lower than real ones. This is the best result obtained by many attempts with the lowest Kd values founded (GERM Database).

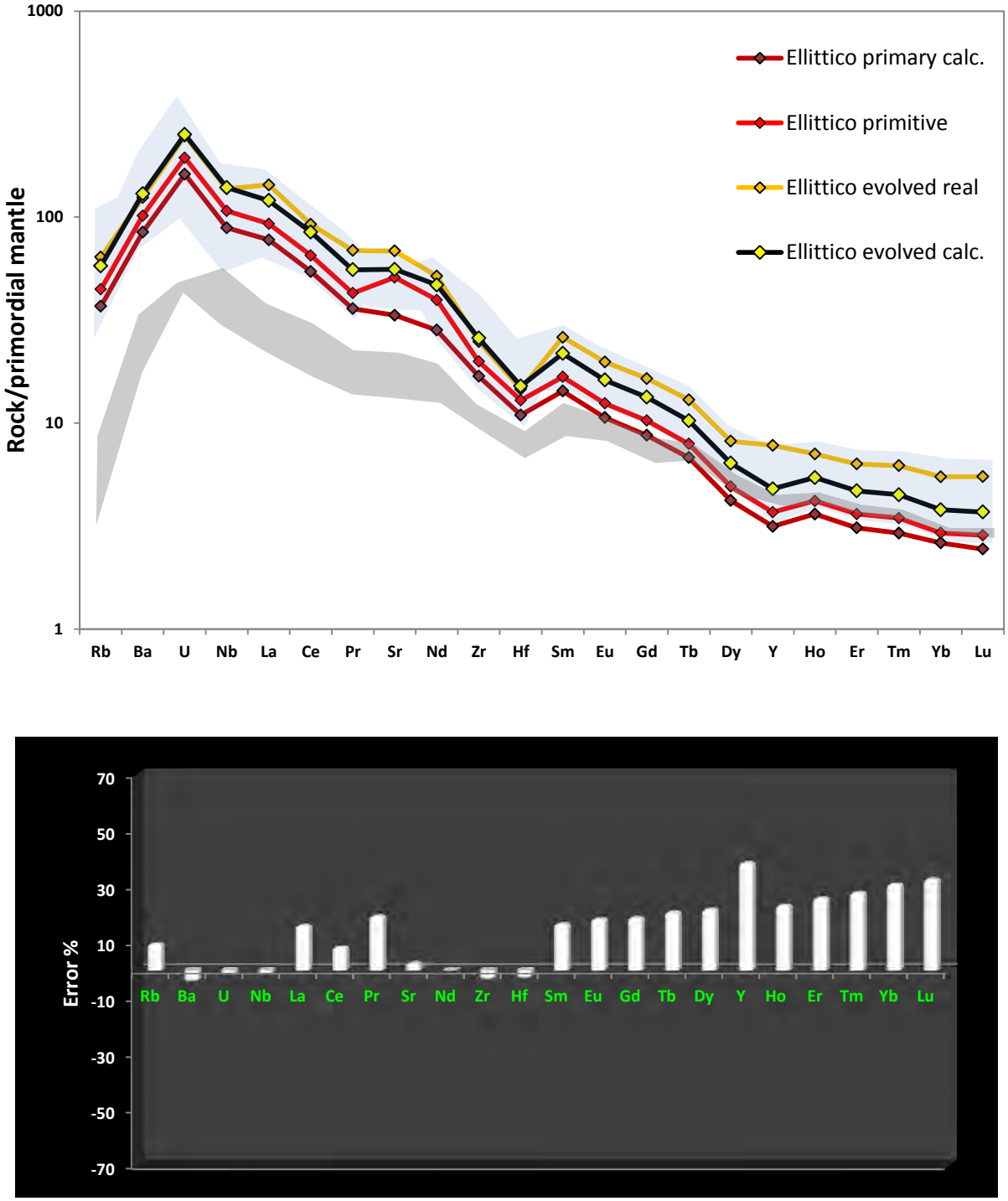


**Fig. 10.2.4 –** a) Trace Element patterns of Ellittico lavas and b) histogram of error percentages from fractionation models.

***Ellittico***

Fig. 10.2.4a displays the trace elements patterns for Ellittico modeled samples, with the primary calculated magma (ET52, Mg# = 50.9%) that plots at the base of the alkaline blue area (as in AAV, see Fig. 10.2.3a). It well represents an un-fractionated magma that could be considered as the eutectic composition of the Etnean system during the Ellittico evolutionary period (Table 4 and 5). Observing the real (ET12) and calculated (ET12 calc.) arrival samples of the direct fractionation, is evident a good matching for LILE and HFSE (errors under 15%), whereas REE are quite different. This is shown in fig. 10.2.4b, where relative percentages errors for REE reaches up 39.5% (Y). The calculated content of Yttrium and other REE values are lower than final ET12 real concentrations by using Rayleigh mass balance fractionation model. It does not reduce the goodness of calculations because absolute values differences never exceed 13.6 ppm.

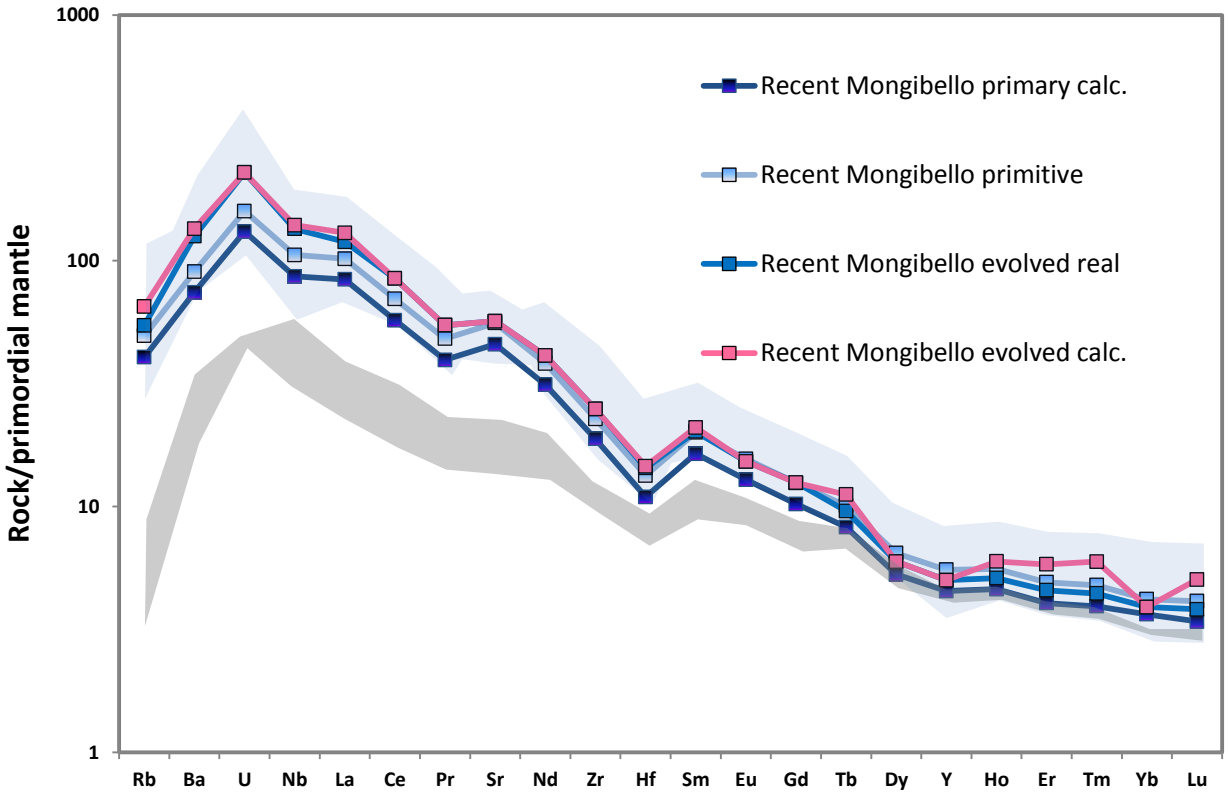

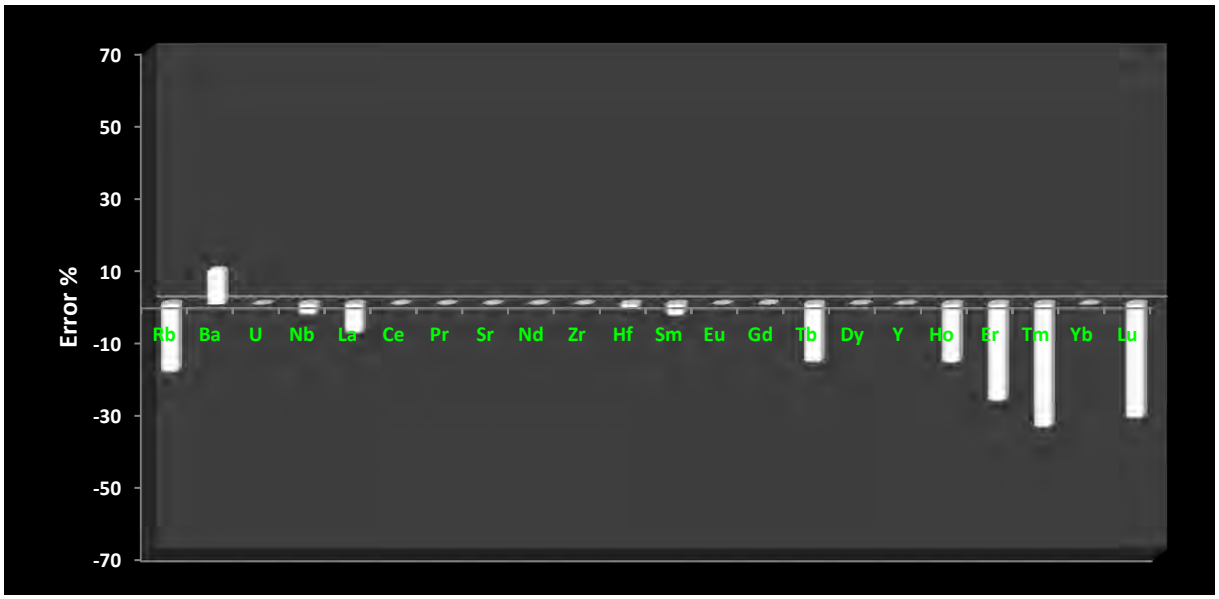


**Fig. 10.2.5 –** a) Trace Element patterns of pre-1971 Recent Mongibello lavas and b) histogram of error percentages from fractionation models.

### *Pre-1971 Recent Mongibello*

Pre-1971 Recent Mongibello calculations, started from the primitive real composition of ET22 (Mg# = 47.5%) and by means of a backward mass balance fractionation model provided a primary magma (Table 4 and 5) that, as well as for the previous described suites (AAV and Ellittico), is located at the bottom of the alkaline envelope (Fig. 10.2.5a). His trend reflects exactly the pattern of the starting magma. Direct fractionation, from ET22 to ET24, gave calculated values that match well with the real concentrations and confirm again the goodness of the modeling. Within the trace elements set, the largest differences are noted for Tm (-34.7%), Lu (-32.2%), Er (-27.5%), Ho (-16.9%), Tb (-16.7%) and Rb (-19.5%) that in absolute values <7 ppm (Rb, Table 5; Fig. 10.2.5b). In this case calculated contents always exceed the real arrival concentrations. All attempted combinations between Kd values does not give lower errors.

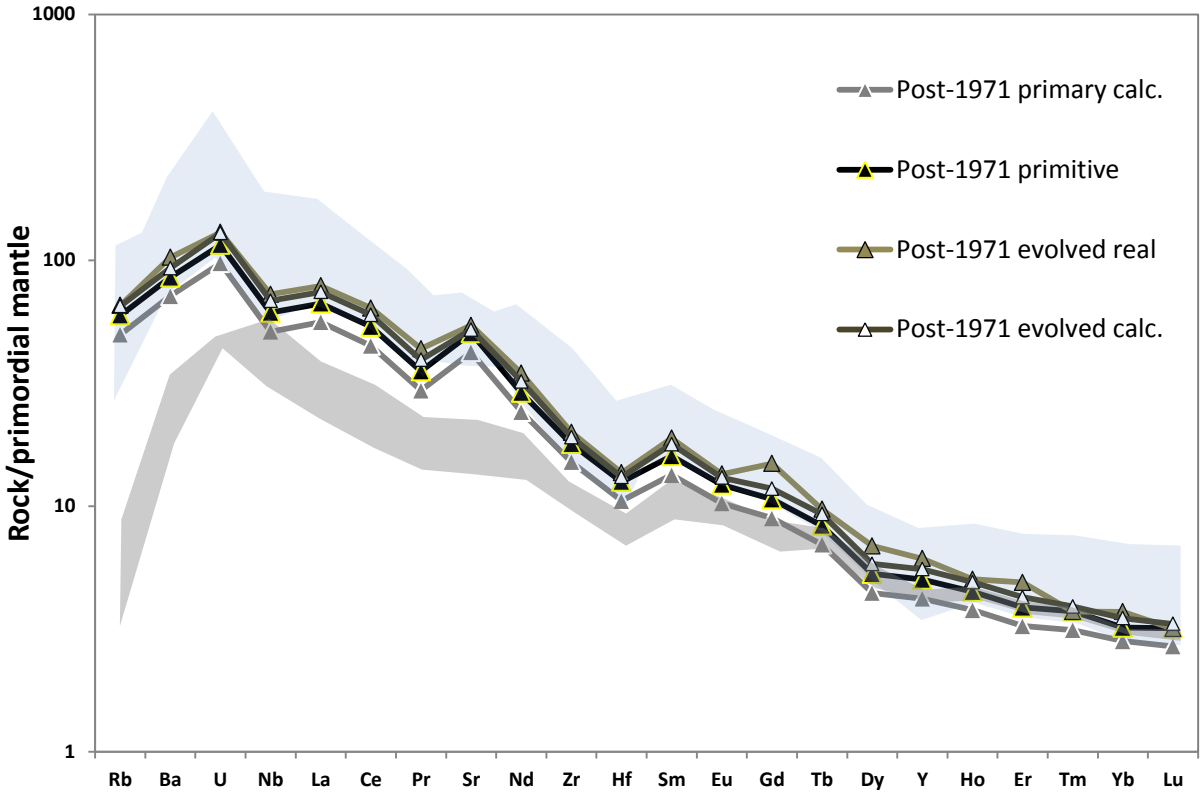


**Fig. 10.2.6** –Trace Element patterns of post-1971 Recent Mongibello lavas.

### *Post-1971 Recent Mongibello*

In this work, to obtain the post-1971 primary magma and compare it with others from AVV, Ellittico and pre-1971 Recent Mongibello, only the backward mass balance fractionation model was developed (Table 4 and 5). The direct differentiation model from the primitive real term Bg1 (primitive in Fig. 10.2.6; Mg# = 53.7%) to the evolved real and calculated Pm2 (evolved real in Fig. 10.2.6; Mg# = 47.85%) was taken from Giacomoni et al. (2012). The first observation, from Fig. 10.2.6, is about the less evolved features of the arrival magma respect to the prievious period models, and it is reflected in the lower trace elements concentrations (Pm2 is located at the base of the blue alkaline area). The choice of Pm2 end-member is related to the absence of a more differentiated term in Mt. Etna 2002-2003 Eruption. In general post-1971 products are more primitive than those of the early magmatic stages as was described in chapter "Whole-rock Geochemistry".

Error percentages, between real and calculated trace elements contents of the arrival magma, are always very low save Gd (24.7%) and Dy (20.1%) (Giacomoni et al. 2012).

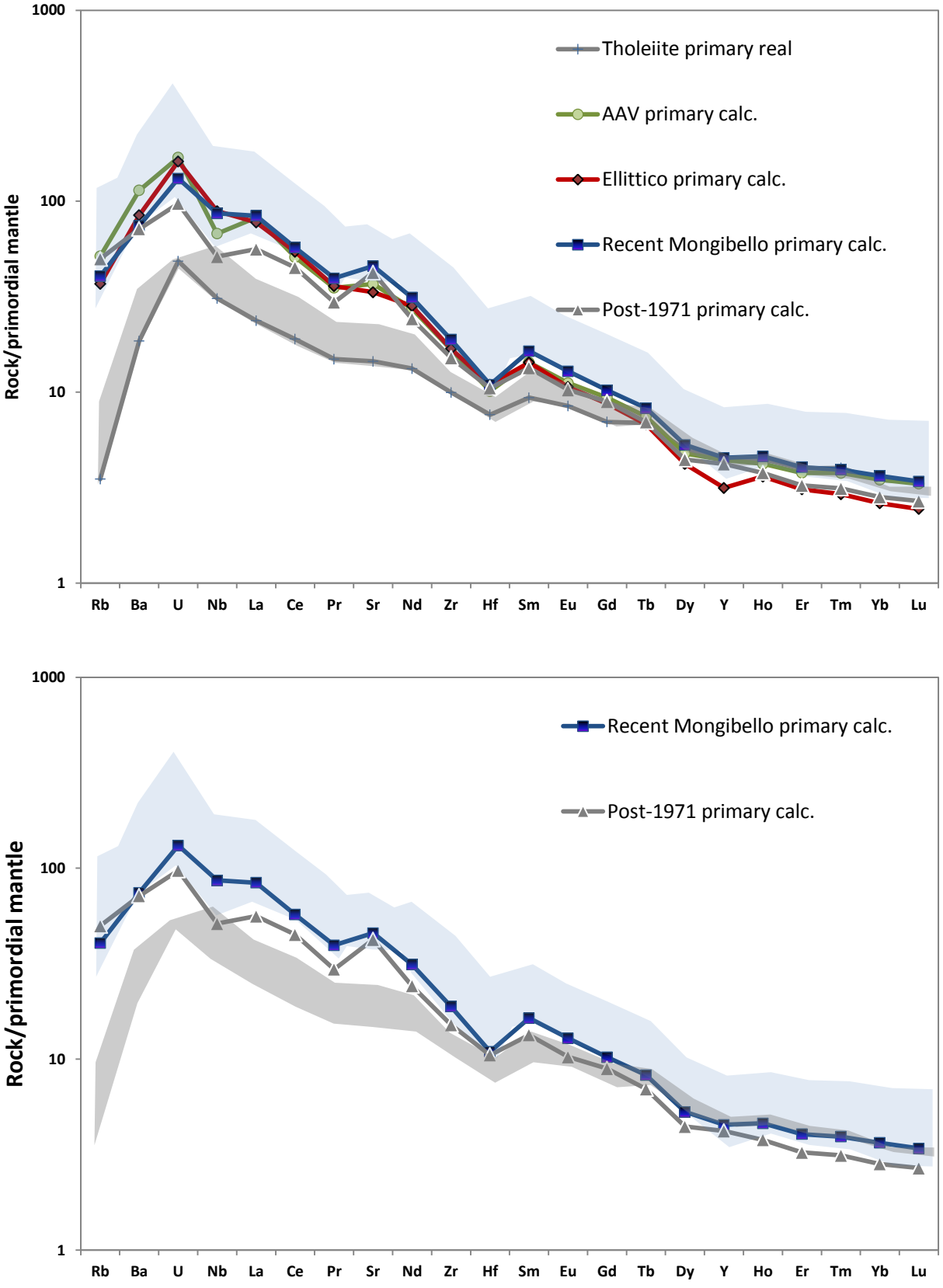


**Fig. 10.2.7** – a) Trace Element patterns of the five primary reconstructed magmas and b) comparison between pre- and post-1971 primary, calculated compositions.

In order to compare the geochemical features of the source of the different primary magmas they are plotted in Fig. 10.2.7. The tholeiitic and alkaline envelopes are also reported for comparison (Fig. 10.2.7). The primary eutectic compositions are less fractionated than the analyzed samples and follow the same trend. The comparison between pre- and post-1971 primary magmas evidences a more marked negative spike in Nb and positive in La for the post-1971 end member. These data will be integrated with partial melting models (Chapter "Melt Modeling") to constrain the Etnean mantle source features and propose a hypothesis for the debated nature of the post-1971 shifting to K-alkaline terms.

**Table 5 -Backward and direct mass balance fractionation models**

| | Backward fract. C.a.a. | | Backward Fract. Ellittico | |
|---|---|---|---|---|
| | **Starting magma ET39** | **Arrival magma primary ET39** | **Starting magma ET52** | **Arrival magma primary ET52** |
| **$SiO_2$** | 54.5 | 52.6 | 50.1 | 48.8 |
| **$TiO_2$** | 1.30 | 1.13 | 1.70 | 1.47 |
| **$Al_2O_3$** | 17.0 | 14.8 | 18.1 | 15.4 |
| **$FeO_{tot}$** | 7.03 | 8.88 | 8.48 | 9.88 |
| **MnO** | 0.14 | 0.16 | 0.16 | 0.14 |
| **MgO** | 4.03 | 8.85 | 4.24 | 9.77 |
| **CaO** | 8.88 | 7.80 | 10.1 | 8.92 |
| **$Na_2O$** | 4.74 | 4.12 | 4.78 | 4.06 |
| **$K_2O$** | 1.88 | 1.64 | 1.77 | 1.50 |
| **$P_2O_5$** | 0.50 | 0.00 | 0.54 | 0.00 |
| **Tot** | 100 | 100 | 100 | 100 |
| **Mg#** | 54.4 | 66.8 | 50.9 | 66.6 |
| | | **% abs.** | | **% abs.** |
| | **Ol** | **96.9** | **Ol** | **87.0** |
| | **Cpx** | **3.13** | **Cpx** | **13.0** |
| | **Plg** | **-** | **Plg** | **-** |
| | **Ti-mt** | **-** | **Ti-mt** | **-** |
| | **F%** | **15.0** | **F%** | **18.0** |
| | | **Rayleigh model** | | **Rayleigh model** |
| **Rb** | 38.3 | 32.7 | 28.3 | 23.4 |
| **Ba** | 927 | 797 | 710 | 590 |
| **U** | 4.13 | 3.55 | 4.08 | 3.40 |
| **Nb** | 56.4 | 48 | 76.4 | 63.3 |
| **La** | 65.6 | 56 | 63.7 | 53.3 |
| **Ce** | 106 | 90 | 116 | 97 |
| **Pr** | 11.3 | 9.7 | 11.8 | 9.9 |
| **Sr** | 909 | 778 | 849 | 704 |
| **Nd** | 43.3 | 37.1 | 45.3 | 38.3 |
| **Zr** | 217 | 187 | 223 | 189 |
| **Hf** | 3.64 | 3.12 | 3.98 | 3.38 |
| **Sm** | 7.39 | 6.35 | 7.45 | 6.3 |
| **Eu** | 2.18 | 1.88 | 2.10 | 1.79 |
| **Gd** | 6.50 | 5.59 | 6.13 | 5.20 |
| **Tb** | 0.94 | 0.81 | 0.86 | 0.73 |
| **Dy** | 4.09 | 3.52 | 3.63 | 3.10 |
| **Y** | 23.4 | 20.1 | 16.8 | 14.3 |
| **Ho** | 0.80 | 0.69 | 0.69 | 0.59 |
| **Er** | 2.10 | 1.81 | 1.73 | 1.49 |
| **Tm** | 0.32 | 0.28 | 0.26 | 0.22 |
| **Yb** | 1.91 | 1.71 | 1.44 | 1.29 |
| **Lu** | 0.28 | 0.25 | 0.21 | 0.18 |

| | Backward fract. Pre-1971 | | Backward fract. Post-1971 | |
|---|---|---|---|---|
| | **Starting magma ET22** | **Arrival magma primary ET22** | **Starting magma Bg1** | **Arrival magma primary Bg1** |
| **$SiO_2$** | 48.5 | 47.2 | 49.87 | 48.5 |
| **$TiO_2$** | 1.62 | 1.36 | 1.68 | 1.43 |
| **$Al_2O_3$** | 18.5 | 15.5 | 17.25 | 14.7 |
| **$FeO_{tot}$** | 9.70 | 11.0 | 8.72 | 10.3 |
| **MnO** | 0.19 | 0.16 | 0.17 | 0.16 |
| **MgO** | 4.23 | 10.71 | 5.02 | 10.5 |
| **CaO** | 11.2 | 9.39 | 10.8 | 9.23 |
| **$Na_2O$** | 3.97 | 3.32 | 4.09 | 3.49 |
| **$K_2O$** | 1.68 | 1.41 | 1.92 | 1.64 |
| **$P_2O_5$** | 0.38 | 0.00 | 0.50 | 0.00 |
| **Tot** | 100 | 100 | 100 | 100 |
| **Mg#** | 47.5 | 66.2 | 53.7 | 67.3 |
| | | **% abs.** | | **% abs.** |
| | **Ol** | **100** | **Ol** | **100** |
| | **Cpx** | **-** | **Cpx** | **-** |
| | **Plg** | **-** | **Plg** | **-** |
| | **Ti-mt** | **-** | **Ti-mt** | **-** |
| | **F%** | **19.0** | **F%** | **17.0** |
| | | **Rayleigh model** | | **Rayleigh model** |
| **Rb** | 31.4 | 25.7 | 37.9 | 31.7 |
| **Ba** | 631 | 519 | 595 | 500 |
| **U** | 3.35 | 2.76 | 2.43 | 2.04 |
| **Nb** | 75.3 | 61.6 | 43.7 | 36.5 |
| **La** | 70.0 | 57.6 | 45.9 | 38.5 |
| **Ce** | 124 | 102 | 95.4 | 79.7 |
| **Pr** | 13.3 | 10.9 | 9.8 | 8.2 |
| **Sr** | 1179 | 965 | 1067 | 892 |
| **Nd** | 51.7 | 42.4 | 39.1 | 32.7 |
| **Zr** | 255 | 211 | 201 | 169 |
| **Hf** | 4.13 | 3.38 | 3.88 | 3.24 |
| **Sm** | 8.88 | 7.28 | 7.10 | 5.94 |
| **Eu** | 2.63 | 2.16 | 2.05 | 1.73 |
| **Gd** | 7.44 | 6.10 | 6.35 | 5.32 |
| **Tb** | 1.09 | 0.89 | 0.90 | 0.75 |
| **Dy** | 4.76 | 3.90 | 3.91 | 3.27 |
| **Y** | 25.1 | 20.6 | 22.9 | 19.1 |
| **Ho** | 0.91 | 0.76 | 0.73 | 0.62 |
| **Er** | 2.36 | 1.94 | 1.86 | 1.56 |
| **Tm** | 0.35 | 0.29 | 0.28 | 0.23 |
| **Yb** | 2.07 | 1.80 | 1.58 | 1.39 |
| **Lu** | 0.31 | 0.25 | 0.24 | 0.20 |

| | Direct fract. Thol. 1° step | | | Direct fract. Thol. 2° step | | |
|---|---|---|---|---|---|---|
| | Starting magma ET4 | Arrival magma ET6 | Calculated magma | Starting magma ET6 | Arrival magma ET9 | Calculated magma |
| $SiO_2$ | 47.6 | 51.0 | 51.1 | 51.0 | 51.2 | 51.1 |
| $TiO_2$ | 1.47 | 1.76 | 1.79 | 1.76 | 1.67 | 2.20 |
| $Al_2O_3$ | 13.5 | 13.6 | 13.7 | 13.6 | 16.2 | 16.1 |
| $FeO_{tot}$ | 11.8 | 10.5 | 10.6 | 10.5 | 10.8 | 10.6 |
| MnO | 0.15 | 0.12 | 0.15 | 0.12 | 0.15 | 0.09 |
| MgO | 14.9 | 10.9 | 10.9 | 10.9 | 5.70 | 5.71 |
| CaO | 8.07 | 8.44 | 8.50 | 8.44 | 9.78 | 9.64 |
| $Na_2O$ | 2.16 | 2.87 | 2.64 | 2.87 | 3.85 | 3.59 |
| $K_2O$ | 0.28 | 0.34 | 0.36 | 0.34 | 0.40 | 0.46 |
| $P_2O_5$ | 0.17 | 0.34 | 0.22 | 0.34 | 0.27 | 0.47 |
| Tot | 100 | 100 | 100 | 100 | 100 | 100 |
| Mg# | 72.4 | 68.3 | | 68.3 | 52.4 | |

| | % abs. | % rel. | | % abs. | % rel. |
|---|---|---|---|---|---|
| Ol | 9.50 | 36.4 | Ol | 4.88 | 18.1 |
| Cpx | 5.20 | 19.9 | Cpx | 2.20 | 8.15 |
| Opx | 0.65 | 2.49 | Opx | 14.7 | 54.4 |
| Plg | 2.70 | 10.3 | Plg | 5.10 | 18.9 |
| Cr-sp | 8.05 | 30.8 | Cr-sp | 0.12 | 0.44 |
| F% | 26.1 | 100 | F% | 27.0 | 100 |
| $r^2$=0.30 | | | $r^2$=0.69 | | |

| | Rayleigh model | | | | Rayleigh model | | | |
|---|---|---|---|---|---|---|---|---|
| | ET4 | ET6 | Calculated | % err. | ET6 | ET9 | Calculated | % err. |
| Rb | 2.22 | 2.29 | 2.95 | -28.6 | 2.29 | 5.38 | 3.14 | 41.6 |
| Ba | 130 | 199 | 175 | 11.9 | 199 | 225 | 220 | 1.96 |
| U | 1.02 | 0.98 | 1.35 | -38.3 | 0.98 | 0.93 | 1.30 | -39.6 |
| Nb | 22.1 | 34.0 | 29.9 | 12.1 | 34.0 | 39.3 | 46.0 | -17.1 |
| La | 16.3 | 25.0 | 22.0 | 11.8 | 25.0 | 24.5 | 32.6 | -32.9 |
| Ce | 33.6 | 49.5 | 45.5 | 8.07 | 49.5 | 53.3 | 63.3 | -18.7 |
| Pr | 4.11 | 5.60 | 5.56 | 0.77 | 5.60 | 5.99 | 7.16 | -19.5 |
| Sr | 306 | 423 | 414 | 2.02 | 423 | 457 | 422 | 7.73 |
| Nd | 18.0 | 23.5 | 23.4 | 0.16 | 23.5 | 25.1 | 27.3 | -8.77 |
| Zr | 112 | 135 | 135 | -0.21 | 135 | 129 | 168 | -30.3 |
| Hf | 2.35 | 2.53 | 2.85 | -12.8 | 2.53 | 2.78 | 3.28 | -17.9 |
| Sm | 4.16 | 5.11 | 5.11 | 0.02 | 5.11 | 5.30 | 5.73 | -8.12 |
| Eu | 1.42 | 1.79 | 1.79 | -0.06 | 1.79 | 1.70 | 1.93 | -13.8 |
| Gd | 4.17 | 5.09 | 5.08 | 0.19 | 5.09 | 5.00 | 5.54 | -10.8 |
| Tb | 0.74 | 0.85 | 0.89 | -5.01 | 0.85 | 0.83 | 0.93 | -12.3 |
| Dy | 3.69 | 3.93 | 4.10 | -4.38 | 3.93 | 3.91 | 4.81 | -23.1 |
| Y | 20.0 | 20.2 | 23.0 | -13.4 | 20.2 | 19.5 | 24.7 | -26.8 |
| Ho | 0.73 | 0.75 | 0.86 | -15.1 | 0.75 | 0.74 | 0.95 | -27.8 |

| | ET4 | ET6 | Calculated | % err. | ET6 | ET9 | Calculated | % err. |
|---|---|---|---|---|---|---|---|---|
| **Er** | 1.91 | 1.87 | 2.35 | -25.9 | 1.87 | 1.88 | 2.39 | -27.0 |
| **Tm** | 0.30 | 0.27 | 0.37 | -37.2 | 0.27 | 0.28 | 0.34 | -21.7 |
| **Yb** | 1.71 | 1.52 | 1.81 | -18.8 | 1.52 | 1.58 | 1.67 | -5.37 |
| **Lu** | 0.25 | 0.22 | 0.31 | -41.2 | 0.2 | 0.2 | 0.2 | -7.50 |

| | Direct fract. C.a.a. | | | Direct fract. Ellittico | | |
|---|---|---|---|---|---|---|
| | Starting magma ET39 | Arrival magma ET36 | Calculated magma | Starting magma ET52 | Arrival magma ET12 | Calculated magma |
| **$SiO_2$** | 54.5 | 59.1 | 59.2 | 50.1 | 51.0 | 51.2 |
| **$TiO_2$** | 1.30 | 0.91 | 0.93 | 1.70 | 1.44 | 1.70 |
| **$Al_2O_3$** | 17.0 | 19.0 | 19.1 | 18.1 | 19.1 | 19.0 |
| **$FeO_{tot}$** | 7.03 | 4.09 | 4.17 | 8.48 | 7.05 | 7.10 |
| **MnO** | 0.14 | 0.13 | 0.12 | 0.16 | 0.15 | 0.16 |
| **MgO** | 4.03 | 1.03 | 1.09 | 4.24 | 2.52 | 2.50 |
| **CaO** | 8.88 | 5.81 | 5.76 | 10.1 | 10.1 | 10.0 |
| **$Na_2O$** | 4.74 | 6.56 | 6.36 | 4.78 | 5.71 | 5.30 |
| **$K_2O$** | 1.88 | 2.95 | 2.59 | 1.77 | 2.09 | 2.22 |
| **$P_2O_5$** | 0.50 | 0.44 | 0.70 | 0.54 | 0.85 | 0.70 |
| **Tot** | 100 | 100 | 100 | 100 | 100 | 100 |
| **Mg#** | 54.4 | 34.3 | | 50.9 | 42.6 | |
| | | **% abs.** | **% rel.** | | **% abs.** | **% rel.** |
| | **Ol** | **1.94** | **6.91** | **Ol** | **4.23** | **18.4** |
| | **Cpx** | **15.6** | **55.4** | **Cpx** | **5.95** | **25.9** |
| | **Plg** | **7.00** | **24.9** | **Plg** | **11.0** | **48.0** |
| | **Ti-mt** | **3.60** | **12.8** | **Ti-mt** | **1.75** | **7.63** |
| | **F%** | **28.1** | **100** | **F%** | **22.9** | **100** |
| | **$r^2$=0.51** | | | **$r^2$=0.57** | | |

| | | Rayleigh model | | | | Rayleigh model | | |
|---|---|---|---|---|---|---|---|---|
| | ET39 | ET36 | Calculated | % err. | ET52 | ET12 | Calculated | % err. |
| **Rb** | 38.3 | 67.1 | 53.2 | 20.7 | 28.3 | 40.6 | 36.7 | 9.44 |
| **Ba** | 927 | 1047 | 1046 | 0.05 | 710 | 869 | 908 | -4.50 |
| **U** | 4.13 | 5.00 | 5.48 | -9.53 | 4.08 | 5.19 | 5.29 | -1.88 |
| **Nb** | 56.4 | 111 | 77.1 | 30.7 | 76.4 | 97.8 | 99.2 | -1.38 |
| **La** | 65.6 | 104 | 91.2 | 12.6 | 63.7 | 98.5 | 82.7 | 16.0 |
| **Ce** | 106 | 159 | 147 | 7.64 | 116 | 164 | 150 | 8.26 |
| **Pr** | 11.3 | 17.1 | 15.8 | 7.63 | 11.8 | 19.0 | 15.3 | 19.4 |

| | ET39 | ET36 | Calculated | % err. | ET52 | ET12 | Calculated | % err. |
|---|---|---|---|---|---|---|---|---|
| **Sr** | 909 | 1171 | 1165 | 0.56 | 1075 | 1444 | 1176 | 18.5 |
| **Nd** | 43.3 | 57.3 | 57.4 | -0.14 | 53.6 | 70.1 | 63.4 | 9.49 |
| **Zr** | 217 | 390 | 301 | 22.7 | 223 | 279 | 289 | -3.76 |
| **Hf** | 3.64 | 5.83 | 5.06 | 13.2 | 3.98 | 4.52 | 4.67 | -3.32 |
| **Sm** | 7.39 | 8.40 | 8.39 | 0.09 | 7.45 | 11.6 | 9.7 | 16.6 |
| **Eu** | 2.18 | 2.43 | 2.41 | 0.49 | 2.10 | 3.33 | 2.72 | 18.4 |
| **Gd** | 6.50 | 7.26 | 7.25 | 0.22 | 6.13 | 9.80 | 7.96 | 18.8 |
| **Tb** | 0.94 | 1.00 | 1.00 | 0.10 | 0.86 | 1.40 | 1.11 | 20.8 |
| **Dy** | 4.09 | 4.35 | 4.35 | 0.04 | 3.63 | 6.02 | 4.70 | 21.8 |
| **Y** | 23.4 | 25.9 | 25.9 | -0.31 | 16.8 | 35.4 | 21.8 | 38.5 |
| **Ho** | 0.80 | 0.87 | 0.89 | -2.84 | 0.69 | 1.16 | 0.89 | 23.2 |
| **Er** | 2.10 | 2.37 | 2.37 | -0.25 | 1.73 | 3.04 | 2.25 | 25.9 |
| **Tm** | 0.32 | 0.37 | 0.38 | -0.39 | 0.26 | 0.46 | 0.33 | 27.8 |
| **Yb** | 1.91 | 2.24 | 2.24 | 0.09 | 1.44 | 2.70 | 1.87 | 30.8 |
| **Lu** | 0.28 | 0.34 | 0.34 | -0.07 | 0.21 | 0.41 | 0.27 | 32.6 |

| | Direct fract. Pre-1971 | | | Direct fract. Post-1971 | | |
|---|---|---|---|---|---|---|
| | **Starting magma ET22** | **Arrival magma ET24** | **Calculated magma** | **Starting magma Bg1** | **Arrival magma Pm2** | **Calculated magma** |
| **$SiO_2$** | 48.5 | 51.2 | 51.2 | 49.9 | 50.4 | 50.6 |
| **$TiO_2$** | 1.62 | 1.50 | 1.36 | 1.68 | 1.69 | 1.68 |
| **$Al_2O_3$** | 18.5 | 20.1 | 20.1 | 17.3 | 17.9 | 17.9 |
| **$FeO_{tot}$** | 9.70 | 7.21 | 7.21 | 8.72 | 8.20 | 8.29 |
| **MnO** | 0.19 | 0.16 | 0.20 | 0.17 | 0.17 | 0.17 |
| **MgO** | 4.23 | 1.94 | 1.92 | 5.02 | 4.03 | 4.00 |
| **CaO** | 11.2 | 10.0 | 10.0 | 10.8 | 10.2 | 10.3 |
| **$Na_2O$** | 3.97 | 5.18 | 4.99 | 4.09 | 4.72 | 4.45 |
| **$K_2O$** | 1.68 | 2.06 | 2.45 | 1.92 | 2.08 | 2.11 |
| **$P_2O_5$** | 0.38 | 0.61 | 0.57 | 0.50 | 0.57 | 0.55 |
| **Tot** | 100 | 100 | 100 | 100 | 100 | 100 |
| **Mg#** | 47.5 | 35.9 | | 53.7 | 47.9 | |

| | **% abs.** | **% rel.** | | **% abs.** | **% rel.** |
|---|---|---|---|---|---|
| **Ol** | **2.20** | **6.63** | **Ol** | **1.68** | **18.4** |
| **Cpx** | **12.1** | **36.4** | **Cpx** | **4.80** | **52.7** |
| **Plg** | **14.2** | **42.8** | **Plg** | **1.95** | **21.4** |
| **Ti-mt** | **4.70** | **14.2** | **Ti-mt** | **0.68** | **7.46** |
| **F%** | **33.2** | **100** | **F%** | **9.11** | **100** |
| **$r^2$=0.46** | | | **$r^2$=0.32** | | |

| | | Rayleigh model | | | | Rayleigh model | | |
|---|---|---|---|---|---|---|---|---|
| | **ET22** | **ET24** | **Calculated** | **% err.** | **Bg1** | **Pm2** | **Calculated** | **% err.** |
| **Rb** | 31.4 | 34.6 | 41.4 | -19.5 | 37.9 | 41.6 | 41.4 | 0.48 |
| **Ba** | 631 | 880 | 944 | 9.83 | 595 | 719 | 650 | 9.60 |
| **U** | 3.35 | 4.80 | 4.80 | -0.02 | 2.43 | 2.73 | 2.71 | 0.73 |
| **Nb** | 75.3 | 96.1 | 99.5 | -3.56 | 43.7 | 51.8 | 48.8 | 5.79 |
| **La** | 70.0 | 82.1 | 89.2 | -8.65 | 45.9 | 54.1 | 51.1 | 5.55 |
| **Ce** | 124 | 150 | 150 | 0.05 | 95.4 | 113 | 106 | 6.19 |
| **Pr** | 13.3 | 15.1 | 15.1 | 0.00 | 9.76 | 12.0 | 10.9 | 9.17 |
| **Sr** | 1179 | 1198 | 1197 | 0.02 | 1067 | 1146 | 1103 | 3.75 |
| **Nd** | 51.7 | 55.6 | 55.7 | -0.01 | 39.1 | 47.0 | 43.5 | 7.45 |
| **Zr** | 255 | 279 | 279 | 0.00 | 201 | 224 | 214 | 4.46 |
| **Hf** | 4.13 | 4.44 | 4.51 | -1.60 | 3.88 | 4.22 | 4.06 | 3.79 |
| **Sm** | 8.88 | 8.96 | 9.31 | -3.82 | 7.10 | 8.38 | 7.93 | 5.37 |
| **Eu** | 2.63 | 2.57 | 2.57 | 0.00 | 2.05 | 2.27 | 2.19 | 3.52 |
| **Gd** | 7.44 | 7.46 | 7.45 | 0.13 | 6.35 | 8.87 | 7.02 | 20.9 |
| **Tb** | 1.09 | 1.04 | 1.21 | -16.7 | 0.90 | 1.05 | 1.00 | 4.76 |
| **Dy** | 4.76 | 4.40 | 4.40 | 0.00 | 3.91 | 5.07 | 4.29 | 15.4 |
| **Y** | 25.1 | 22.8 | 22.8 | 0.03 | 22.9 | 27.8 | 25.2 | 9.35 |
| **Ho** | 0.91 | 0.84 | 0.98 | -16.9 | 0.73 | 0.83 | 0.80 | 3.61 |
| **Er** | 2.36 | 2.19 | 2.79 | -27.5 | 1.86 | 2.35 | 2.04 | 13.2 |
| **Tm** | 0.35 | 0.33 | 0.44 | -34.7 | 0.28 | 0.28 | 0.29 | -3.57 |
| **Yb** | 2.07 | 1.92 | 1.92 | -0.01 | 1.58 | 1.83 | 1.73 | 5.46 |
| **Lu** | 0.31 | 0.28 | 0.37 | -32.2 | 0.24 | 0.23 | 0.25 | -8.70 |

# 12. MELTING MODELING

Mt. Etna is one of the most studied volcano in the world, especially in the last 40 years, but nevertheless the nature of his mantle source is still debated because mantle xenoliths have never been found. The scarcity of direct information could be balanced through melt modeling that take into account the reconstructed primary magmas (see "Fractionation modeling" chapter) and the whole-rock and in situ analyses of mantle xenoliths from the near Iblean magmatic province. In this context, Mt. Iblei mantle source, could represent a realistic paragenesis (Mt. Iblei are only about 50 kilometers far), to take into account for comparison. Iblean volcanism in fact is characterized by lavas with different magmatic affinities (as well as Mt. Etna with tholeiitic and alkaline suites) from tholeiitic to nephelinitic. Viccaro and Cristofolini (1998) developed a partial melt model starting from Mt. Spagnolo/Maletto primitive magmas (from literature) with the aim to explain the pre- and post-1971 geochemical variations of emitted lavas. In this work five models were developed, representative of each Etnean periods to constrain the entire magmatic cycle. In addition "primary" and un-fractionated magmas compatible with a direct origin by partial melting processes were used. Only tholeiites show primitive features and do not necessitated of backward reconstructions to obtain the original composition.

### 12.1 MAJOR ELEMENTS MELTING MODELING

These calculations aim at obtaining the estimation of the degrees of partial melting and the modal compositions of the minerals entering the melt to reproduce the primary eutectic etnean magmas. Melting proportions were obtained by least-squares mass balance calculations between the chemical composition of the primary reconstructed lavas and that of the mineralogical phases assumed to be present in the mantle source invoked in the melting process. The refractory hazburgitic residua was obtained in the same way from their modeled chemical composition and their constituent phases. The composition of fertile and residual main peridotite minerals (olivine, orthopyroxene, clinopyroxene, spinel, amphibole and phlogopite) from Iblean mantle xenoliths were taken from Beccaluva et al. (1998).

Mantle Source $S_1$, from Beccaluva et al. (1998), was chosen for the tholeiitic modeling whereas $S_2$ was used for the alkaline suites reconstructions. These mantle sources are linked in Table 6 to the mineral melting proportions (E), the respective restitic hazburgites (R) for distinct partial melting degrees.

This overview lets us to distinguish two main partial-melting regimes for the Etnean magmas one for the productions of tholeiitic magmas and one for the alkaline successive suites. The $S_1$ mantle source generates tholeiitic lavas by partial melting degrees in the order of 16-17%. The calculation shows negative olivine and high positive orthopyroxene and amphibole melting proportions. These values are not so far from what obtained for tholiitic Iblean modeling. Beccaluva et al. (1998), referring to experimental data (Kushiro, 1972; Mysen and Boettcher, 1975; Green, 1976; Hirose and Kawamoto, 1995) hypothesized that these liquids may be generated in the P-T range of 10-20 Kbar and 1100-1200 °C, by melting a fertile lherzolite under hydrated conditions. These melting conditions are consistent with the amphibole dehydration solidus of mantle peridotite ($H_2O$<0.4 wt%) at pressures lower than 28 Kbar and temperatures of 1100-1200 °C (Beccaluva et al., 1998). The $S_2$ peridotitic composition represents the mantle source of AAV, Ellittico and Recent Mongibello products. Primary reconstructed alkaline magmas result to be generated by about 7% of partial melting degree that Is lower than in previous mentioned tholeiitic model. In this case, olivine is still negative in melting proportions but with lower percentages (from -13.7 to -10.3%), whereas less orthopyroxene (22-25.3%) and more clinopyroxene (29.6-31.8%) is necessary to take into account the primary alkaline melt composition. For this alkaline regime, the involvement of spinel in the partial melting is negative and amphibole reaches 55.8%. The largest difference is given by the presence of phlogopite in the alkaline groups melting, which is reflected in the

higher primary $Na_2O$ and $K_2O$ magma contents (Table 6). Comparing pre- and post-1971 partial melting models is shown a higher contribution of phlogopite, from 9.79 to 13.6%, for the more recent primary reconstructed composition. This evidence can justify the different original $K_2O$ wt% contents observed prevalently in the last 40 years products. Respect to the tholeiitic mantle source setting, the alkaline melt-models reflect $SiO_2$ undersaturated conditions due to the increased alkalinity of the source and to the reduced melting degree.

## 12.2 TRACE ELEMENTS MELTING MODELING

Trace elements were elaborated for the two mantle sources $S_1$ and $S_2$, by means of mass balance melt models, using the modal source and calculated eutectic compositions and the obtained partial melting degrees. Composition of the resulting melt was calculated according to the following formula $Cl = Co/(D+F*^{(1-P)})$, where "$C_l$" is the calculated composition of the resulting melt, "$C_o$" is the composition of the starting lherzolite, "F" is the partial melting degree, "D" the total weighted partition coefficients of the peridotites and "P" the total weighted partition coefficients of the primary magmas (Shaw, 1970). Kd used in the calculations were downloaded from the GERM database (http://earthref.org/GERM/).

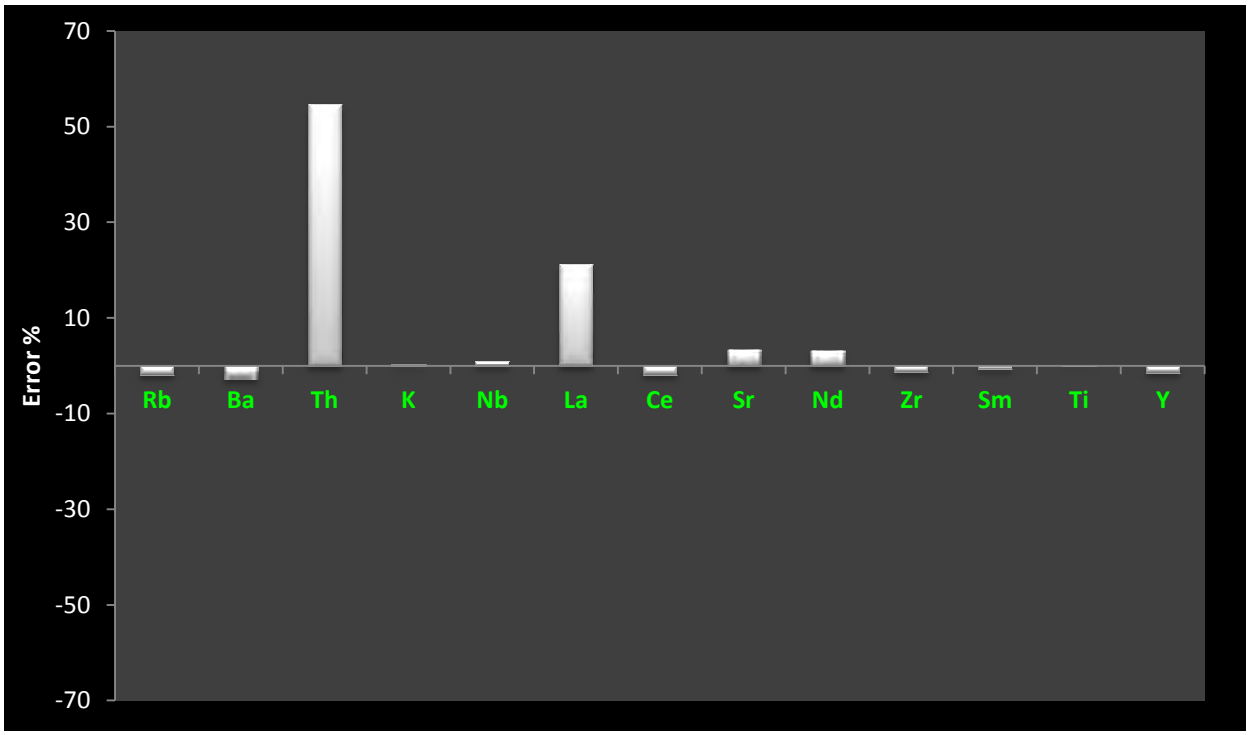

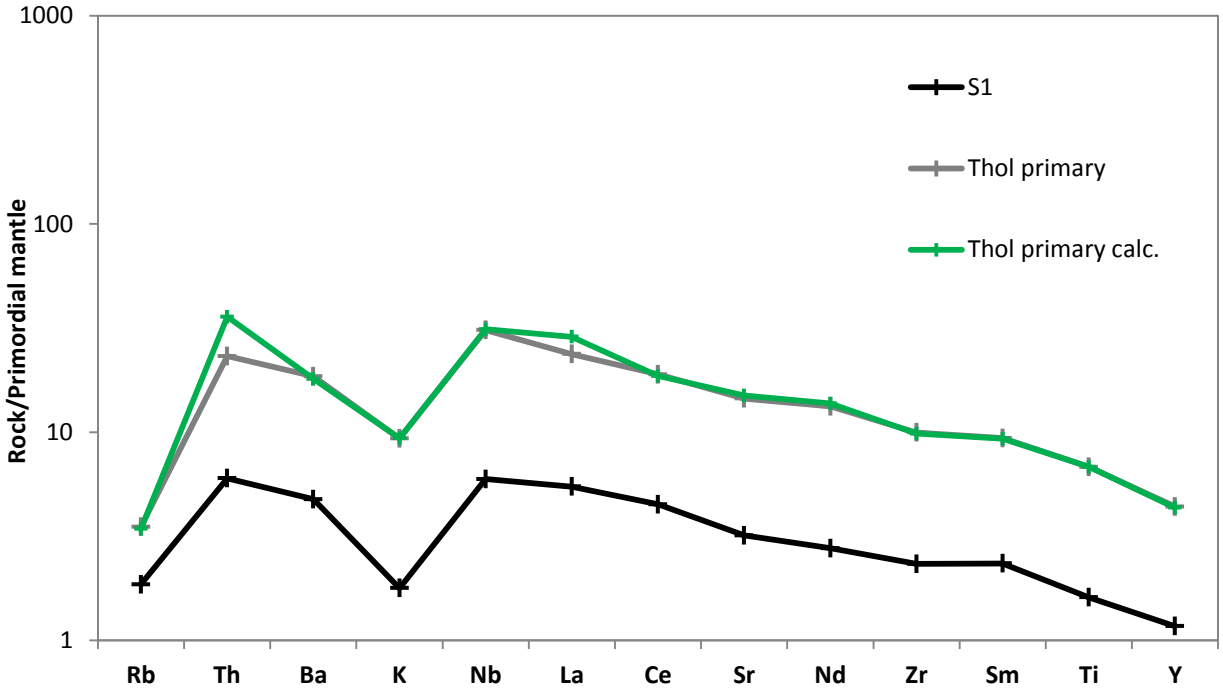


**Fig. 12.2.1 –** a) Trace element patterns of mantle source, real and calculated eutectic compositions for Tholeiitic modelling and b) histogram of error percentages.

### *Tholeiites*

Tholeiitic modeling shows satisfactory results with a good matching between real and calculated eutectic compositions (Fig. 12.2.1a). Only Th and La display high errors (%) up to 54.6 % (but only 1.1 ppm in absolute value) (Fig. 12.2.1b). $S_1$ represents the Iblean source taken from Beccaluva et al. (1998) and its meliing lead to pattern for the primary (in this case also primitive) magma anlalyzed for Mt. Etna, with positive spikes in Th, Nb and negative in K and Rb.

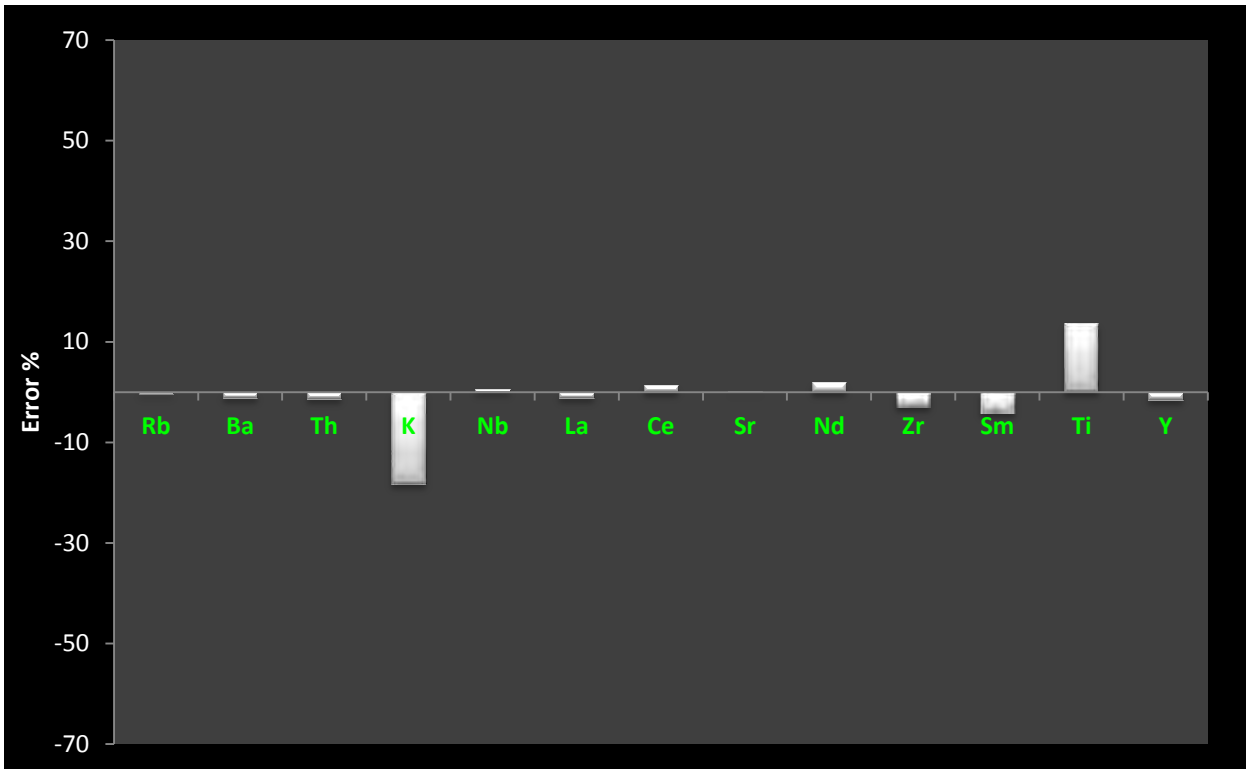


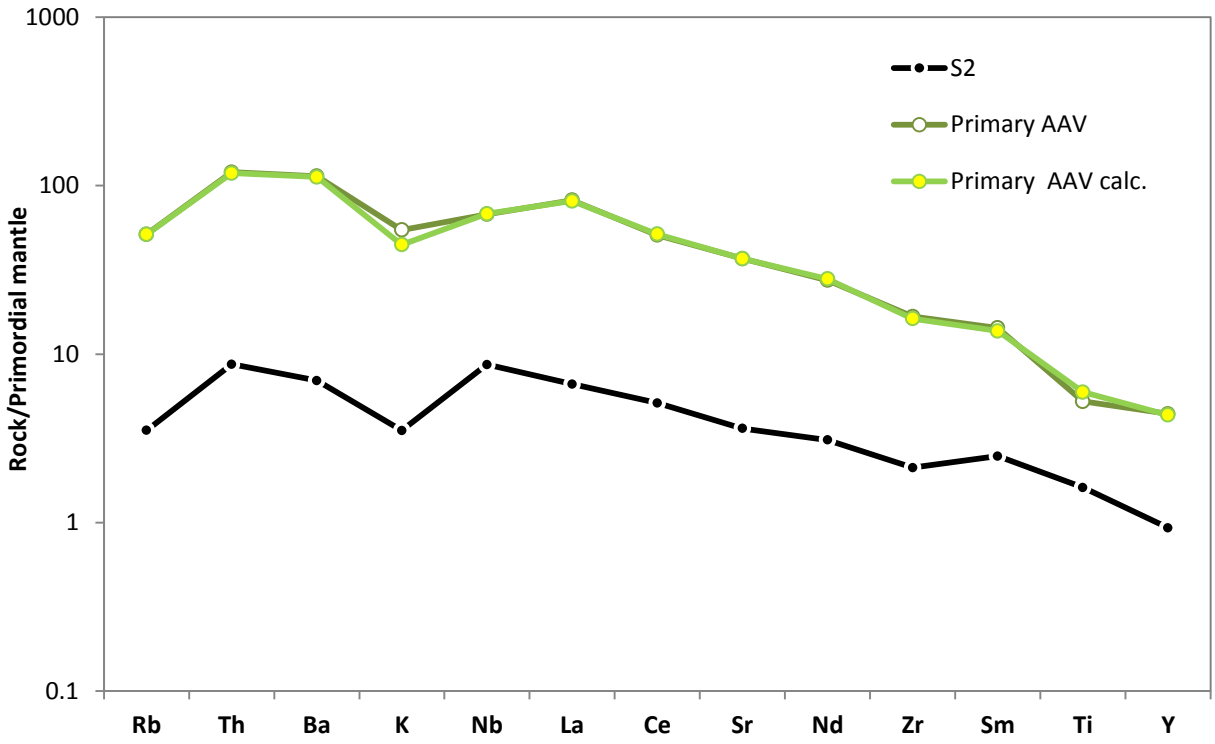


**Fig. 12.2.2 –** a) Trace element patterns of mantle source, real and calculated eutectic compositions for AVV modelling and b) histogram of error percentages.

*AAV*

Real and calculated eutectic compositions from AVV fit very well demonstrating the goodness of modeling (Fig. 12.2.2a). Only K and Ti show sligth high error (-18.1% and 13.6 respectively) (Fig. 12.2.2b).

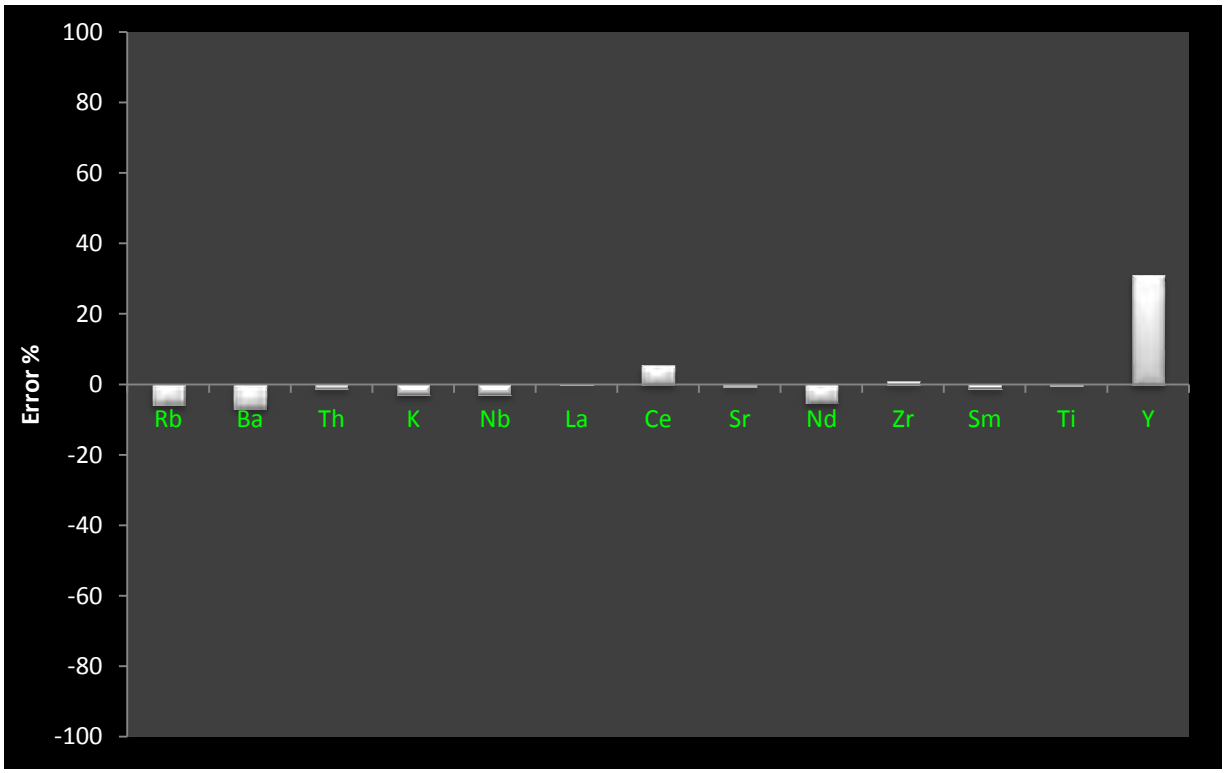


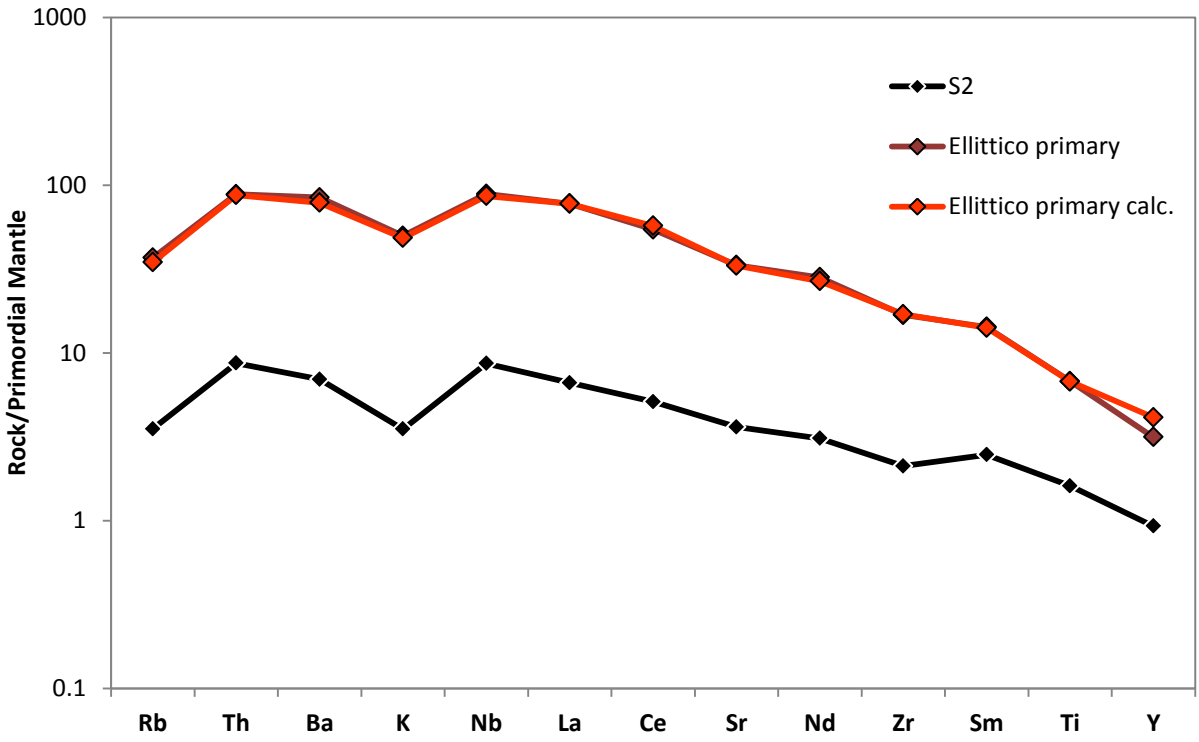

**Fig. 12.2.3 –** a) Trace element patterns of mantle source, real and calculated eutectic compositions for Ellittico modelling and b) histogram of error percentages.

***Ellittico***

Real and calculated eutectic compositions from Ellittico fit very well demonstrating the goodness of modeling (Fig. 12.2.3a). Only Y shows an high error (31.1% and 4.5 ppm in absolute value) because the low original concentration in the primary reconstructed eutectic (Fig. 12.2.3b). Melting The Iblean source $S_2$ (Beccaluva et al., 1998) was obtained an eutectic composition well comparable to the primary Etnean magma, even if this last trend appears enriched in the most incompatible element.

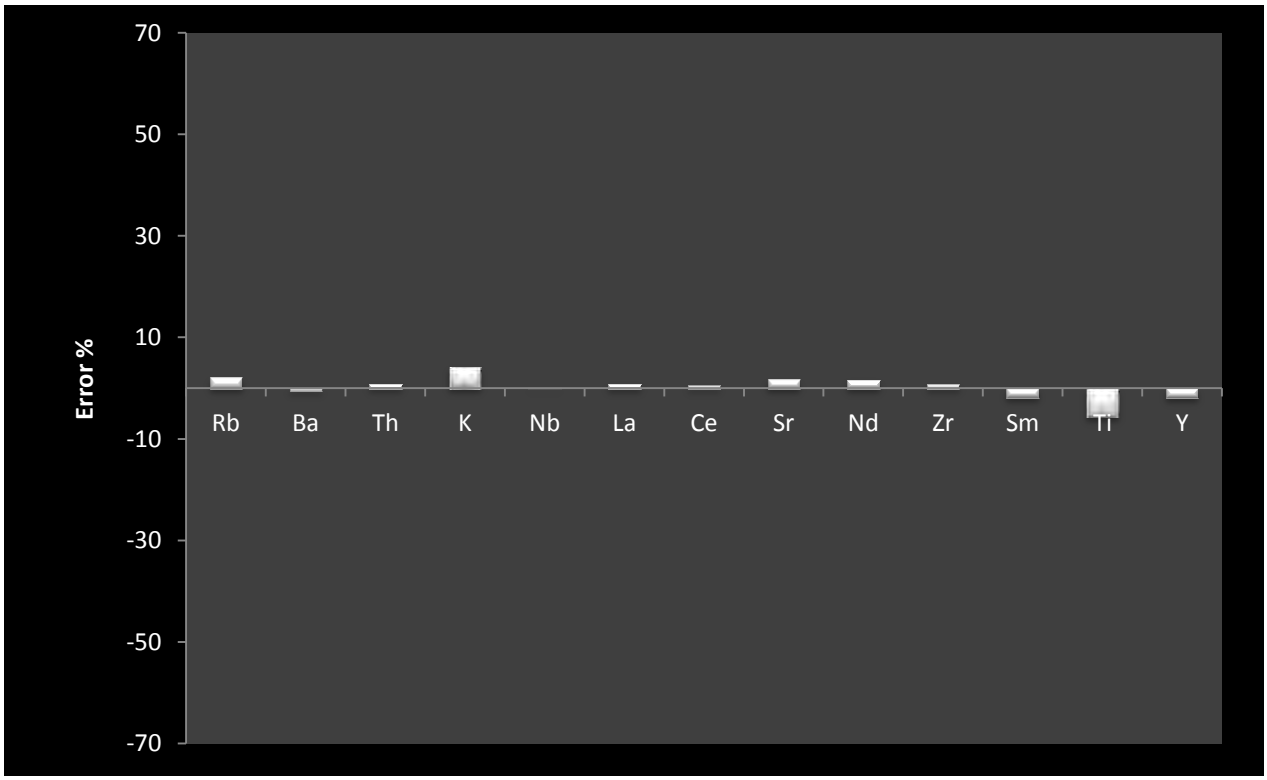

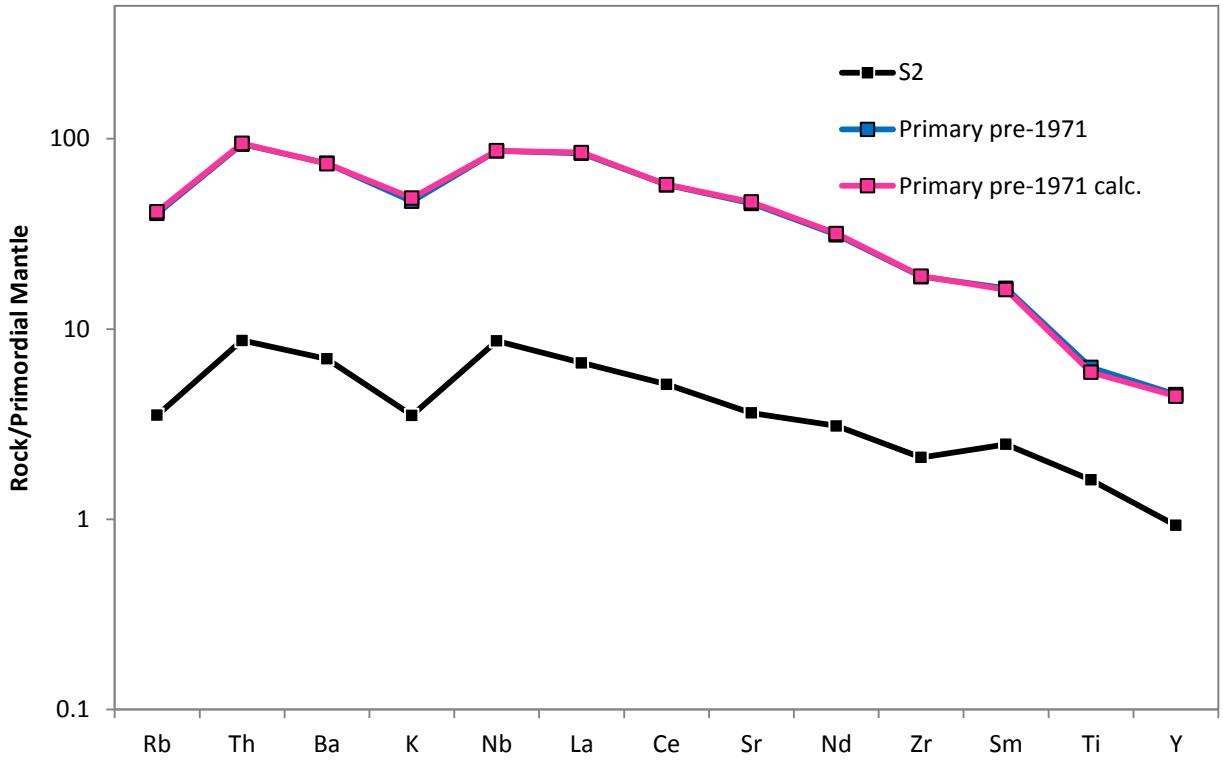


**Fig. 12.2.4 –** a) Trace element patterns of mantle source, real and calculated eutectic compositions for pre-1971 Recent Mongibello modelling and b) histogram of error percentages.

### *Pre-1971 Recent Mongibello*

Recent Mongibello (pre-1971) partial melting model is not so different from the Ellittico one, showing a good match between real and calculated primary compositions (Fig. 12.2.4a) . The chosen mantle source is still $S_2$ that well reproduces the peridotitic composition from which alkaline etnean magmas are originated. Error percentages are very limited and always below 5.6% (Fig. 12.2.4b). Pre-1971 Recent Mongibello primary magma shows a trend similar to Ellittico one but with an enrichment in more compatible trace elements.

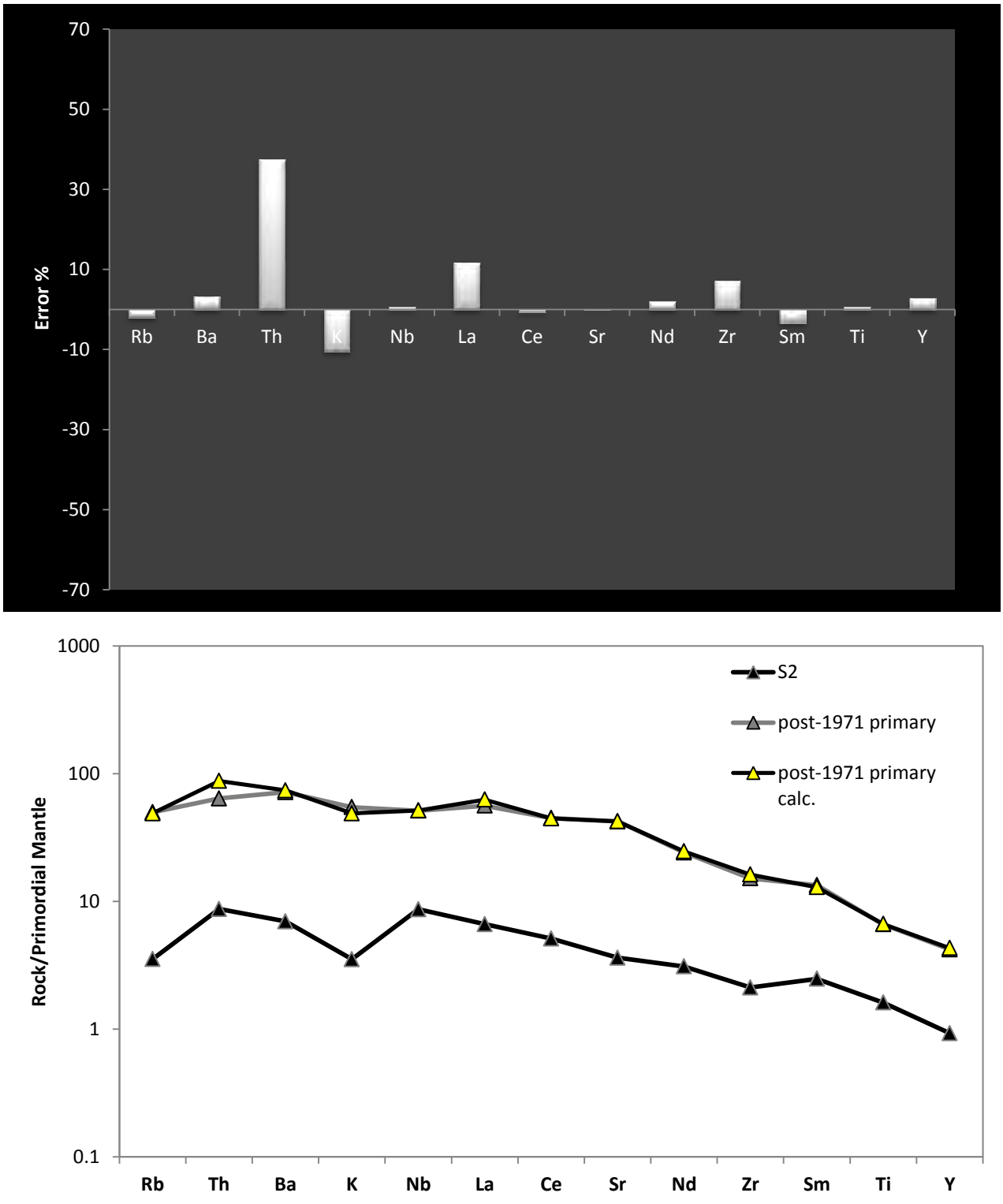


**Fig. 12.2.5 –** a) Trace element patterns of mantle source, real and calculated eutectic compositions for post-1971 Recent Mongibello modelling and b) histogram of error percentages.

***Post-1971 Recent Mongibello***

For post-1971 primary magma the negative spike in Ti is less marked than in Pre-1971 as well as for potassium (Fig 12.2.5a). At the same time the “flat” behavior of Nb, the not so high content in Th and the relative enrichment in Rb respect to the earlier magmatic stage suggests a change in the partial melting processes as shown in Table 6.

**Table 6 - Mass balance partial-melting models for each magmatic series.**

**Inferred mantle source compositions**

| | $S_1$Thol | | | $S_2$ alK. AAV | | |
|---|---|---|---|---|---|---|
| **$SiO_2$** | 44.24 | | | 44.1 | | |
| **$TiO_2$** | 0.20 | | | 0.24 | | |
| **$Al_2O_3$** | 4.76 | **Ol** | 50 | 4.86 | **Ol** | 50 |
| **FeOtot** | 8.76 | **Opx** | 27 | 8.77 | **Opx** | 27 |
| **MgO** | 37.26 | **Cpx** | 9 | 37.4 | **Cpx** | 8 |
| **CaO** | 2.99 | **Sp** | 5 | 2.71 | **Sp** | 5 |
| **$Na_2O$** | 0.64 | **Amph** | 10 | 0.60 | **Amph** | 9 |
| **$K_2O$** | 0.04 | **Phlo** | - | 0.22 | **Phlo** | 1 |
| **$Cr_2O_3$** | 1.11 | | | 1.11 | | |

**Mineral melting proportions (E) and magma compositions**

| | E Thol | E alk. AAV |
|---|---|---|
| **Ol** | -21.1 | -25.3 |
| **Opx** | 42.3 | 31.6 |
| **Cpx** | 22.7 | 17.4 |
| **Sp** | 13.2 | -12.15 |
| **Amph** | 42.9 | 75.0 |
| **Phlo** | - | 13.5 |
| | **ET4** | **ET39 calc.** |
| **$SiO_2$** | 47.8 | 52.6 |
| **$TiO_2$** | 1.43 | 1.26 |
| **$Al_2O_3$** | 13.7 | 14.8 |
| **FeOtot** | 11.8 | 9.02 |
| **MgO** | 14.9 | 8.81 |
| **CaO** | 8.13 | 7.81 |
| **$Na_2O$** | 1.92 | 4.00 |
| **$K_2O$** | 0.31 | 1.67 |
| **$Cr_2O_3$** | 0.00 | 0.00 |
| **$r^2$** | 0.30 | 0.24 |

**Inferred mantle source compositions**

| | $S_2$ alk. Ellittico | | | $S_2$ alk. Pre-1971 | | | $S_2$ alk. Post-1971 | | |
|---|---|---|---|---|---|---|---|---|---|
| **$SiO_2$** | 44.1 | | | 44.1 | | | 44.1 | | |
| **$TiO_2$** | 0.24 | | | 0.24 | | | 0.24 | | |
| **$Al_2O_3$** | 4.86 | **Ol** | 50 | 4.86 | **Ol** | 50 | 4.86 | **Ol** | 50 |
| **FeOtot** | 8.77 | **Opx** | 27 | 8.77 | **Opx** | 27 | 8.77 | **Opx** | 27 |
| **MgO** | 37.4 | **Cpx** | 8 | 37.4 | **Cpx** | 8 | 37.4 | **Cpx** | 8 |
| **CaO** | 2.71 | **Sp** | 5 | 2.71 | **Sp** | 5 | 2.71 | **Sp** | 5 |
| **$Na_2O$** | 0.60 | **Amph** | 9 | 0.60 | **Amph** | 9 | 0.60 | **Amph** | 9 |
| **$K_2O$** | 0.22 | **Phlo** | 1 | 0.22 | **Phlo** | 1 | 0.22 | **Phlo** | 1 |
| **$Cr_2O_3$** | 1.11 | | | 1.11 | | | 1.11 | | |

**Mineral melting proportions (E) and magma compositions**

| | E alk. Ellittico | E alk. Pre-1971 | E alk. Post-1971 |
|---|---|---|---|
| **Ol** | -15.5 | -10.3 | -12.5 |
| **Opx** | 27.9 | 22.6 | 25.3 |
| **Cpx** | 24.0 | 29.6 | 31.8 |
| **Sp** | -7.52 | -1.70 | -5.03 |
| **Amph** | 57.8 | 50.0 | 46.9 |
| **Phlo** | 13.2 | 9.79 | 13.6 |
| | **ET 52 calc.** | **ET 22 calc.** | **Bg1 calc.** |
| **$SiO_2$** | 48.9 | 47.3 | 48.6 |
| **$TiO_2$** | 1.5 | 1.34 | 1.52 |
| **$Al_2O_3$** | 15.4 | 15.6 | 14.8 |
| **FeOtot** | 10.0 | 11.0 | 10.3 |
| **MgO** | 9.78 | 10.7 | 10.5 |
| **CaO** | 9.01 | 9.34 | 9.31 |
| **$Na_2O$** | 3.92 | 3.40 | 3.32 |
| **$K_2O$** | 1.61 | 1.27 | 1.58 |
| **$Cr_2O_3$** | 0.00 | 0.00 | 0.00 |
| **$r^2$** | 0.22 | 0.20 | 0.25 |

**Mantle residua after partial melting**

| | F%= 16.6 | F%= 7.88 | | F%= 7.27 | F%= 7.21 | F%= 7.22 |
|---|---|---|---|---|---|---|
| $SiO_2$ | 44.00 | 38.96 | $SiO_2$ | 39.69 | 39.69 | 39.69 |
| $TiO_2$ | 0.66 | 1.31 | $TiO_2$ | 1.29 | 1.29 | 1.29 |
| $Al_2O_3$ | 7.91 | 10.15 | $Al_2O_3$ | 9.59 | 9.59 | 9.59 |
| FeOtot | 6.19 | 7.75 | FeOtot | 8.07 | 8.07 | 8.07 |
| MgO | 31.13 | 26.12 | MgO | 26.20 | 26.20 | 26.20 |
| CaO | 6.58 | 5.75 | CaO | 5.30 | 5.30 | 5.30 |
| $Na_2O$ | 1.92 | 0.79 | $Na_2O$ | 0.82 | 0.82 | 0.82 |
| $K_2O$ | 0.36 | 1.77 | $K_2O$ | 1.77 | 1.77 | 1.77 |
| $Cr_2O_3$ | 1.24 | 7.41 | $Cr_2O_3$ | 7.27 | 7.27 | 7.27 |
| | R Thol | R alk. AAV | | R alk. Ellittico | R alk. Pre-1971 | R alk. Post-1971 |
| Ol | 65.11 | 64.53 | Ol | 61.36 | 59.83 | 60.63 |
| Opx | 16.80 | 19.64 | Opx | 21.33 | 22.63 | 21.69 |
| Cpx | 7.22 | 6.24 | Cpx | 5.92 | 5.85 | 5.64 |
| Sp | 4.53 | 5.78 | Sp | 5.71 | 5.28 | 5.42 |
| Amph | 6.34 | 2.46 | Amph | 4.27 | 5.04 | 5.32 |
| Phlo | 0.00 | 1.36 | Phlo | 1.41 | 1.36 | 1.30 |

# 13. CONCLUSIONS

This work furnished a complete overview of the entire evolutionary cycle of Etnean magmatism. The stratigraphically controlled sampling from Tholeiitic to Recent Mongibello periods gave us the possibility the investigate the variations in the petrographic and geochemistry features of the emitted magmas and in the eruptive styles. By means of these direct studies it was possible to reproduce deep fractionation processes and improve the knowledge on the Etnean feeding system (Fig. 13.1). Mass balance modeling allowed to identifie five original magmas (Tholeiites, AAV, Ellittico, pre-1971 and post-1971 Recent Mongibello) with "primary" features, representing un-fractionated terms. They were compared to melt inclusions data (from literature) showing realistic compositions. Starting from the reconstructed primary magmas (chapter "Fractionation modeling") the most evolved lavas for each series were obtained. On average an estimation of about 40% of material should be considered beneath the volcano taking account the entire volume of the products emitted by the volcano. According to Neri and Rossi (2002) if the whole volcano edifice amounts to 374 $km^3$, about 150 $km^3$ of magma should be left behind from the magma on its way from the mantle to the surface (Tanguy et al., 1997, hypothesize the beginning of magma fractionation at 10 Kbar pressure). As confirmed by seismic tomography a positive P-wave anomaly (Murru et al., 1999, Patanè et al., 2006; Allard et al., 2006) underneath the volcanic edifice is noticed and Allard et al. (2006) hypothized that the absence of significant magma emissions could be balanced by the presence of an un-erupted, 10 km wide, intrusive body extending from the crystalline basement for 5 km inside the lower crust (its volume could be 3-4 times greater than the exposed volcanic succession one). Patanè et al. (2006) suggested that magma ascent can occur through this plutonic body. This calculation allowed us to give a first estimation of the entire magma volume produced by the Etnean source in his magmatic evolution. However this assumption is in contrast to the volume estimation obtained by the fractionation modeling. The value of 150 $km^{3,}$ derived from mass balance calculations applied to the Neri and Rossi (2002) study, is about 9 times smaller than Allard et al. (2006) estimation. Ferlito et al. (2014) further support our hypothesize stating that is not necessary the presence of such a wide intrusive body to produce the volume of magma erupted and the massive magmatic gasses released. They suppose the presence of a volatile flushing inside the primitive magma that resides into the plumbing system. This process allows $H_2O$ content to overcome the saturation threshold, exsolving and promoting eruption of primitive and volatile-rich magmas.

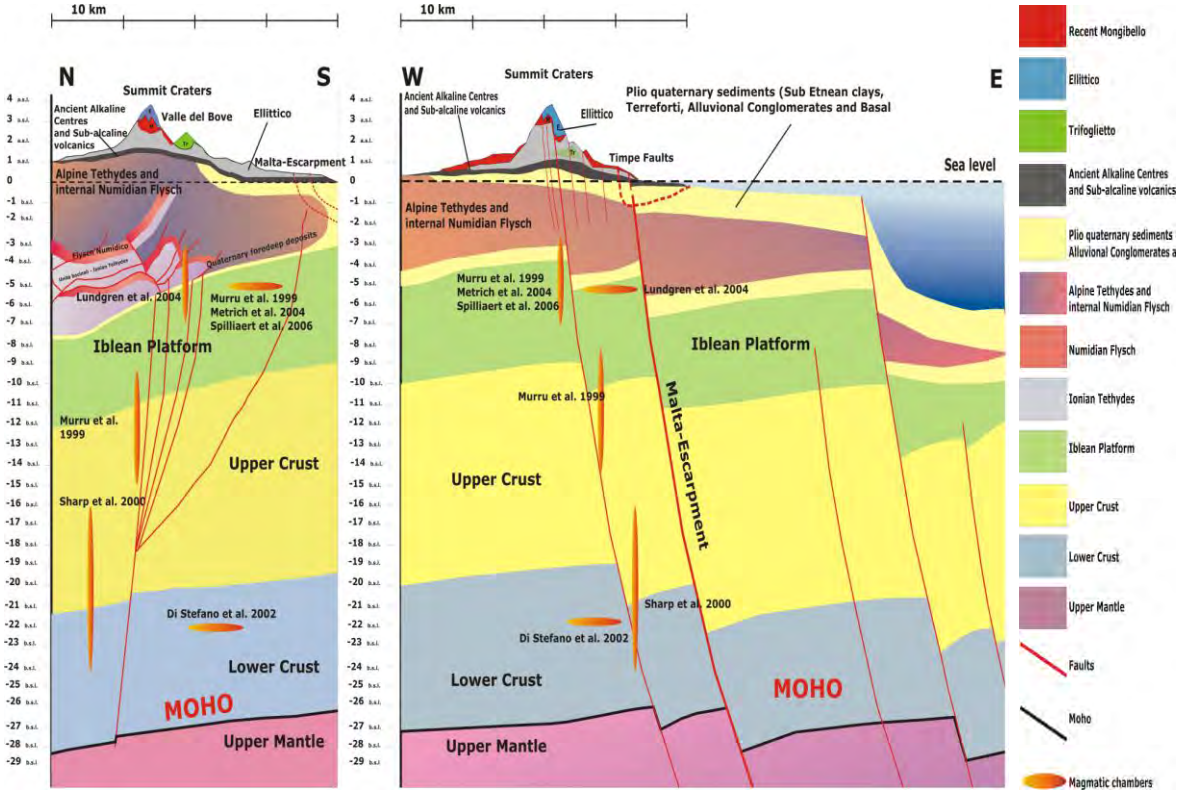


**Fig. 13.1** – Bidimensional model of Mt. Etna feeding system based on data from literature (Murru et al., 1999; Sharp et al., 2000; Metrch et al., 2004; Spilliaert et al., 2006; Di Stefano et al., 2002)

Another aim of this work was to investigate the Etnean mantle source, and it was possible only using Iblean mantle xenoliths from Beccaluva et al. (1998).

The results, displayed in Fig. 12.2.1., 12.2.2., 12.2.3., 12.2.4. and 12.2.5., show two evident different sources for tholeiites and alkaline suites that are attributable to Mt. Iblei modeling from Beccaluva et al. (1998). Post-1971 (Fig. 12.2.5.), prevalently K-alkaline terms, derive probably from the same mantle source $S_2$ of pre-1971 (Fig. 12.2.4.) products that melt in different proportions with a more involvement of phlogopite (Table 6). This could partially explain the shifting to potassium affinitiy that is not prerogative of recent lavas but is evidenced in AAV and Ellittico stages too. Modal proportions of melted peridotite show the same percentage of phlogopite in AAV, Ellittico and post-1971 models (about 13%) and a lower participation in pre-1971 calculation (about 9%). This is in agreement with Ferlito and Lanzafame (2010) that recognized a cyclic recurrence of potassium term in Mt. Etna magmatic evolution.

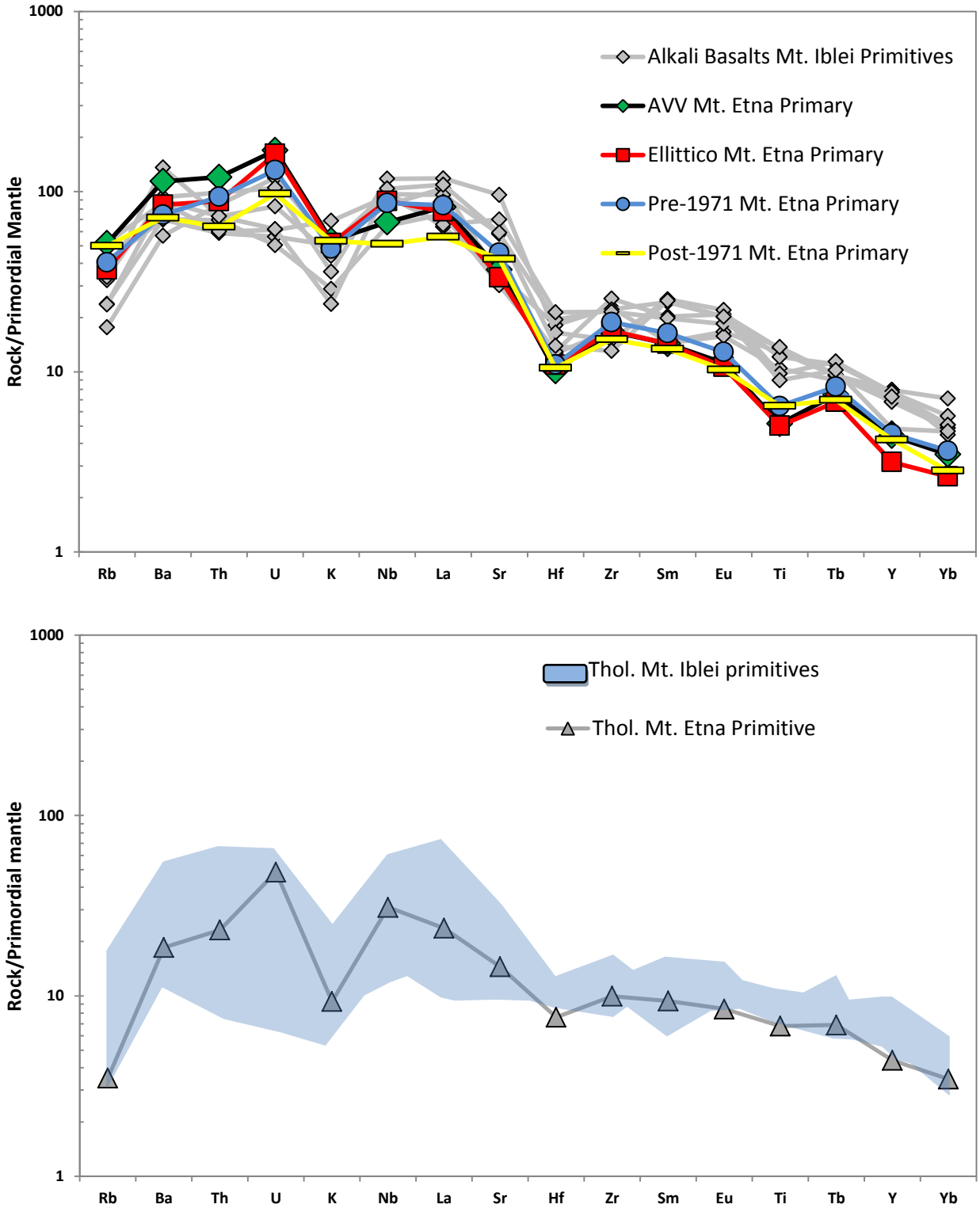


**Fig. 13.2 –** Comparison between Mt. Etna and Mt. Iblei a) primary and primitive Alkali basalts; b) primitive Tholeiites.

Fig. 13.2a tries to evidence the difference between Etnean and Iblein tholeiitic trace elements patterns. The primitive sample ET4, from Mt. Etna, plots inside the Iblean envelope, showing an enrichment in Uranium and a depletion in Hf. Also a comparison between Incompatible elements of primary (reconstructed) Etnean alkaline lavas and Iblean primitive magmas was developed (Fig. 13.2b). The first ones appear to be slightly enriched in Rb, Th, K and U and depleted in REE. On the whole, according to Correale et al. (2014) it can be pointed out that mantle sources beneath Mt. Iblei and Mt. Etna are very similar.

## 14. REFERENCES


- Adam J. and Green T. (2006) Trace element partitioning between mica- and amphibole-bearing garnet lherzolite and hydrous basanitic melt: 1. Experimental results and the investigation of controls on partitioning behavoiur. Contrib. Mineral. Petrol. 152: 1-17.
- Aigner-Torres M., Blundy J., Ulmer P. and Pettke T. (2007) Laser Ablation ICPMS study of trace elements partitioning between plagioclase and basaltic melts: an experimental approach. Contrib. Mineral. Petrol. 153: 647-667.
- Aiuppa A., Moretti R., Federico C., Giudice G., Gurrieri S., Liuzzo M., Papale P., Shinohara H. and Valenza M. (2007b) Forecasting Etna eruptions by real-time observation of volcanic gas composition. Geology 35: 1115–1118.
- Aiuppa A., Shinohara H., Tamburello G., Giudice G., Liuzzo M. and Moretti R. (2011) Hydrogen in the gas plume of an open-vent volcano, Mount Etna, Italy. J Geophys Res 116 DOI: 10.1029/2011JB008461.
- Alesci G. (2009-2010) Petrologia delle lave etnee nell'evento eruttivo 2002-2003: un possibile collegamento tra I sistemi dir if di Sud e di Nord. Master degree thesis.
- Alesci G., Giacomoni P. P., Coltorti M. and Ferlito C. (2013) Primary magmas, fractionation modelling and mantle sources of Etnenan lavas. Goldschmidt 2013 Conference abstract, Min. Soc. Mag. DOI: 10.1180/minmag.2013.077.5.1.
- Allard P., Carbonnelle J., Dajlevic D., Lebronec J., Morel P. Robe M. C., Maurenas J.M., Faivrepierret R., Martin D., Sabroux J. and Zettwoog P. (1991) Eruptive and diffuse emissions of $CO_2$ from Mt Etna. Nature 351: 387–391.
- Allard P., Carbonelle J., Métrich N., Loyer H. and Zettwoog P. (1994) Sulphur output and magma degassing budget of Stromboli volcano. Nature 368: 326-330.
- Allard P., D'Alessandro W., Jean-Baptiste P., Parello F., Flehoc C. and Parisi B. (1997) Mantle-derived helium and carbon in water springs and gases of Mount Etna. Earth Planet Sci Letters 148: 501-516.
- Allard P. (1997) Endogenous magma degassing and storage at Mount Etna. Geophys Res Lett 24: 2219-2222.
- Allard P., Behncke B., D'Amico S., Neri M. and Gambino G. (2006) Mount Etna 1993–2005: Anatomy of an evolving eruptive cycle. Earth-Science Reviews 78: 85-114.

- Anderson A. T. Jr. and Wright T. L. (1972) Phenocrysts and glass inclusions and their bearing on oxidation and mixing of basaltic magmas, Kilauea Volcano, Hawaii. Am Mineral 57: 188-216.
- Anderson A. T. Jr. (1976) Magma mixing: petrological processes and volcanological tools. J Volcanol Geotherm Res 1: 3-33.
- Anderson H. and Jackson J. (1987) The deep seismicity of the Tyrrhenian Sea. Geophys J R Astron Soc 91: 613-637.
- Andronico D., Branca S., Calvari S., Burton M., Caltabiano T., Corsaro R. A., Del Carlo P., Garfi G., Lodato L., Miraglia L., Murè F., Neri M., Pecora E., Pompilio M., Salerno G. and Spampinato L. (2005) A multy-disciplinary approach study of the 2002-03 Etna eruption: insights into a complex plumbing system. Bull Volcanol 67: 314-330.
- Andronico D., Cristaldi A., Del Carlo P. and Taddeucci J. (2009) Shifting styles of basaltic explosive activity during the 2002-2003 eruption of Mt. Etna, Italy. J Volcanol Geoth Res 180: 110-122.
- Anzà S., Dongarrà G., Giammanco S., Gottini V., Hauser S. and Valenza M. (1989) Geochimica dei fluidi dell'Etna. Le acque sotterranee. Mineral Petrogr Acta 23: 231–251.
- Armienti P., Innocenti F., Petrini P., Pompilio M. and Villari L. (1988) Sub-aphyric alkali basalt from Mt Etna: inferences on the depth and composition of the source magma, Rend. Sot Ital Miner Petrol Spec Issue: 877-891.
- Armienti P. (1994) Volatile control on the modal composition of Mt. Etna lavas. Mid-term scientific report of EEC contract no. EV5V-CT92-0177:Etna's volatiles. CEC RDT Program "Environment – natural hazards". European Volcano Laboratories, Paris.
- Armienti P., Tonarini S., D'Orazio M. and Innocenti F. (2004) Genesis and evolution of Mt. Etna alkaline lavas: petrological and Sr-Nd-B isotope constraints. Per Mineral 73: 29-52.
- Armienti P., Perinelli C. and Putirka K. (2013) A new model to estimate deep-level magma scent rates, with applications to Mt. Etna (Sicily, Italy). J Petrol 45: 1-19.
- Azzaro R. and Neri M. (1992) L'attività eruttiva dell'Etna nel corso del ventennio 1971–1991. Primi passi verso la costituzione di un data-base relazionale. CNR-IIV Oper file report 3/92, Catania 1–10.
- Azzaro R. (1999) Earthquake surface faulting at Mount Etna volcano (Sicily) and implications for active tectonics. Geodynamics 28: 193-213.
- Barberi F., Carapezza M. L., Valenza M. and Villari L. (1993) The control of lava flow during the 1991–1992 eruption of Mt. Etna. J Volcanol Geotherm Res 56: 1-34.

- Barsanti M., Papale P., Moretti R., Boschi E., Hauri E. and Longo A. (2009) Heterogeneous large total $CO_2$ abundance in the shallow magmatic system of Kilauea volcano, Hawaii. J Geophysi Res 114, B12201.
- Beccaluva L., Siena F., Coltorti M., Di Grande A., Lo Giudice A., Macciotta G., Tassinari R. and Vaccaro C. (1998) Nephelinitic to tholeiitic magma generation in a transtensional tectonic setting: an integrated model for the Iblean volcanism, Sicily. J Petrol 39: 1547-1576.
- Ben-Avraham Z. and Grasso M. (1990) Collisional zone segmentation in Sicily and surrounding areas in the Central Mediterranean. Ann Tectonicae 4: 131-139.
- Butler R. W. H., Grasso M. and La Manna F. (1992) Origin and deformation of the Neogene-Recent Maghrebian foredeep at the Gela Nappe, SE Sicily. J Geol Soc Lond 149: 547-556.
- Braiato M. (2011-2012) Studio petrologico dei prodotti emessi durante gli eventi parossistici dell'Etna tra gennaio 2011 a aprile 2012. Bachelor degree thesis.
- Branca S., Coltelli M., De Beni E. and Wijbrans J. (2008) Geological evolution of Mount Etna Volcano (Italy) from earliest products until the first central volcanism (between 500 and 100 Ka ago) inferred from geochronological and stratigraphical data. Int J Earth Sci 97: 135-152.
- Burton M., Mader H. M. and Polacci M. (2007) The role of gas percolation in quiescent degassing of persistently active basaltic volcanoes. Earth Planet Sci Lett 264: 46-50.
- Calvari S., Coltelli M., Neri M., Pompilio M. and Scribano V. (1994) The 1991–1993 Etna eruption: chronology and lava flow-field evolution. Acta Vulcanol 4: 1-14.
- Calvari S., Groppelli G. and Pasquarè G. (1994) Preliminary geological data on the south-western wall of the Valle del Bove, Mt. Etna, Sicily. Acta Vulcanol 5:15-30.
- Carroll M. R. and Holloway J. R. (1994) Volatiles in magmas. Rev Mineral 30: 517.
- Cashman K. V., Sturtevant B., Papale P. and Navon O. (2000) Magmatic fragmentation In: Sigurdsson H (ed) Encyclopedia of volcanoes. Academic Press, San Diego: 421-430.
- Catalano R. and D'Argenio B. (1982) Schema geologico della Sicilia. Guide Geologiche Regionali, Mem Soc Geol It, Suppl. A. V.XXIV: 9-41. Palermo.
- Clocchiatti R. and Massare D. (1985) Experimental crystallisation growth in melt inclusions: the possibility and limitation of the method. Contrib Mineral Petrol 89: 193-204.
- Clocchiatti R., Weisz J., Mosbah M. and Tanguy J. C. (1992) Coexistence de "verres" alcalins et tholéiitiques saturés en CO2 dans les olivines des hyaloclastites d'Aci Castello

(Etna, Sicile, Italie). Arguments en faveur d'un manteau anormal et d'un réservoir profond. Acta Vulcanol 2: 161-173.

- Clocchiatti R., Condomines M., Guenot N. and Tanguy J. C. (2004) Magma changes at Mount Etna: the 2001 and 2002-2003 eruptions. Earth Planet Sci Lett 226: 397-414.
- Collins S. J., Pyle M. D. and Maclennan J. (2011) Melt inclusions track pre-eruptive storage and dehydration of magmas at Etna. Geology 37: 571-574.
- Coltelli M., Garduno V. H., Neri M., Pasquarè G. and Pompilio M. (1994) Geology of the northern wall of the Valle del Bove, Mt. Etna (Sicily). Acta Vulcanol 5:55-68.
- Condomines M., Tanguy J. C., Kieffer G. and Allègre C. J. (1982) Magma evolution of a volcano studied by $^{230}$Th-$^{238}$U disequilibrium and trace elements systematics: The Etna case. Geochim Cosmochim Acta 46: 1397-1416.
- Continisio R., Ferrucci F., Gaudiosi G., Lo Bascio D. and Ventura G. (1997) Malta escarpment and Mt. Etna: early stages of an asymmetric rifting process? Evidences from geophysical and geological data. Acta Vulcanol 9 (1/2): 45-53.
- Correale A., Paonita A., Martelli M., Rizzo A., Rotolo G. S., Corsaro R. A. and Di Renzo V. (2014) A two component mantle source feeding Mt. Etna magmatism: insights from the geochemistry of primitive magmas. Lithos 184-187: 243-258.
- Corsaro R. A. and Cristofolini R. (2000) Subaqueous volcanism in the Etnean area: evidence for hydromagmatic activity and regional uplift inferred from the Castle Rock of Acicastello. J volcano Geoth Res 95: 209-225.
- Corsaro R. A. and Pompilio M. (2004) Magma dynamics in the shallow plumbing system of Mt. Etna as recorded by compositional variations in volcanics of recent summit activity (1995-1999). J Volcanol Geoth Res 137: 55-71.
- Corsaro R. A., Miraglia L. and Pompilio M. (2007) Petrology evidence of a complex plumbing system feeding the July-August 2001 eruption of Mt. Etna, Sicily, Italy. Bull Volcanol 69: 401-421.
- Cristofolini R., Lentini F., Patanè G. and Rasà R. (1979b) Integrazione dei dati geologici, geofisici e petrologici per la stesura di un profilo crostale in corrispondenza dell'Etna. Boll Soc Geol It 98: 239-247, 2 ff.
- Cristofolini R. and Tranchina A. (1980) Aspetti petrologici delle vulcaniti etnee: caratteri dei fenocristalli isolati ed in aggregati. Rendiconti della Società Italiana di Mineralogia e Petrologia 36: 751-773.

- Cristofolini R., Puglisi G., Scribano V. and Tranchina A. (1987) Within and among flow petrological variations in a sample from dated eruptions of the last ten centuries on Mount Etna. Periodico di Mineralogia 56: 1-24.
- D'Alessandro W., Giammanco S., Parello F. and Valenza M. (1997) CO2 output and δ13C(CO2) from Mount Etna as indicators of degassing of shallow asthenosphere. Bull Volcanol 58: 455-458.
- D'Orazio M., Tonarini S., Innocenti F. and Pompilio M. (1997) Northern Valle del Bove volcanic succession Mt. Etna, Sicily: petrography, geochemistry and Sr-Nd isotope data. Acta Vulcanol 9: 8-16.
- Del Carlo P. and Pompilio M. (2004) The relationship between volatile content and the eruptive style of basaltic magma: the Etna case. Ann Geophys 47.
- Deloule E., Paillat O., Pichavant M. and Scaillet R. (1995) Ion microprobe determination of water in silicate glasses: methods and applications. Chem Geol 125: 19-28.
- Di Stefano A. and Branca S. (2002). Long-term uplift rate ot the Etna volcano basement (southern Italy) based on biochronological data from Pleistocene sediments. Terra nova 14: 61-68.
- Dixon J. E., Stolper E. M. and Holloway J. R. (1995) An Experimental Study of Water and Carbon Dioxide Solubilities in Mid-Ocean Ridge Basaltic Liquids. Part I: Calibration and Solubility Models. J Petrol 36: 1607-1631.
- Ehlers K., Grove T. L., Sisson T. W., Recca S. I. and Zervas D. A.(1992) The effect of oxygen fugacity on the partitioning of nickel and and cobalt between olivine, silicate melt and metal. Geochim Cosmochim Acta 56:3733–3743.
- Faccenna C., Molin P., Orecchio B., Olivetti V., Bellier O., Funiciello F., Minelli L., Piromallo C. and Billi A. (2011) Topography of the Calabria subduction zone (southern Italy): Clues for the origin of Mt. Etna. Tectonophysics 30: TC1003.
- Faure F. and Schiano P. (2005) Experimental investigation of equilibration conditions during forsterite growth and melt inclusion formation. Earth Planet Sci Lett 236: 882-898.
- Ferlito C., Viccaro M. and Cristofolini R. (2008) Volatile-induced magma differentiation in the plumbing system of Mt. Etna volcano (Italy): evidence from glass and tephra of the 2001 eruption. Bull Volcanol 70: 455-473.
- Ferlito C., Coltorti M., Cristofolini R. and Giacomoni P. P. (2009) The contemporaneous emission of low-K and high-K trachybasalts and the role of the NE Rift during the 2002 eruptive event, Mt. Etna, Italy. Bull volcanol 71: 575-587

- Ferlito C., Viccaro M., Nicotra E. and Cristofolini R. (2010) Relationship between the flank sliding of the South East Crater (Mt. Etna, Italy) and the paroxysmal event of November 16. Bull Volcanol 72: 1179-1190.
- Ferlito C. and Lanzafame G. (2010) The role of supercritical fluids in the potassium enrichment of magmas at Mount Etna volcano (Italy). Lithos 119: 642-650.
- Ferlito C., Coltorti M., Lanzafame G. and Giacomoni P. P. (2014) The volatile flushing triggers eruptions at open conduit volcanoes: evidence from Mount Etna volcano (Italy). Lithos 184-187: 447-455.
- Finetti I. R. (2005) Depth contour map of the Moho discontinuity in the centra Mediterranean region from new crop seismic data. In: Finetti I. R. (ed.) CROP PROJECT. Deep Seismic Exploration of the Central Mediterranean and Italy 597-606.
- Fini A. (2011-2012) Caratterizzazione tessiturale e geochimica dei clinopirosseni nelle lave dei Centri Alcalini Antichi e confronto con altri periodi eruttivi dell'Etna. Becheler degree thesis.
- France L., Ildefonse B., Koepke J. and Bech F. (2010) A new method to estimate the oxidation state of basaltic series from microprobe analyses. J Volcanol Geoth Res 189: 340-346.
- Francis P., Oppenheimer C. and Stevenson D. S. (1993) Endogenous growth of persistently active volcanoes. Nature 366: 554-557.
- Frezzotti M. L. (2001) Silicate-melt inclusions in magmatic rocks: applications to petrology. Lithos 55: 273-299.
- Gasperini D., Blichert-Toft J., Bosch D., Del Moro A., Macera P and Albarede F. (2002). Upwelling of deep mantlematerial through a plate window: Evidence from the geochemistry of Italian basaltic volcanic. J Geophys Res 107: B12, 2367.
- Giacomoni P.P., Ferlito C., Alesci G., Coltorti M. (2012) A common feeding system of the NE and S rifts as revealed by the bilateral 2002/2003 eruptive event at Mt. Etna (Sicily, Italy). Bull Volcanol 74: 2415-2433.
- Giacomoni P.P., Coltorti M., Ferlito C., Bonadiman C. and Lanzafame G. (2013) Textural and compositional zoning of plagioclase as archive of magmatic evolution: the Mt. Etna case study. Goldschmidt 2013 Conference Abstracts, Mineralogical Magazine. doi:10.1180/minmag.2013.077. 5.1.

- Giammanco S. and Inguaggiato S. (1996) Soil gas emissions on Mount Etna (Sicily, Italy): geochemical characterization and volcanic influences. Proc IV Int Symp on the Geochemistry of the Earth's Surface, Leeds (England), July 1996.
- Gillot P. Y., Kieffer G. and Romano R. (1994) The evolution of Mount Etna in the light of potassium-argon dating. Acta vulcanol 5: 81-87.
- Grasso M. and Reuther C. D. (1988) The western margin of the Hyblean plateau: a neotectonic transform system on the SE Sicilian foreland. Ann Tecton 2: 107-120.
- Gurenko A. A., Sobolev V. A. and Kononkova N. N. (1991) Petrology of the primary magma of the Reykjanes Peninsula rift tholeiites. Geochem Int 28: 8-71.
- Hart S. R. and Davis K. E. (1978). Nickel partitioning between olivine for the development of DMM–HIMU isotopic compositions in a and silicate melt. Earth Planet Sci Lett 40: 203–219.
- Hervig R. L. and Dunbar N. W. (1992) Cause of chemical zoning in the Bishop California and Bandelier New Mexico Magma chambers. Earth Planet Sci Lett 111: 97-108.
- Huppert, H. E. and Hallworth, M. A. (2007) Bi-directional flows in constrained systems. J Fluid Mech 578: 95-112.
- Ihinger P. D., Hervig R. L. and McMillian P. F. (1994) Analytical methods for volatiles in magmas. Volatiles in Magmas. In: Carrol M. R. and Holloway J.R. Eds Rev Mineral 30: 67-129.
- Imposa S., Coco G. and Corrao M. (2004) Site effects close to structural lineaments in eastern Sicily (Italy). Eng Geol 72: 331.341.
- Joron J. L. and Treuil M. (1984) Etude geochimiche et petrogenese des laves de l'Etna, Sicile, Italie. Bull Volcanol 47: 1125-1144.
- Kamenetsky V. and Clocchiatti R. (1994) Melt inclusions as a potential guide into Mt. Etna magma chemistry. In: De Vivo B. and Frezzotti M. L. Eds, Fluid Inclusions in Minerals: Methods and Applications. Pontignano Siena: Short Course of the IMA Working Group A Inclusions in Minerals B. Virginia Polytechnic Institute and State Univ. Press, Blacksburg, VA: 363–376.
- Kamenetsky, V., Clocchiatti, R., 1996. Primitive magmatism of Mt. Etna: insights from mineralogy and melt inclusions. Earth Planet Sci Lett 142, 553–572.
- Kazahaya K., Shinohara H. and Saito G. (1994) Excessive degassing of Izu–Oshima volcano: magma convection in a conduit. Bull Volcanol 56: 207-216.

- Kovalenko V. I., Hervig R. I. and Sheridan M. F. (1988) Ion microprobe analyses of trace elements in anorthoclase, hedembergite, aenigmatites, quartz, apatite, and glass in pantellerite: evidence for high H2O contents in pantellerite melt. Am Mineral 73: 1038-1045.
- Kress V. C. and Carmichael I. S. E. (1988) Stoichiometry of the iron oxidation reaction in silicate melts. Am Mineral 73: 1267-1274.
- Lachance G. R. and Trail R. J. (1966) Practical solution to the matrix problem in X-ray analysis. Can Spectrosc 11:43–48.
- Loddo M., Patella D., Quarto R., Ruina G., Tramacenere A. and Zito G. (1989). Application of gravity and deep dipole geoelectrics in the volcanic area of Mt. Etna (Sicily). J. Volcanol. Geoth. Res. 39: 17-39, Elsevier Sci Pub B V, Amsterdam.
- Le Maitre R. W., Bateman P., Dudek A., Keller J., Lameyre J., Le Bas M. J. Sabine, P. A. Schmid, R. Sorensen, H. Streckeisen A., Woolley A. R. and Zanettin B. (1989). *A Classification of Igneous Rocks and Glossary of Terms: Recommendations of the International Union of Geological Sciences Subcommission on the Systematics of Igneous Rocks.* Oxford: Blackwell Scientific.
- Lowenstern J. B. and Mahood G. A. (1991) New data on magmatic $H_2O$ contents of pantellerites with implication for petrogenesis and eruptive dynamics at Pantelleria. Bull Volcanol 54: 78–83.
- Lowenstern J. B. (1994b) Chlorine, fluid immiscibility, and degassing in peralkaline magmas from Pantelleria, Italy. Am Mineral 79: 353-369.
- Liu Y., Zhang Y. and Behrens H. (2005) Solubility of $H_2O$ in rhyolitic melts at low pressures and a new empirical model for mixed $H_2O$–$CO_2$ solubility in rhyolitic melts. J Volcanol Geoth Res 143: 219-235.
- Lu F. Q., Anderson A. T. and Davies A. M. (1992) Melt inclusions and crystal-liquid separation in rhyolitic magmas of the Bishop tuff. Contrib Mineral Petrol 110: 113-120.
- Lupton J. (1983) Terrestrial inert gases: isotope tracer studies and clues to primordial components. Annu Rev Earth Planet Sci 11: 371–414.
- Maugeri G. M. (2014) Studio petrologico delle "Melt Inclusions": metodologie ed applicazioni all'evoluzione dei magmi primitivi etnei. Master degree thesis.
- McDonough W. F. and Sun S. S. (1995) The composition of Earth. Chemical Geology 120: 223-253.

- Metrich N., Sigurdsonn H., Meyer P. S. and Devine J. D. (1991) The 1783 Lakagigar eruption in Iceland: geochemistry, CO2 and sulfur degassing. Contrib Mineral Petrol 107: 435-447.
- Metrich N., Allard P., Spilliaert N., Andronico D. and Burton M. (2004) 2001 flank eruption of the alkali- and volatile-rich primitive basalt responsible for Mount Etna's evolution in the last three decades. Earth Planet Sci Lett 228: 1-17.
- Metrich N. and Wallace P. J. (2008) Volatile abundances in basaltic magmas and their degassing paths tracked by melt inclusions. Rev Mineral Geochem 69: 363-402.
- Michaud V. (1995) Crustal xenoliths in recent hawaiites from Mount Etna, Italy: evidence for alkali exchanges during magma – wall rock interaction. Chem Geol 122: 21-42.
- Monaco C., Catalano S., Cocina O., De Guidi G., Ferlito C., Gresta S., Musumeci C and Tortorici L. (2005) Tectonic control on the eruptive dynamics at Mount Etna Volcano (Sicily) during the 2001 and 2002-2003 eruptions. J Volcanol Geoth Res 144: 211-233.
- Murru M., Montuori C., Wyss M. and Privitera E. (1999) The locations of magma chambers at Mt. Etna, Italy, mapped by *b*-values. Geophys Res Lett 26: 2553-2556.
- Neri M., Orombelli G., Pasquarè G.and Pelfini M. (1995). Possible existence and extent of a late Pleistocene glacier on Mt. Etna. Project Seavolc: Sea-level change and the stability and activity of coastal and island volcanoes, Commission of the European Communities, Environment programme contract EV5VCT92-0170, Final Report, May 1995.
- Neri M. and Rossi M. (2002) Geometria e volume dell'apparato vulcanico etneo: il contributo offerto dall'uso di mappe digitali. Quaderni di geofisica – Istituto Nazionale di Geofisica e Vulcanologia 20.
- Neri M., Acocella V. and Behncke B. (2004) The role of the Pernicana Fault System in the spreading of Mt. Etna (Italy) during the 2002-2003 eruption. Bull Volcanol 66:417-430.
- Neri M., Acocella V., Behncke B., Maiolino V., Ursino A. and Velardita R. (2005) Contrasting triggering mechanisms of the 2001 and 2002–2003 eruptions of Mount Etna (Italy). J Volcanol Geoth Res 144: 235-255.
- Nicolich R., Cernobori L., Hirn A., Sapin M. and Gallart J. ETNASEIS Group (1996) Etna: lithospheric heterogeneity as the deep framework to magmatism. Abstracts 2nd Workshop on European Laboratory Volcanoes, Santorini (Greece) 2–4 May 1996.
- Nicolich R., Laigle M., Hirn A., Crenobori L. and Gallart J. (2000) Crustal structure of the Ionian margin of Sicily: Etna volcano in the frame of regional evolution. Tectonophysics 329: 121-139.

- Nicotra E., Ferlito C., Viccaro M. and Cristofolini R. (2011) Volcanic geology and petrology of The Val Calanna succession (Mt. Etna, Southern Italy): discovery of a new eruptive center. Period Mineral 80, 2: 287-307.
- Nielsen H. C. and Sigurdsonn H. (1981) Quantitative methods of electron microprobe analyses of sodium in natural and synthetic glasses. Am Mineral 66: 547-552.
- Oppenheimer C. and Yirgu G. (2002) Thermal imaging of an active lava lake: ErtaAle volcano, Ethiopia. Int J Remote Sens 23: 4777-4782.
- Oppenheimer C., Lomakina A. S., Kyle P. R., Kingsbury N. G. and Boichu M. (2009) Pulsatory magma supply to a phonolite lava lake. Earth Planet Sci Lett 28: 392-398.
- Papale P. (1999) Modeling of the solubility of a two-component $H_2O + CO_2$ fluid in silicate liquids. Am Mineral 84: 477-492.
- Patella D. and Quarto R. (1987). Interpretation of shallow Schlumberger soundings in the western sector of Mt. Etna, Sicily. Boll Geof Teor Appl, Vol.XXIX 116: 309-320.
- Patanè D., Barberi G., Cocina O., De Gori P. and Chiarabba C. (2006) Time-Resolved Seismic Tomography Detects Magma Intrusions at Mount Etna. Science 313: 821-823.
- Patanè G., La Delfa S. and Tanguy J. C. (2006) Volcanism and mantle-crust evolution: The Etna case. Earth Planet Sci Lett 241: 831-843. -257.
- Peccerillo A. (2005) Plio-Quaternary Volcanism in Italy. Petrology, Geochemistry, Geodynamics. Springer book.
- Pennisi M. and Le Cloarec M. (1998) Variations of Cl, F, and S in Mount Etna's plume, Italy, between 1992 and 1995. J Geophys Res 103: 5061-5066.
- Romano R. (1982) Succession of the volcanic activity in the etnean area. Mem Soc Geol It 23: 27-48, 10 ff.
- Rymer H., van Wyk de Fries B., Stix J. and Williams-Jones G. (1998) Pit crater structure and processes governing persistent activity at Masaya Volcano, Nicaragua. Bull Volcanol 59: 345-355.
- Schiano P., Clocchiatti R., Ottolini L. and Busà T. (2001) Transition of Mount Etna lavas from a mantle-plume to an island-arc magmatic source. Nature 412: 900-904.
- Schmincke H. U., Behncke B., Grasso M., and Raffi S. (1997) Evolution of the northwestern Iblean Mountains, Sicily: uplift, Plicocene/Pleistocene sea-level changes, paleoenvironment and volcanism. Geol Rundsch 86: 637-669.
- Selvaggi G. and Chiarabba C. (1995) Seismicity and P-wave velocity image of the Southern Tyrrhenian subduction zone. Geophys J Int 121: 818-826.

- Sharp A. D. L., Davis P. M. and Gay F. (1980) A low velocity zone beneath Etna and magma storage. Nature 287: 587- 591.
- Shaw D. M. (1970) Trace-element fractionation during anatexis. Geochim Cosmochim Acta 34:237–243.
- Sobolev A. V. and Shimizu N. (1993) Ultra-depleted primary melt included in olivine from the Mid-Atlantic ridge. Nature 363: 151-153.
- Sobolev A. V. and Danyushevsky L. V. (1994) Petrology and geochemistry of boninites from the north termination of the Tonga Trench: constraints on the generation conditions of primary high Ca-boninite magmas. J Petrol 27: 865-897.
- Spampinato L., Calvari S., Oppenheimer C. and Lodato L. (2008) Shallow magma transport for the 2002-03 Mt. Etna eruption inferred from thermal infrared surveys. J Volcanol Geoth Res 177: 301-312.
- Spilliaert N., Allard P., Metrich N. and Sobolev A. V. (2006) Melt inclusion record of the conditions of ascent, degassing, and extrusion of volatile-rich alkali basalt during the powerful 2002 flank eruption of Mount Etna (Italy). J Geophis Res 111: B04203, doi:10.1029/2005JB003934
- Spilliaert N., Metrich N. and Allard P. (2006) S-Cl-F degassing pattern of water-rich alkali basalt: Modelling and relationship with eruption styles on Mount Etna volcano. Earth Planet Sci Lett 248: 772-786.
- Stelling J., Botcharnikov R. E., Beermann O. and Nowak M. (2008) Solubility of $H_2O$- and chlorine-bearing fluids in basaltic melt of Mount Etna at T= 1050-1250 °C and P= 200 MPa. Chem Geol 256: 102-110.
- Stevenson D. S. and Blake S. (1998) Modelling the dynamics and thermodynamics of volcanic degassing. Bull Volcanol 60:307-317.
- Stoiber R. E., Williams S. N. and Huebert B. J. (1986) Sulfur and halogen gases at Masaya caldera complex, Nicaragua: total flux and variations with time. J Geophys Res 91: 12215-12231.
- Sun S.s. and McDonough W. F. (1989) Chemical and isotopic systematic of oceanic basalts: implications for mantle composition and processe. Geological Society London, Special publications 42: 313-345.
- Tanguy J. C. and Kieffer G. (1977) The 1974 eruption of Mount Etna. Bull Volcanol 40: 239-252

- Tanguy J. C., Condomines M. and Kieffer G. (1997) Evolution of the Mount Etna magma: Constraints on the present feeding system and eruptive mechanism. J Volcanol Geoth Res 75: 221-250.
- Taylor R. P., Jackson S. E., Longerich H. P. and Webster J. D. (1997) In situ trace element analyses of individual silicate melt inclusions by laser microprobe inductively coupled plasma mass spectrometry LAM–ICP–MS. Geochim Cosmochim Acta 61: 2559-2567.
- Tonarini S., Armienti P., D'Orazio M. and Innocenti F. (2001) Subduction-like fluids in the genesis of Mt. Etna magmas: evidences from boron isotopes and fluid mobile elements. Earth Planet Sci Lett 192: 471-483.
- Torelli L., Grasso M., Mazzoldi G. and Peis D. (1998) Plio–Quaternary tectonic evolution and structure of the Catania foredeep, the northern Hyblean Plateau and the Ionian shelf (SE Sicily). Tectonophysics 298: 209-221.
- Tric E., Valet J. P., Gillot P. Y. and Lemeur I. (1994) Absolute paleo-intensities between 60 and 160 K year from Mount Etna (Sicily). Phys Earth Planet Int 85: 113-129.
- Vaggelli G., De Vivo B. and Trigila R. (1993) Silicate-melt inclusions in recent Vesuvius lavas 1631–1944: analytical chemistry. J Volcanol Geotherm Res 58: 367-376.
- Viccaro M., Ferlito C., Cortesogno L., Cristofolini R. and Gaggero L. (2006) Magma mixing during the 2001 event at Mount Etna (Italy): Effects on the eruptive dynamics. Journal of Volcanology and Geothermal Research 149: 139-159.
- Viccaro M. and Cristofolini R. (2008) Nature of mantle heterogeneity and its role in the short-term geochemical and volcanological evolution of Mt. Etna (Italy). Lithos 105: 272-288.
- Viccaro M., Giacomoni P. P., Ferlito C. and Cristofolini R. (2010) Dynamics of magma supply at Mt. Etna volcano (Southern Italy) as revealed by textural and compositional features of plagioclase phenocrysts. Lithos 116: 77-91.
- Villemant B., Jaffrezic H., Joron J. L. and Treuil M. (1981) Distribution coefficient of major and trace elements; fractional crystallization in the alkali basalt series of Chaine des Puys (Massif Central, France). Geochim Cosmochim Acta 45:1997-2016.
- Wallace P. (2005) Volatiles in subduction zone magmas: concentrations and fluxes based on melt inclusion and volcanic gas data. J Volcanol Geoth Res 140: 217-240.
- Wilson B. M. (1989) Igneous Petrogenesis, A Global Tectonic Approach. Book.
- Witham F. and Llewellin E. W. (2006) Stability of lava lakes. J Volcanol Geoth Res 158: 321-332.

- Witham F., Woods A. W. and Gladstone C. (2006) An analogue experimental model of depth fluctuations in lava lakes. Bull Volcanol 69: 51-56.
- Witham F. (2011) Conduit convection, magma mixing, and melt inclusion trends at persistently degassing volcanoes. Earth Planet Sci Lett 301: 345-352.
- Wood B. and Trigila R. (2001) Experimental determination of aluminous clinopyroxene-melt partition coefficients for potassic liquid, with application to the evolution of the Roman province potassic magmas. Chem Geol 172: 213-22.

**APPENDIX A: Whole-rock major elements, trace elements and CIPW norm (CD-ROM).**

**APPENDIX B: Microprobe compositions of constituent minerals in Mt. Etna lavas used in mass balance calculations (CD-ROM).**